# Constructing phase diagrams of block copolymers with A-block-(B-stat-C) architecture

## *Supporting Information*

*Britta Weidinger[§], Nadine von Coelln[§], Guohui Yang, Hermann Nirschl, Irene Wacker, Rasmus R. Schröder, Petra Tegeder, Eva Blasco**

*[§] equal contribution*

**Contents**

## 1. Synthesis and chemical characterization of the block copolymers

### *1.1 P(MMA-stat-HEMA) macroCTAs*

Exemplary synthesis of P(MMA-stat-HEMA) macroCTAs

In a Schlenk tube, MMA (6.40 g, 64.0 mmol, 819 eq.), HEMA (2.08 g, 16.0 mmol, 204 eq.) and CPDB (17.3 mg, 78.1 µmol, 1.0 eq.) were dissolved in 1,4-dioxane (8 mL). AIBN solution (323 mg, 9.78 µmol, 0.125 eq., 10 mg in 2.010 mg 1,4-dioxane) was added. The solution was degassed via freeze-pump-thaw (3 x 8 min), followed by backfilling with nitrogen. The reaction mixture was stirred at 90 °C for 2.5 h, cooled in liquid nitrogen and opened to the atmosphere. After dilution with DCM, the solution was precipitated into diethyl ether twice. After centrifugation and decanting of the supernatant, copolymer macroCTA-38 was received as a light pink solid.

$^1$H NMR 600 MHz ($CD_2Cl_2$): $\delta$ [ppm] = 7.80 (m), 7.47 (m), 7.31 (m), 4.0 (bs), 3.74 (bs), 3.50 (s), 2.00 - 0.61 (m).

Table S1: Monomer ratio, reaction time, molecular weight, and dispersity of the synthesized MacroCTAs-XX, where xx corresponds to the molecular weight in kDa.

| Polymer | MMA:HEMA:CPDB:AIBN | T [h] | $M_n$(GPC) | Đ | Precursor for |
|---|---|---|---|---|---|
| macroCTA-*22* | 304:76:1:0.125 | 4 | 22454 | 1.11 | $S_{0.54}$-$MH_{0.46}$-*45* |
| macroCTA-*29* | 441:110:1:0.125 | 4 | 28749 | 1.12 | $S_{0.52}$-$MH_{0.48}$-*67* |
| macroCTA-*21* | 304:76:1:0.125 | 2 | 20667 | 1.13 | $S_{0.75}$-$MH_{0.25}$-*66* |
| macroCTA-*54* | 819:204:1:0.125 | 5 | 53925 | 1.05 | $S_{0.49}$-$MH_{0.51}$-*92* |
| macroCTA-*23* | 304:76:1:0.125 | 2.5 | 23083 | 1.08 | $S_{0.45}$-$MH_{0.55}$-*42*<br>$S_{0.66}$-$MH_{0.34}$-*70* |
| macroCTA-*48* | 819:204:1:0.125 | 2.5 | 48065 | 1.12 | $S_{0.50}$-$MH_{0.50}$-*91* |
| macroCTA-*39* | 819:204:1:0.125 | 2.5 | 38850 | 1.17 | $S_{0.46}$-$MH_{0.54}$-*81*<br>$S_{0.42}$-$MH_{0.58}$-*89* |
| macroCTA-*43* | 819:204:1:0.125 | 3.2 | 43205 | 1.15 | $S_{0.28}$-$MH_{0.72}$-*67*<br>$S_{0.27}$-$MH_{0.73}$-*70* |
| macroCTA-*38* | 819:204:1:0.125 | 2.5 | 37641 | 1.10 | $S_{0.37}$-$MH_{0.63}$-*65*<br>$S_{0.53}$-$MH_{0.47}$-*94* |
| macroCTA-*34* | 819:204:1:0.125 | 2.6 | 33587 | 1.13 | $S_{0.42}$-$MH_{0.58}$-*57*<br>$S_{0.09}$-$MH_{0.91}$-*39*<br>$S_{0.31}$-$MH_{0.69}$-*48*<br>$S_{0.16}$-$MH_{0.84}$-*45*<br>$S_{0.12}$-$MH_{0.88}$-*40*<br>$S_{0.16}$-$MH_{0.84}$-*43* |
| macroCTA-*19* | 304:76:1:0.125 | 2 | 18985 | 1.10 | $S_{0.39}$-$MH_{0.61}$-*35*<br>$S_{0.28}$-$MH_{0.72}$-*29*<br>$S_{0.50}$-$MH_{0.50}$-*45*<br>$S_{0.56}$-$MH_{0.44}$-*52* |
| macroCTA-*9* | 224:56:1:0.125 | 1 | 9303 | 1.12 | $S_{0.68}$-$MH_{0.32}$-*33* |

NMR spectra of P(MMA-*stat*-HEMA) macroCTAs

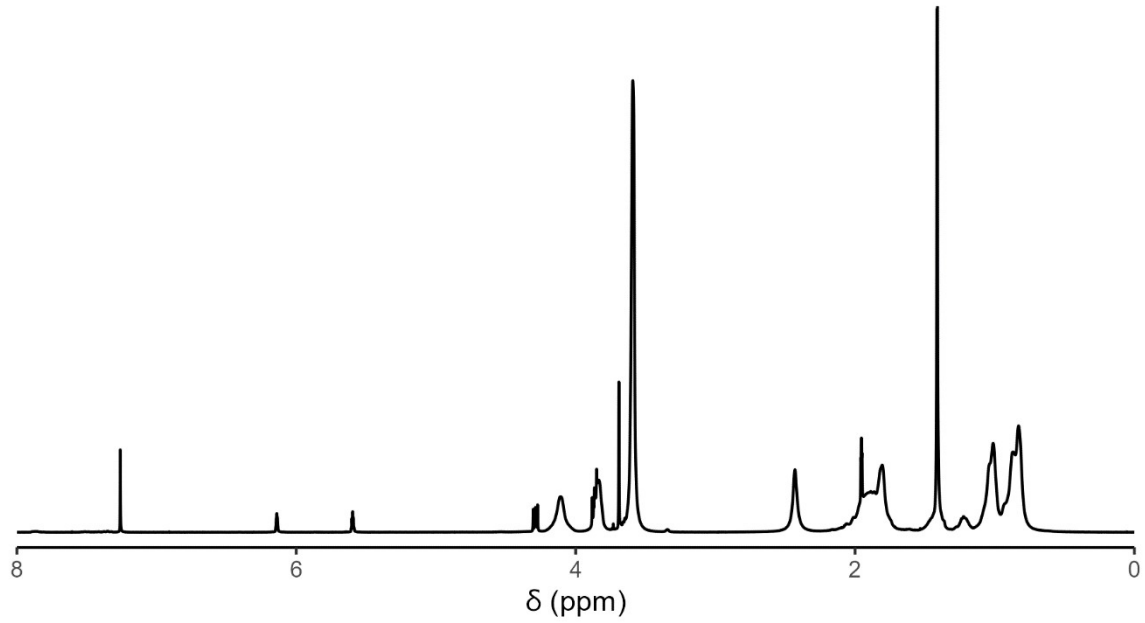


Figur

e S1: $^{1}$H NMR spectrum of macroCTA-*22* in $CDCl_3$.

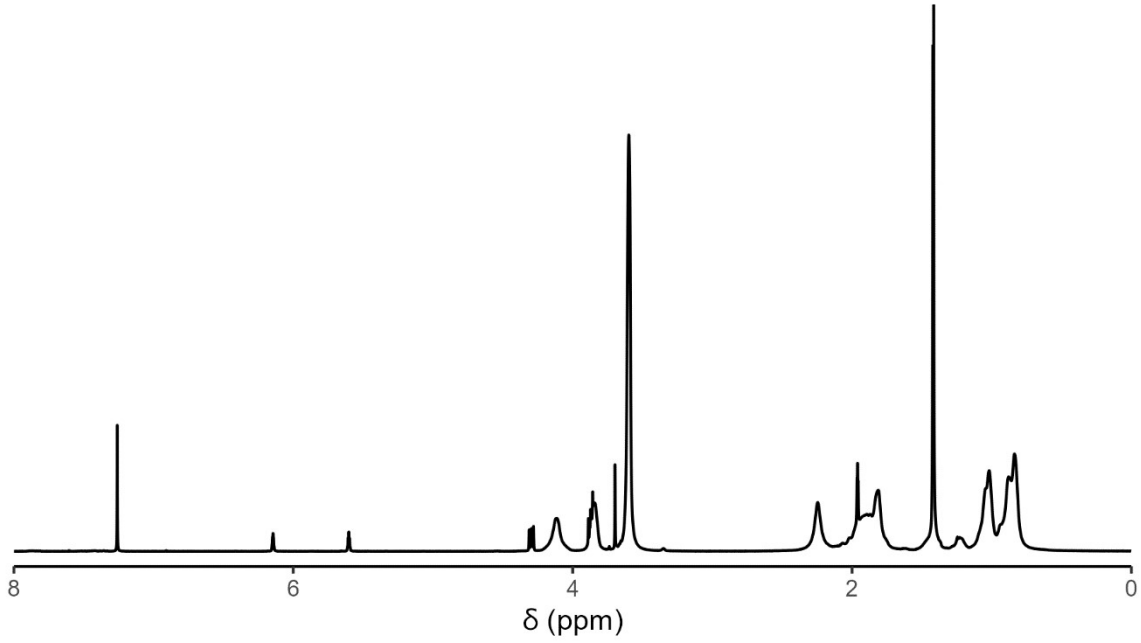


Figure S2: $^{1}$H NMR spectrum of macroCTA-*29* in $CDCl_3$.

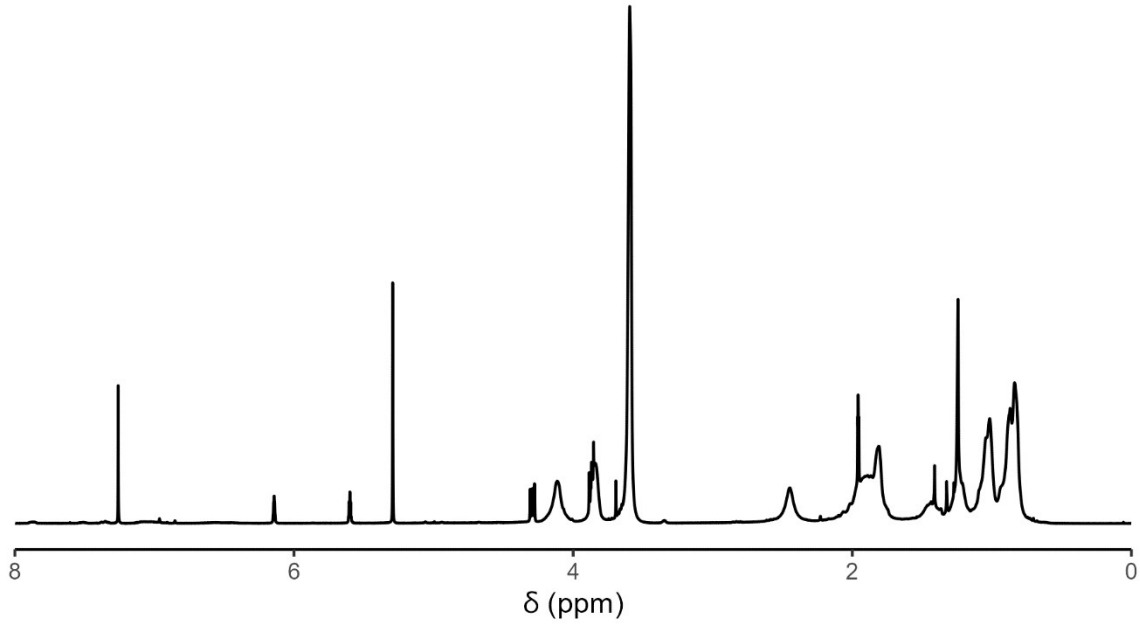


Figure S3: $^{1}$H NMR spectrum of macroCTA-*21* in $CDCl_3$.

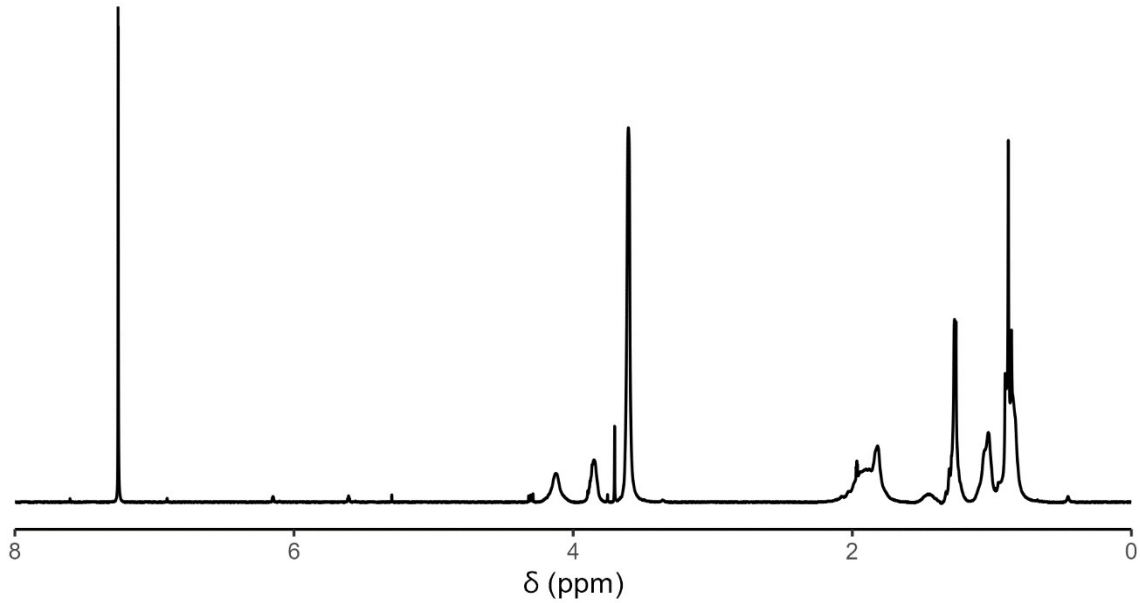


Figure S4: $^{1}$H NMR spectrum of macroCTA-*54* in $CDCl_3$.

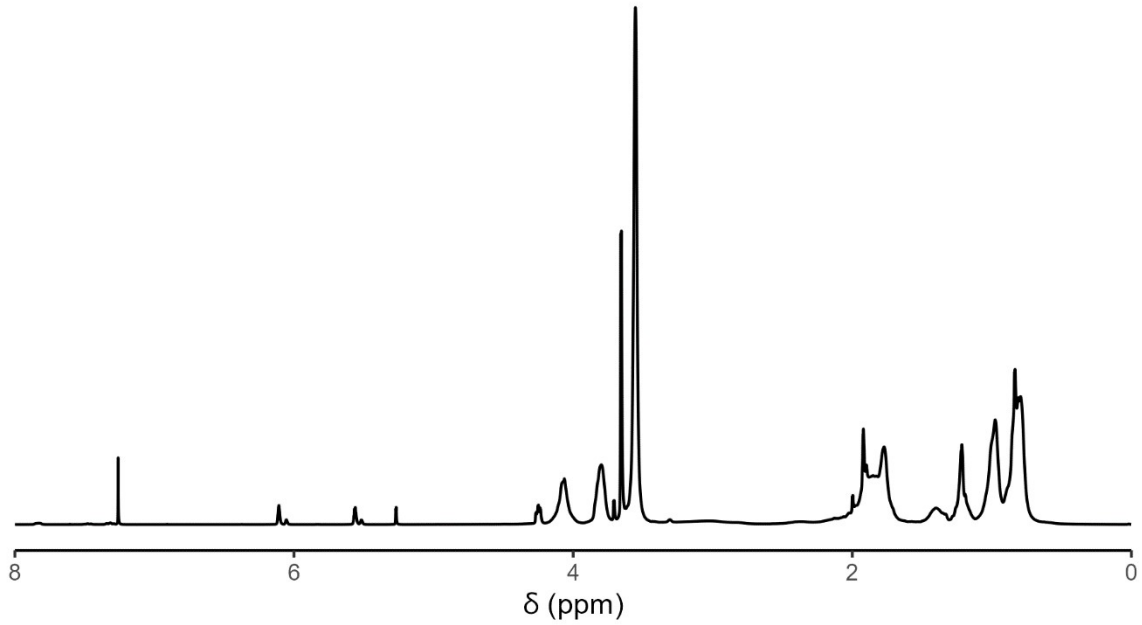


Figure S5: $^{1}H$ NMR spectrum of macroCTA-*23* in $CDCl_3$.

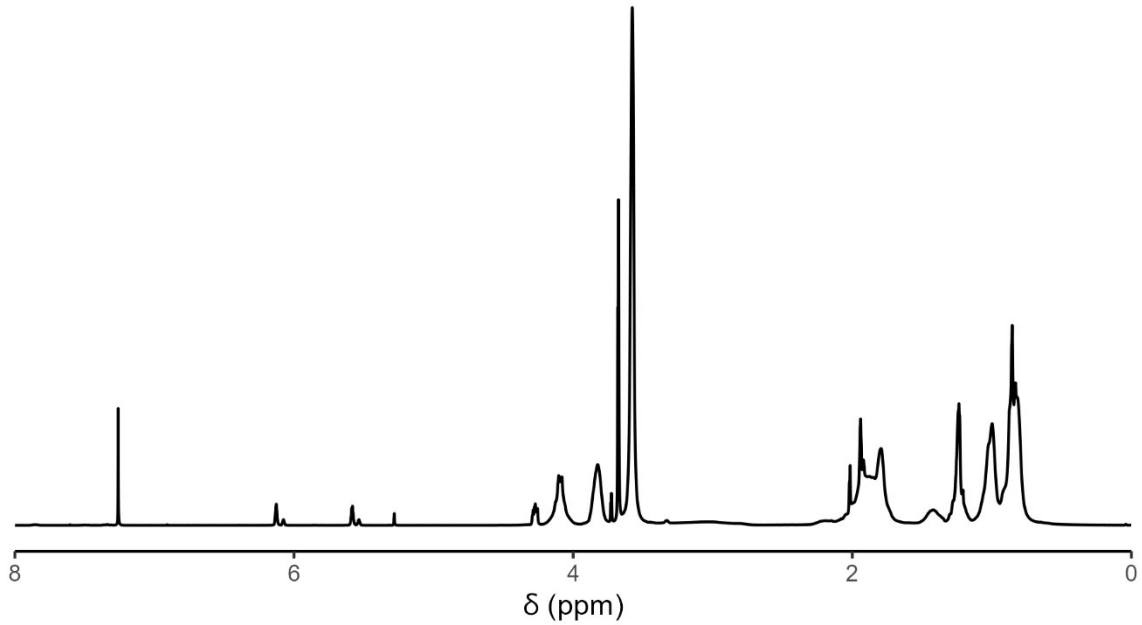


Figure S6: $^{1}H$ NMR spectrum of macroCTA-*48* in $CDCl_3$.

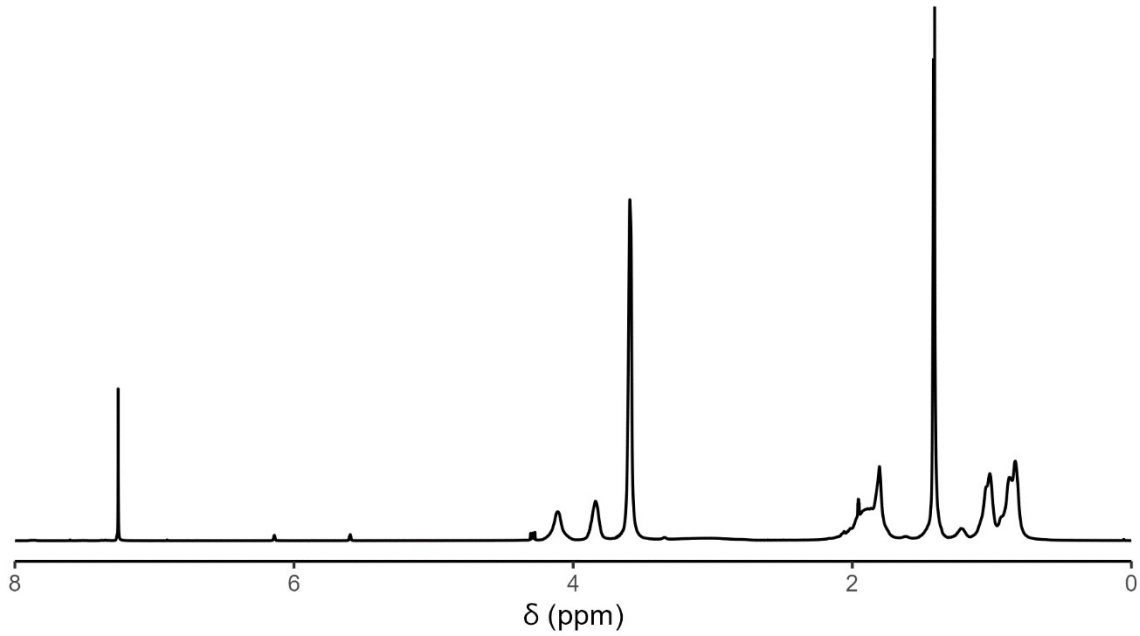


Figure S7: $^{1}H$ NMR spectrum of macroCTA-*39* in $CDCl_3$.

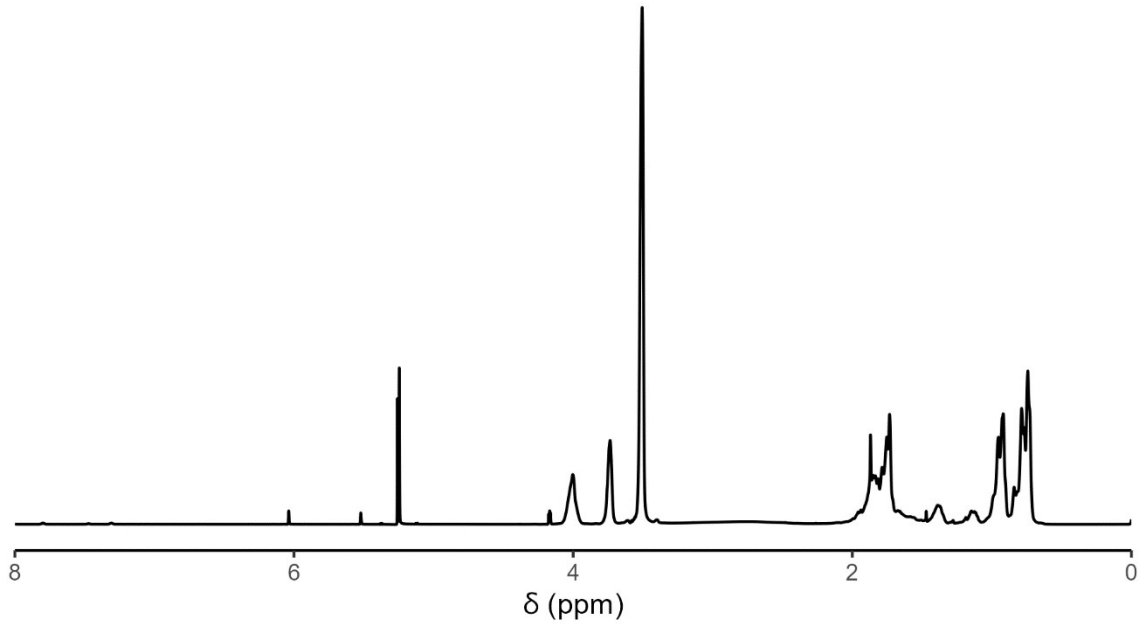


Figure S8: $^{1}H$ NMR spectrum of macroCTA-*43* in $CD_2Cl_2$.

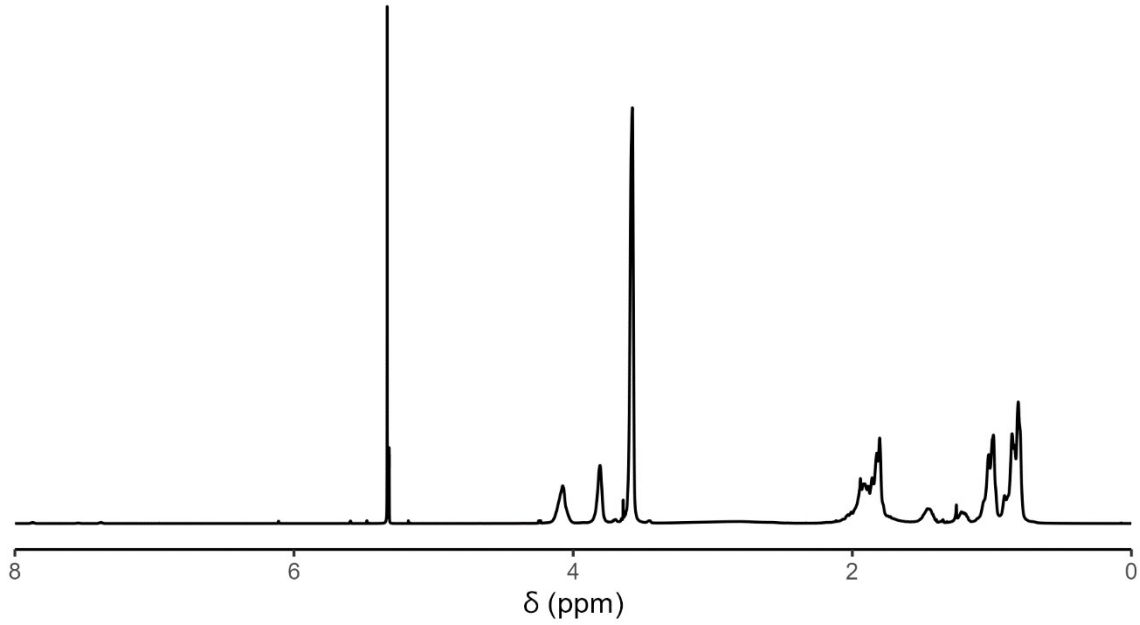


Figure S9: $^{1}H$ NMR spectrum of macroCTA-*38* in $CD_2Cl_2$.

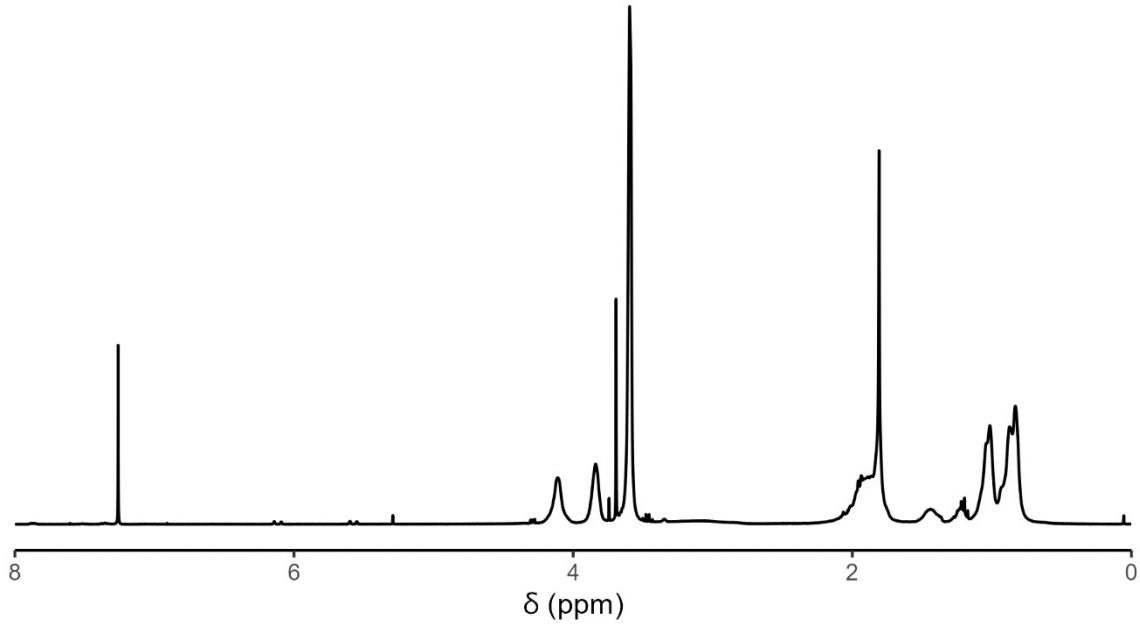


Figure S10: $^{1}H$ NMR spectrum of macroCTA-*34* in $CDCl_3$.

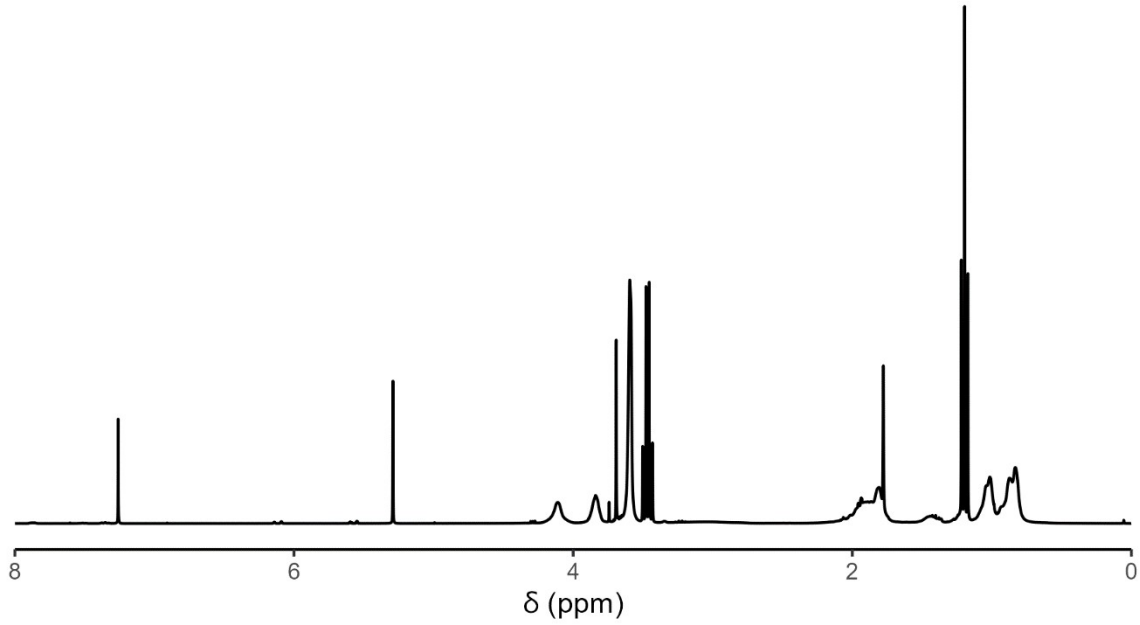


Figure S11: $^{1}H$ NMR spectrum of macroCTA-*19* in $CDCl_3$.

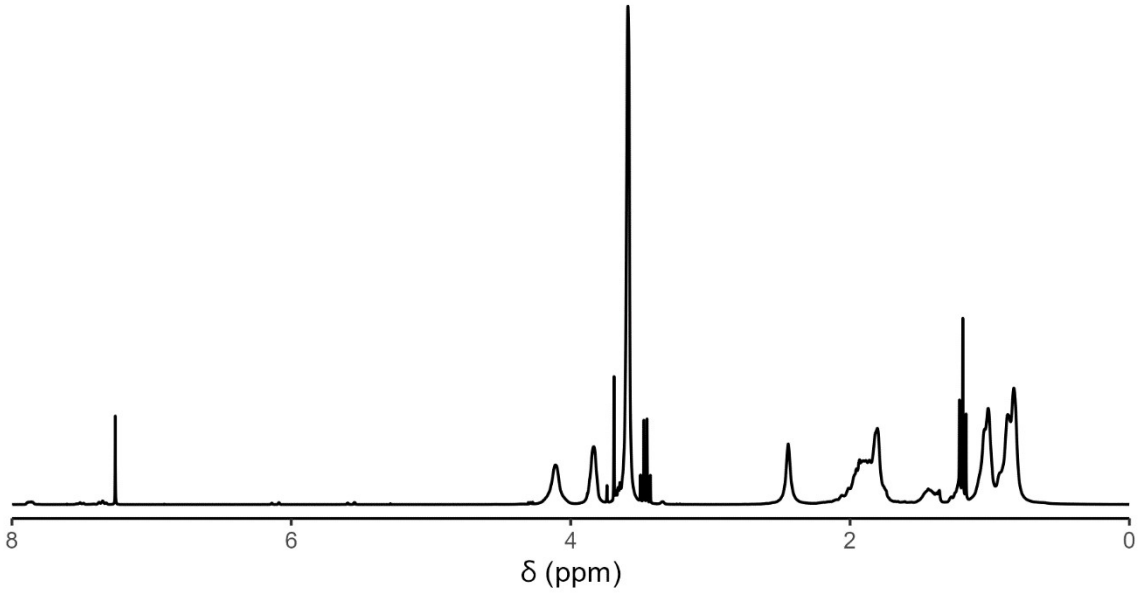


Figure S12: $^{1}H$ NMR spectrum of macroCTA-*9* in $CDCl_3$.

GPC chromatograms of P(MMA-*stat*-HEMA) macroCTAs

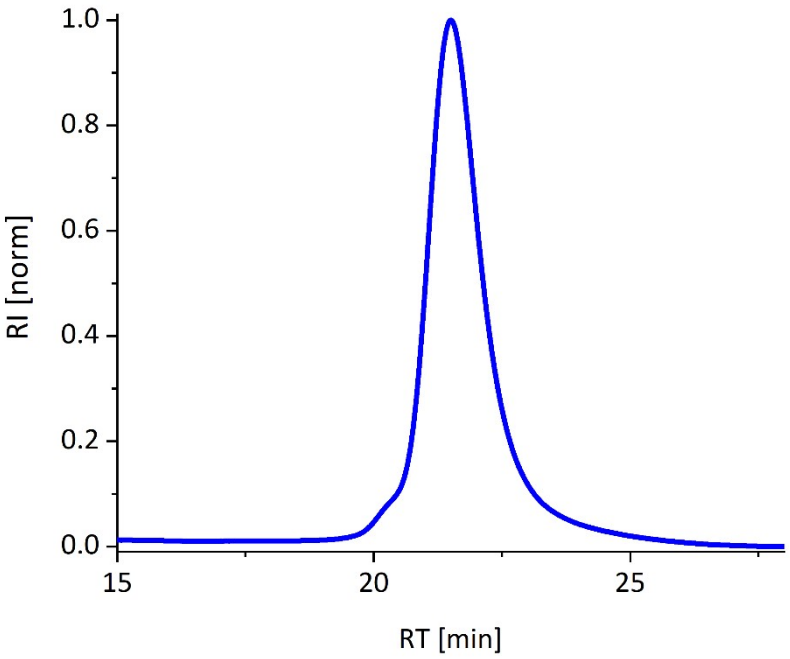


Figure S13: GPC chromatogram (RI detector) of macroCTA-*22*.

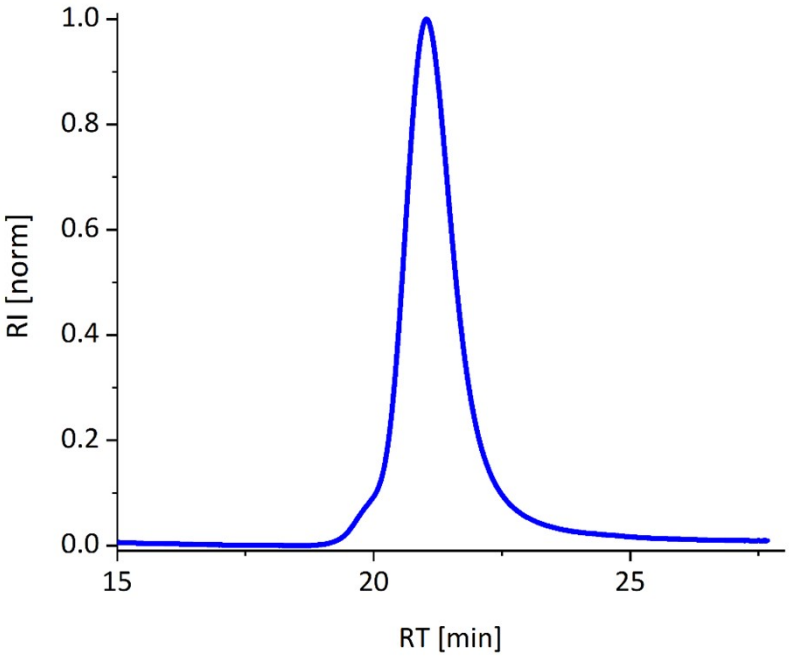


Figure S14: GPC chromatogram (RI detector) of macroCTA-*29*.

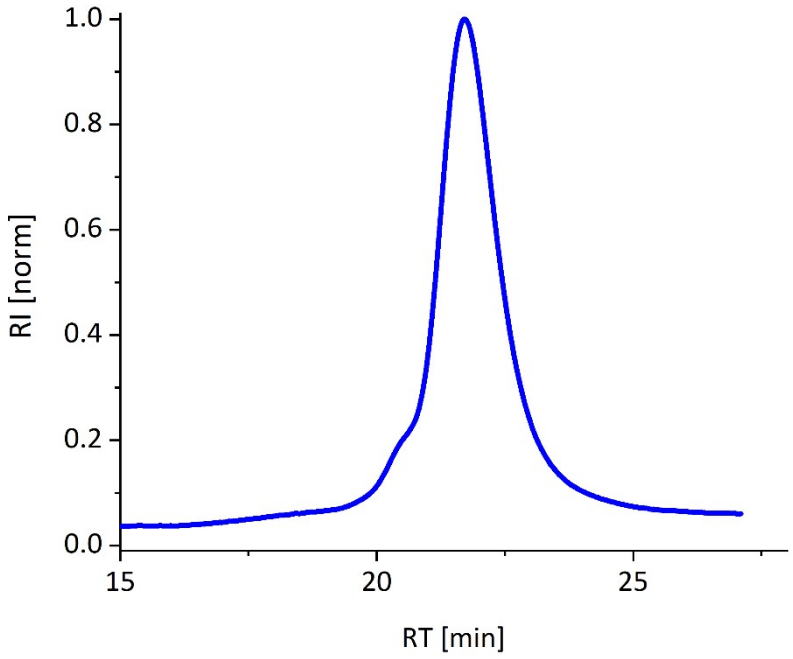


Figure S15: GPC chromatogram (RI detector) of macroCTA-*21*.

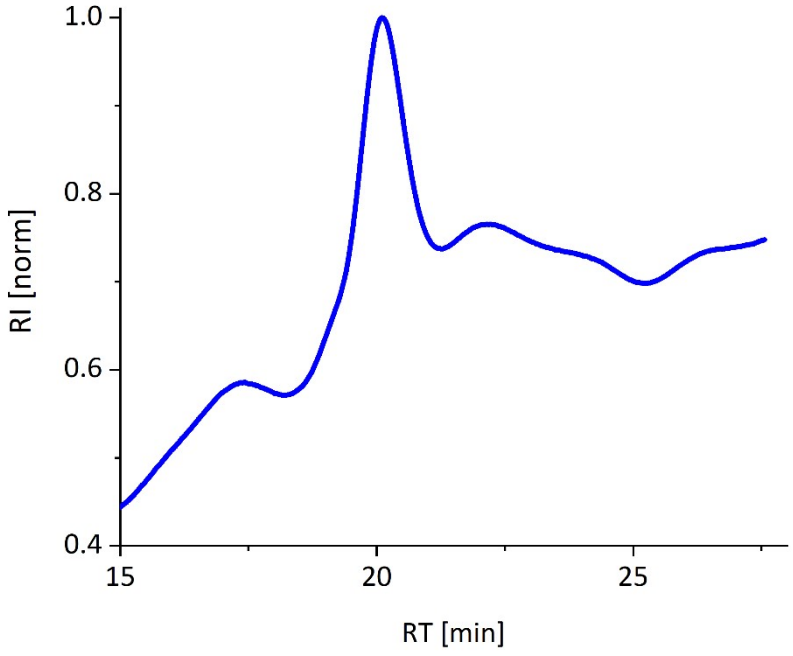


Figure S16: GPC chromatogram (RI detector) of macroCTA-*54*.

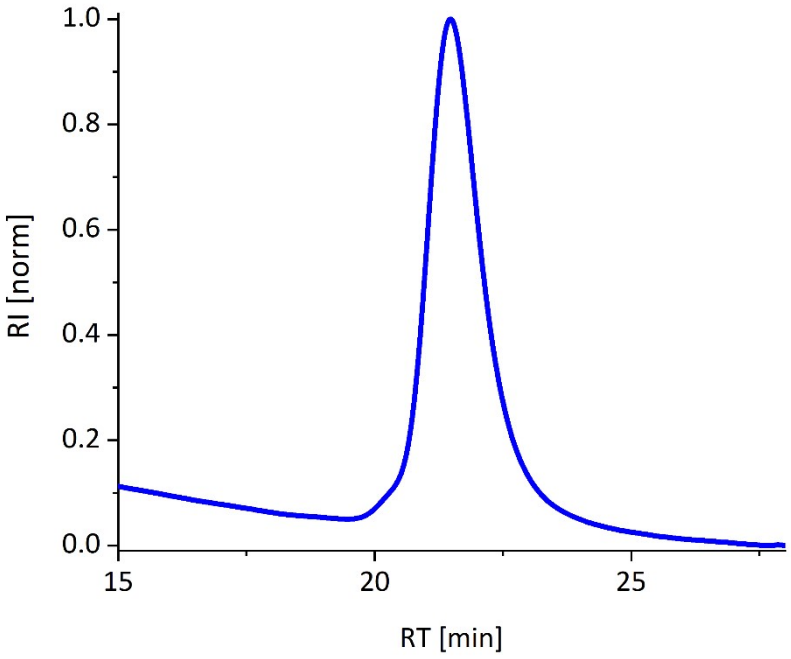


Figure S17: GPC chromatogram (RI detector) of macroCTA-*23*.

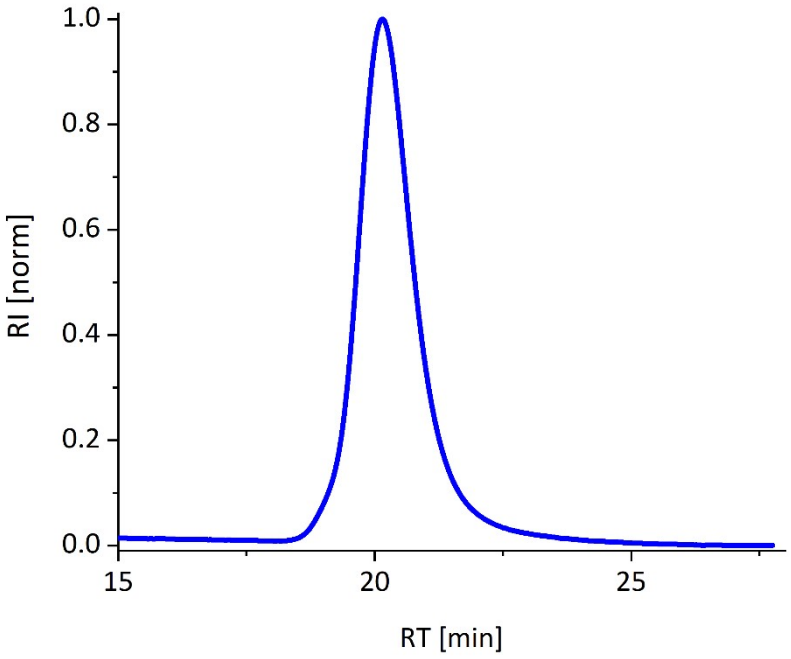


Figure S18: GPC chromatogram (RI detector) of macroCTA-*48*.

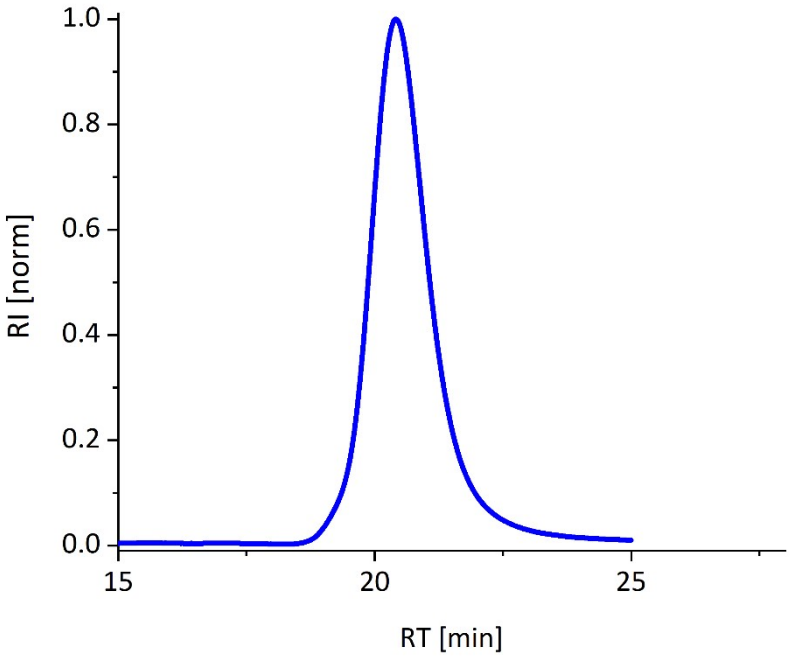


Figure S19: GPC chromatogram (RI detector) of macroCTA-*39*.

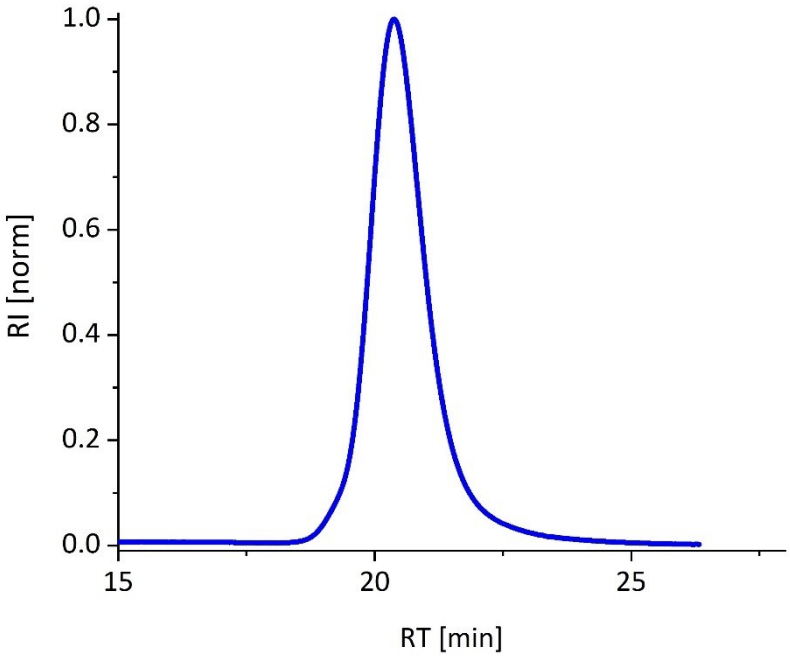


Figure S20: GPC chromatogram (RI detector) of macroCTA-*43*.

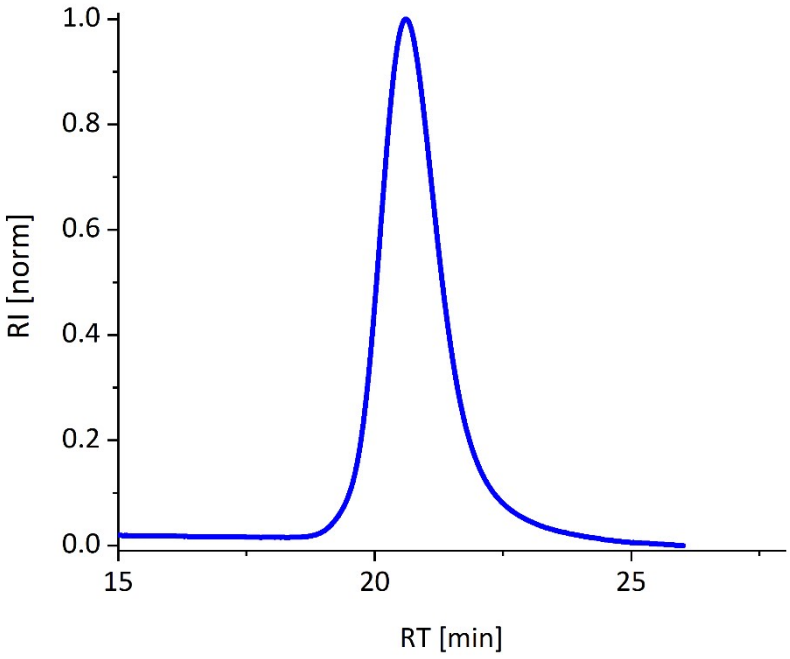


Figure S21: GPC chromatogram (RI detector) of macroCTA-*38*.

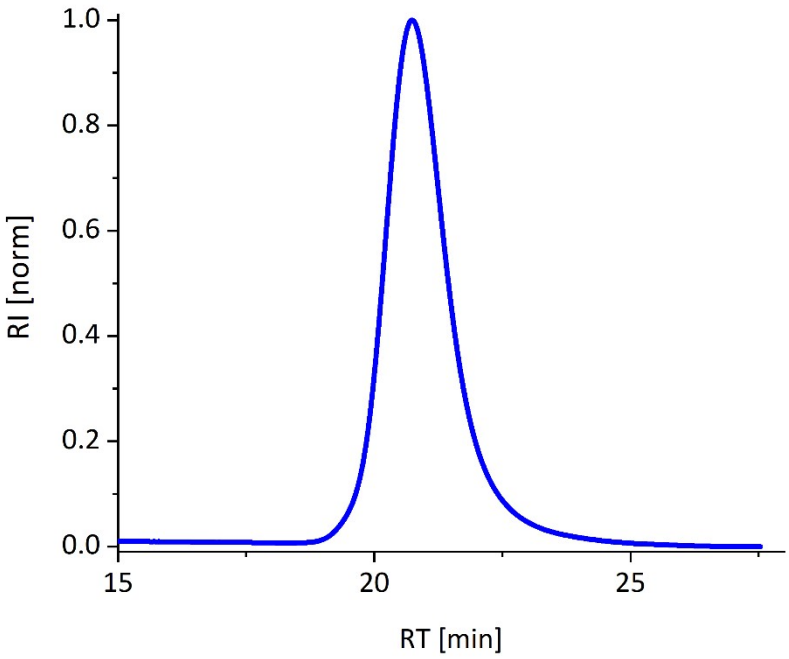


Figure S22: GPC chromatogram (RI detector) of macroCTA-*34*.

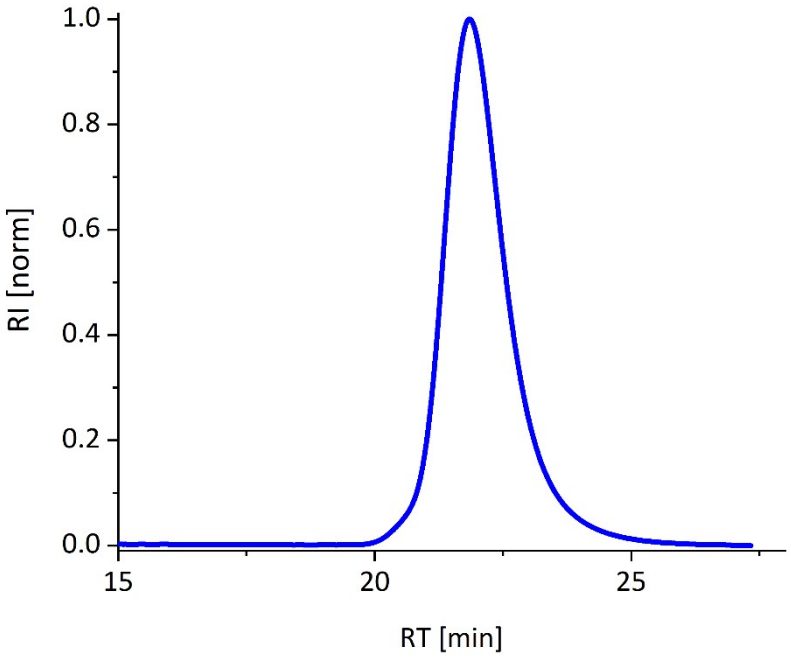


Figure S23: GPC chromatogram (RI detector) of macroCTA-*19*.

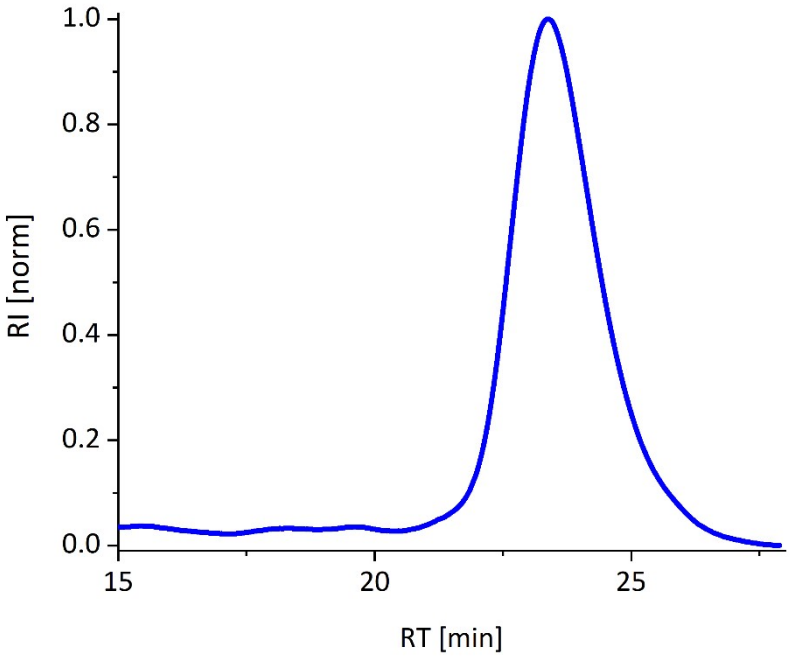


Figure S24: GPC chromatogram (RI detector) of macroCTA-*9*.

### *1.2* PS-*b*-P(MMA-*stat*-HEMA) BCPs

Exemplary synthesis of PS-*b*-P(MMA-*stat*-HEMA) BCPs

In a Schlenk tube, 560 mg (MW = 37641, 0.0149 mmol, 1 eq.) of macroCTA-*38* were dissolved in 18 mL 1,4-dioxane. Styrene (18.3 g, 176 mmol, 11000 eq.) and AIBN stock solution (79 mg, 0.0032 mmol, 7.5 mg in 1.125 g 1,4-dioxane, 0.2 eq.) were added. The solution was degassed via freeze-pump-thaw (3 x 8 min), followed by backfilling with nitrogen. The reaction mixture was stirred at 90 °C for 2 h, cooled in liquid nitrogen and opened to the atmosphere. The solvent and most of the remaining styrene were removed in vacuo, the viscous mixture was dissolved in small amounts of DCM and precipitated into diethyl ether twice. After centrifugation and decanting of the supernatant, $S_{0.53}$-$MH_{0.47}$-*94* was received as a light pink solid.

$^1$H NMR 600 MHz ($CD_2Cl_2$): $\delta$ [ppm] = 7.80 (m), 7.47 (m), 7.31 (m), 7.28 - 6.31 (m), 4.07 (bs), 3.80 (bs), 3.56 (s), 2.14 - 0.63 (m).

Table S2: Table detailing the reaction conditions and analytical data of the BCPs.

| Polymer | MacroCTA | Styrene:MacroCTA:AIBN | T [min] | $M_n$(GPC) | Đ | Funct. polymer |
|---|---|---|---|---|---|---|
| $S_{0.75}$-$MH_{0.25}$-*66* | macroCTA-*21* | 5000:1:0.2 | 120 | 65769 | 1.20 | $S_{0.75}$-$MH^*_{0.25}$-*66* |
| $S_{0.68}$-$MH_{0.32}$-*33* | macroCTA-*9* | 5000:1:0.2 | 80 | 32524 | 1.06 | $S_{0.68}$-$MH^*_{0.32}$-*33* |
| $S_{0.66}$-$MH_{0.34}$-*70* | macroCTA-*23* | 8000:1:0.2 | 120 | 69535 | 1.10 | $S_{0.66}$-$MH^*_{0.34}$-*70* |
| $S_{0.56}$-$MH_{0.44}$-*52* | macroCTA-*19* | 10000:1:0.2 | 60 | 52082 | 1.07 | $S_{0.56}$-$MH^*_{0.44}$-*52* |
| $S_{0.54}$-$MH_{0.46}$-*45* | macroCTA-*22* | 3720:1:0.2 | 60 | 45272 | 1.18 | - |
| $S_{0.53}$-$MH_{0.47}$-*94* | macroCTA-*38* | 11000:1:0.2 | 120 | 93566 | 1.10 | $S_{0.53}$-$MH^*_{0.47}$-*94* |
| $S_{0.52}$-$MH_{0.48}$-*67* | macroCTA-*22* | 7000:1:0.2 | 120 | 66991 | 1.10 | $S_{0.52}$-$MH^*_{0.48}$-*67* |
| $S_{0.50}$-$MH_{0.50}$-*91* | macroCTA-*48* | 6150:1:0.2 | 90 | 91421 | 1.14 | $S_{0.50}$-$MH^*_{0.50}$-*91* |
| $S_{0.50}$-$MH_{0.50}$-*45* | macroCTA-*19* | 6150:1:0.2 | 60 | 45136 | | $S_{0.50}$-$MH^*_{0.50}$-*45* |
| $S_{0.49}$-$MH_{0.51}$-*92* | macroCTA-*54* | 6150:1:0.2 | 100 | 56600 | 1.39 | |
| $S_{0.46}$-$MH_{0.54}$-*81* | macroCTA-*39* | 6150:1:0.2 | 90 | 81005 | 1.14 | $S_{0.46}$-$MH^*_{0.54}$-*81* |
| $S_{0.45}$-$MH_{0.55}$-*42* | macroCTA- | 3720:1:0.2 | 40 | 42064 | 1.11 | $S_{0.45}$-$MH^{50\%*}_{0.55}$-*42* |

| | | | | | | |
|---|---|---|---|---|---|---|
| | *23* | | | | | |
| $S_{0.42}$-$MH_{0.58}$-*89* | macroCTA-*39* | 6150:1:0.2 | 90 | 89172 | 1.16 | $S_{0.42}$-$MH^*_{0.58}$-*89* |
| $S_{0.42}$-$MH_{0.58}$-*57* | macroCTA-*34* | 10000:1:0.2 | 120 | 56861 | 1.11 | $S_{0.42}$-$MH^*_{0.58}$-*57* |
| $S_{0.39}$-$MH_{0.61}$-*35* | macroCTA-*19* | 3720:1:0.2 | 40 | 35156 | 1.09 | - |
| $S_{0.37}$-$MH_{0.63}$-*65* | macroCTA-*38* | 6150:1:0.2 | 90 | 65036 | 1.09 | $S_{0.37}$-$MH^*_{0.63}$-*65* |
| $S_{0.31}$-$MH_{0.69}$-*48* | macroCTA-*34* | 5000:1:0.2 | 90 | 47659 | 1.09 | $S_{0.31}$-$MH^*_{0.69}$-*48* |
| $S_{0.28}$-$MH_{0.72}$-*67* | macroCTA-*43* | 3720:1:0.2 | 90 | 67188 | 1.13 | $S_{0.28}$-$MH^*_{0.72}$-*67* |
| $S_{0.28}$-$MH_{0.72}$-*29* | macroCTA-*19* | 2000:1:0.2 | 40 | 29291 | 1.09 | $S_{0.28}$-$MH^*_{0.72}$-*29* |
| $S_{0.27}$-$MH_{0.73}$-*70* | macroCTA-*43* | 3720:1:0.2 | 60 | 70191 | 1.13 | $S_{0.27}$-$MH^*_{0.73}$-*70* |
| $S_{0.16}$-$MH_{0.84}$-*45* | macroCTA-*34* | 13200:1:0.2 | 120 | 45079 | 1.23 | - |
| $S_{0.16}$-$MH_{0.84}$-*43* | macroCTA-*34* | 3500:1:0.2 | 30 | 42621 | 1.13 | $S_{0.16}$-$MH^*_{0.84}$-*43* |
| $S_{0.12}$-$MH_{0.88}$-*40* | macroCTA-*34* | 2400:1:0.2 | 28 | 39858 | 1.13 | - |
| $S_{0.09}$-$MH_{0.91}$-*39* | macroCTA-*34* | 2500:1:0.2 | 23 | 38743 | 1.13 | - |

NMR spectra of PS-*b*-P(MMA-*stat*-HEMA) BCPs

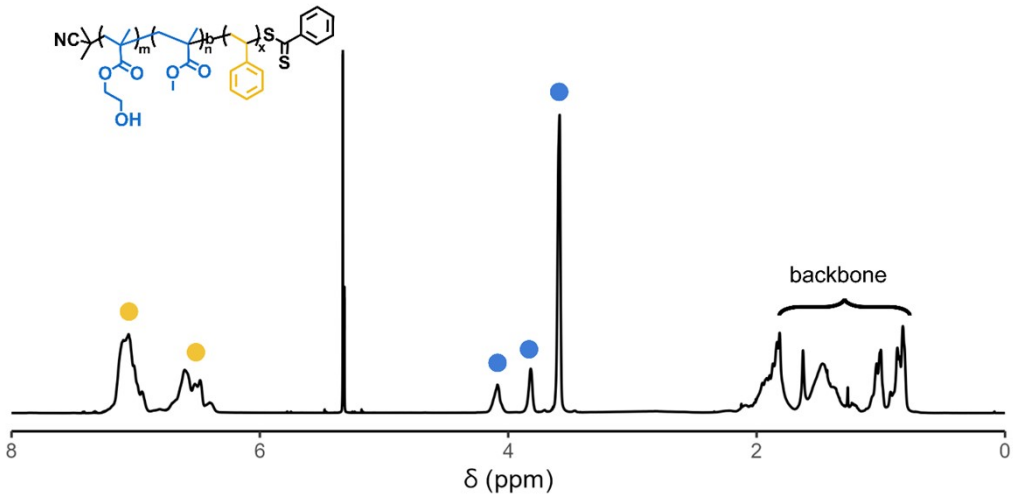


Figure S25: $^{1}$H NMR spectrum of $S_{0.53}$-$MH_{0.47}$-*94* in $CDCl_3$ with peak assignment.

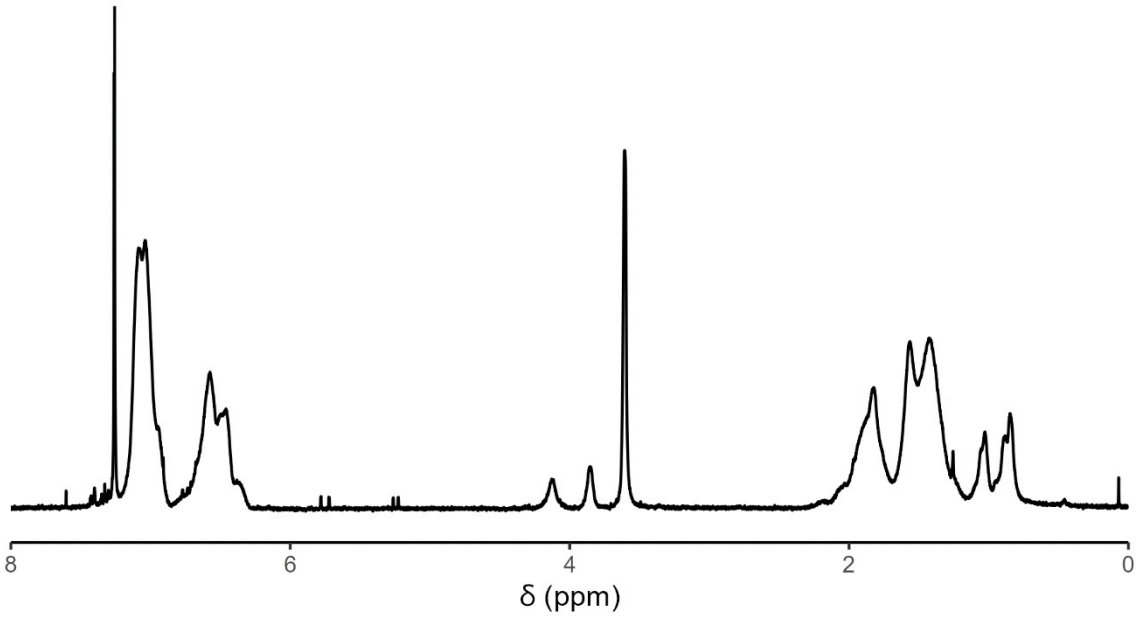


Figure S26: $^{1}$H NMR spectrum of $S_{0.75}$-$MH_{0.25}$-*66* in $CDCl_3$.

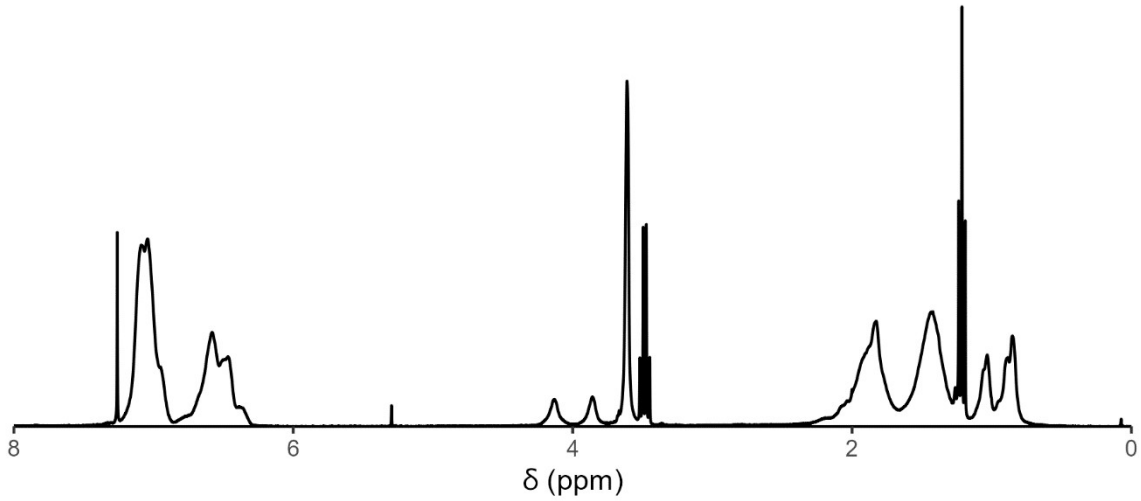


Figure S27: $^{1}$H NMR spectrum of $S_{0.68}$-$MH_{0.32}$-*33* in $CDCl_3$.

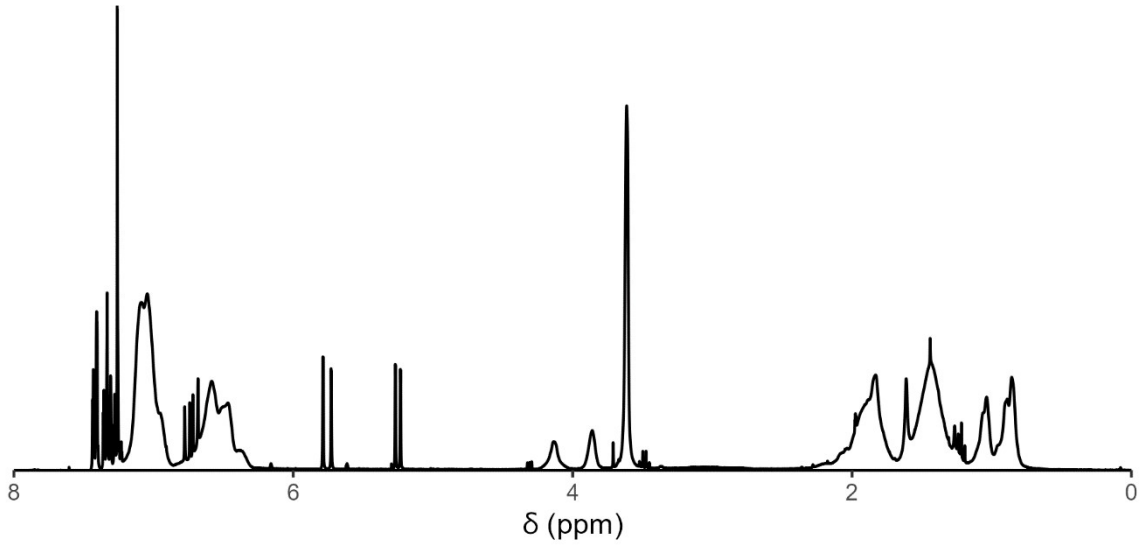


Figure S28: $^{1}$H NMR spectrum of $S_{0.66}$-$MH_{0.34}$-*70* in $CDCl_3$.

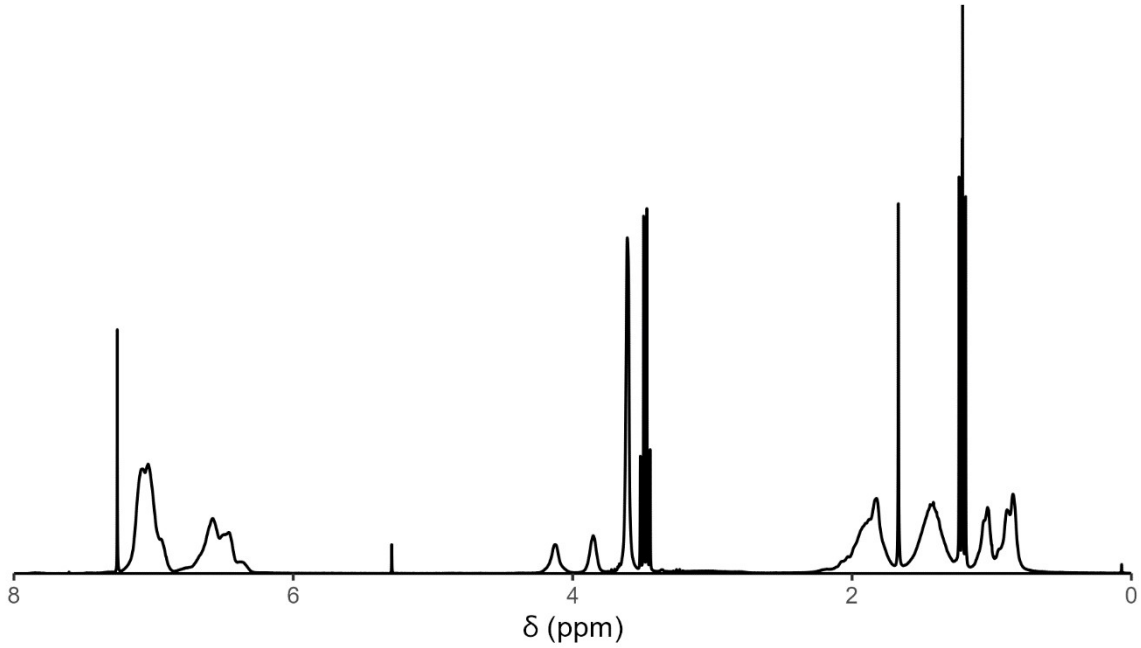


Figure S29: $^{1}$H NMR spectrum of $S_{0.56}$-$MH_{0.44}$-*52* in $CDCl_3$.

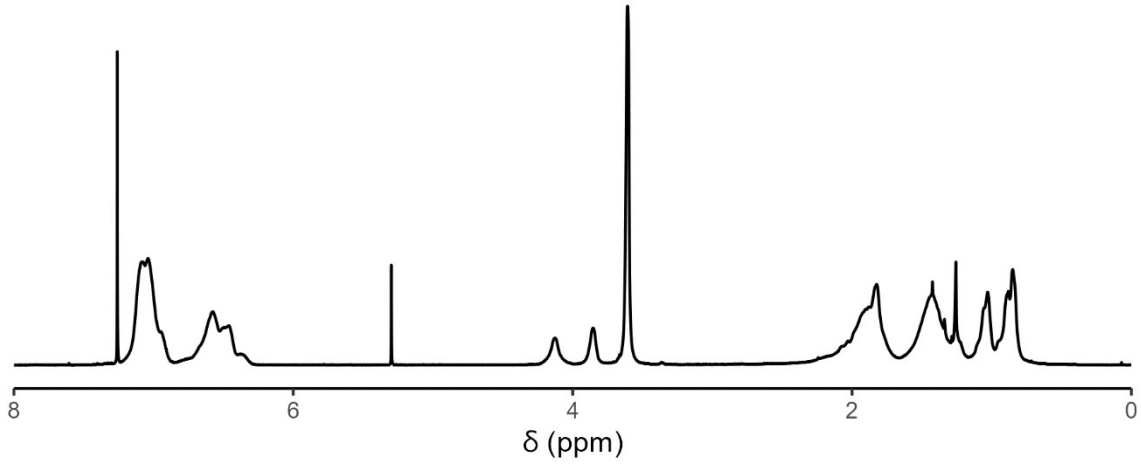


Figure S30: $^{1}$H NMR spectrum of $S_{0.54}$-$MH_{0.46}$-*45* in $CDCl_3$.

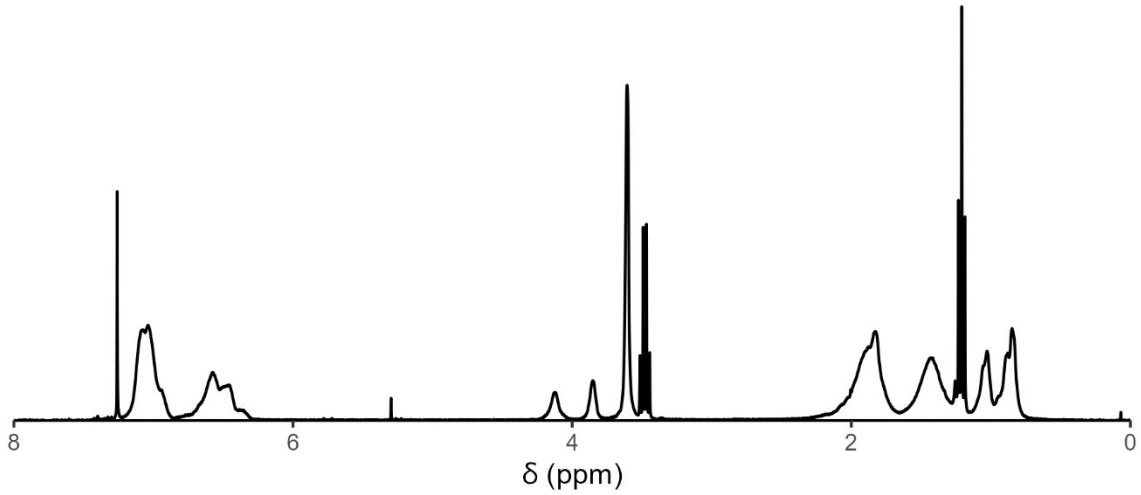


Figure S31: $^{1}$H NMR spectrum of $S_{0.52}$-$MH_{0.48}$-*67* in $CDCl_3$.

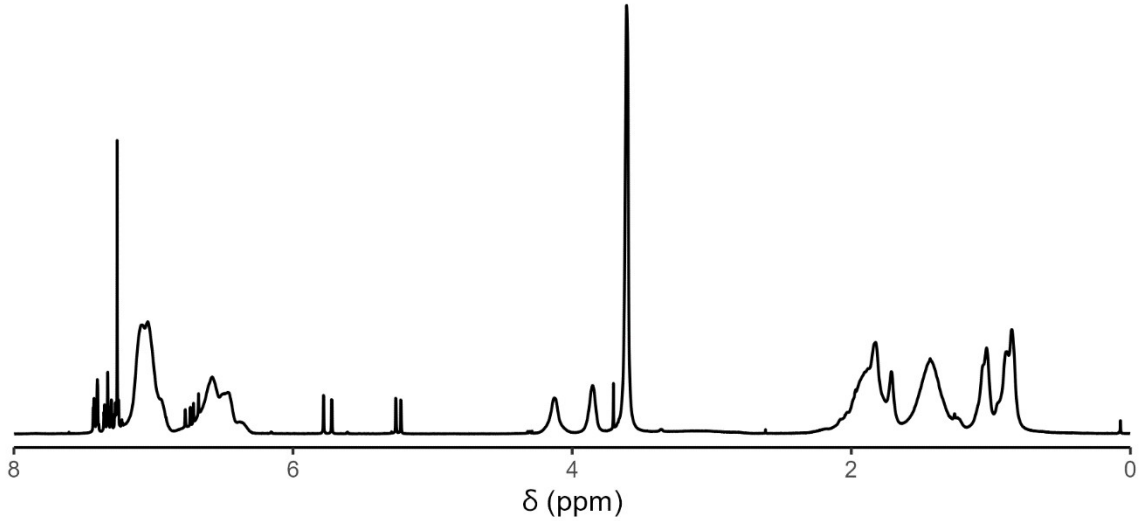


Figure S32: $^{1}$H NMR spectrum of $S_{0.50}$-$MH_{0.50}$-*91* in $CDCl_3$.

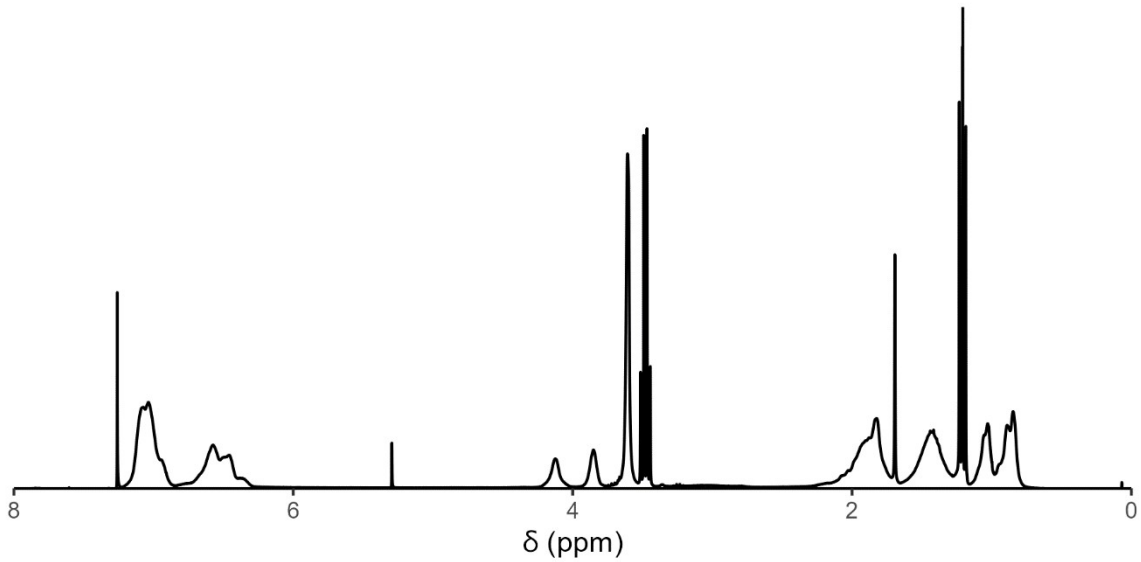


Figure S33: $^{1}$H NMR spectrum of $S_{0.50}$-$MH_{0.50}$-*45* in $CDCl_3$.

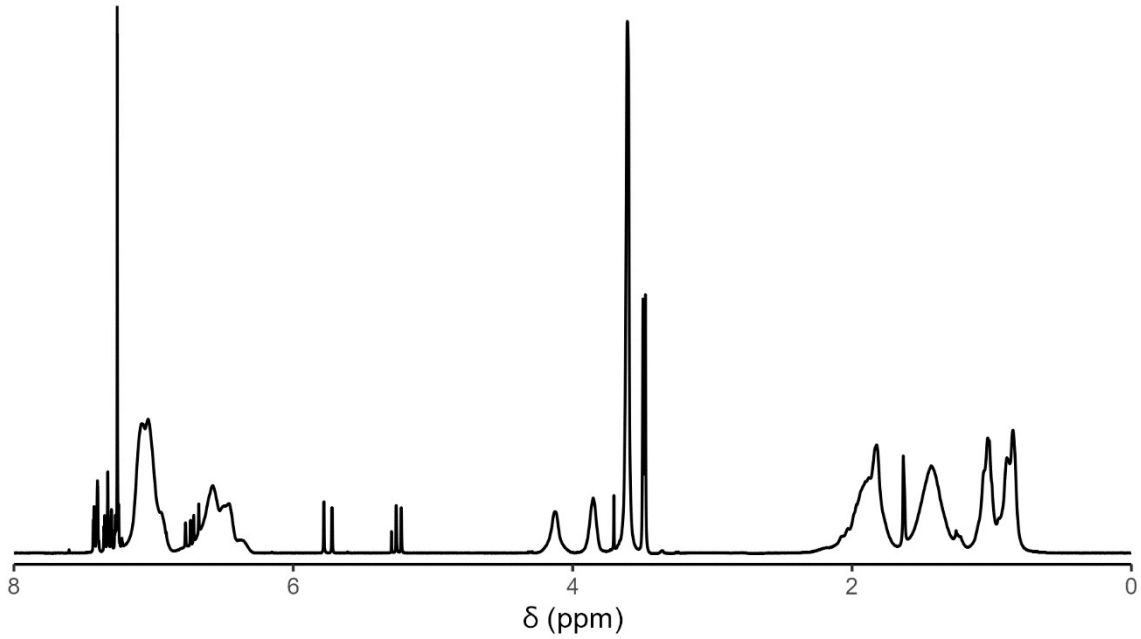


Figure S34: $^{1}$H NMR spectrum of $S_{0.49}$-$MH_{0.51}$-*92* in $CDCl_3$.

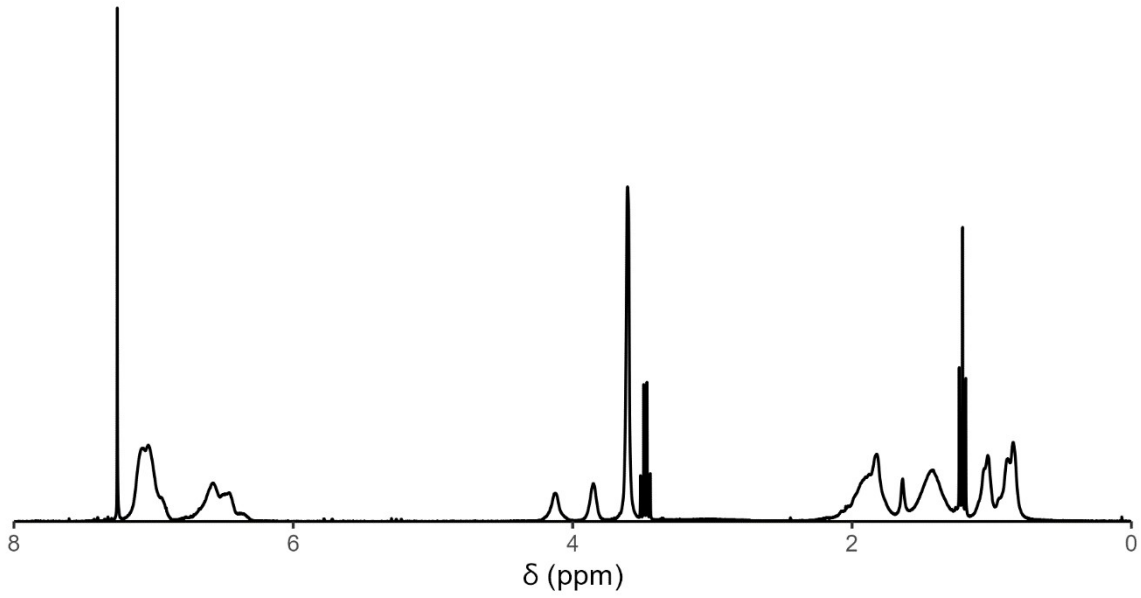


Figure S35: $^{1}$H NMR spectrum of $S_{0.46}$-$MH_{0.54}$-*81* in $CDCl_3$.

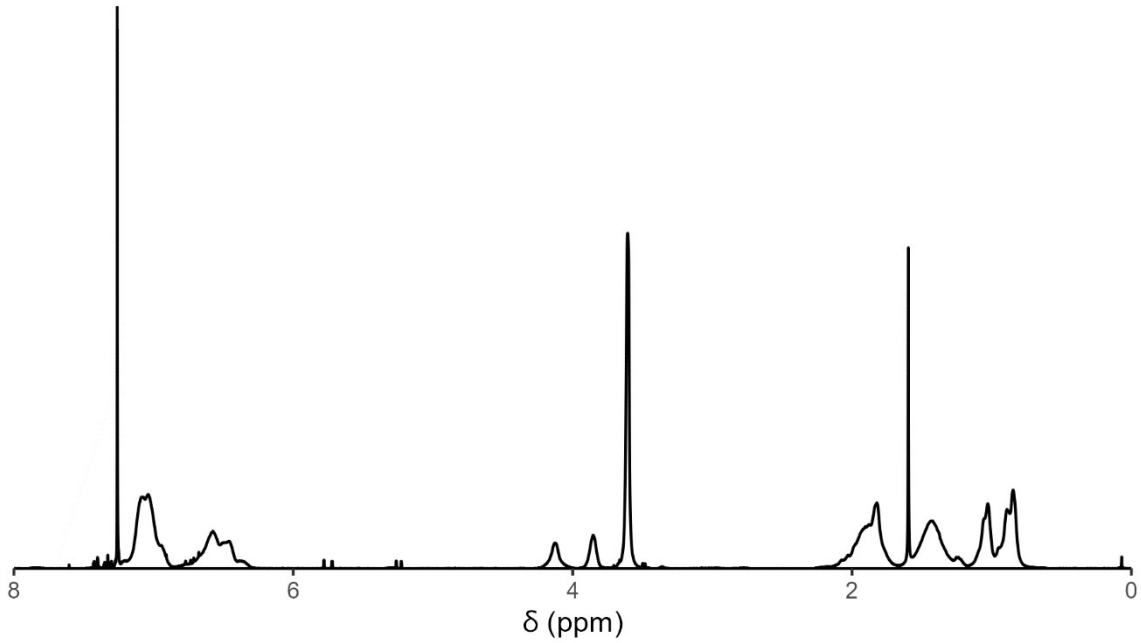


Figure S36: $^{1}$H NMR spectrum of $S_{0.45}$-$MH_{0.55}$-*42* in $CDCl_3$.

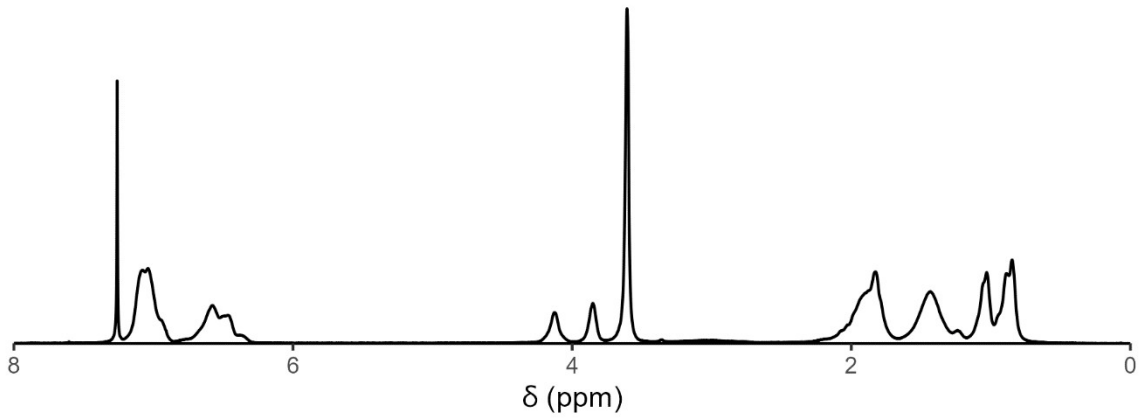


Figure S37: $^{1}$H NMR spectrum of $S_{0.42}$-$MH_{0.58}$-*89* in $CDCl_3$.

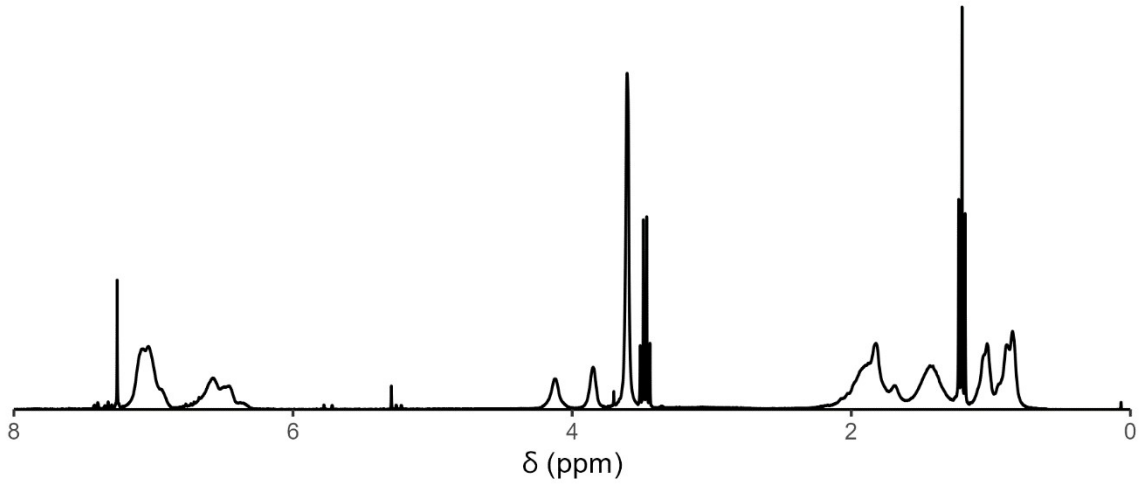


Figure S38: $^{1}$H NMR spectrum of $S_{0.42}$-$MH_{0.58}$-*57* in $CDCl_3$.

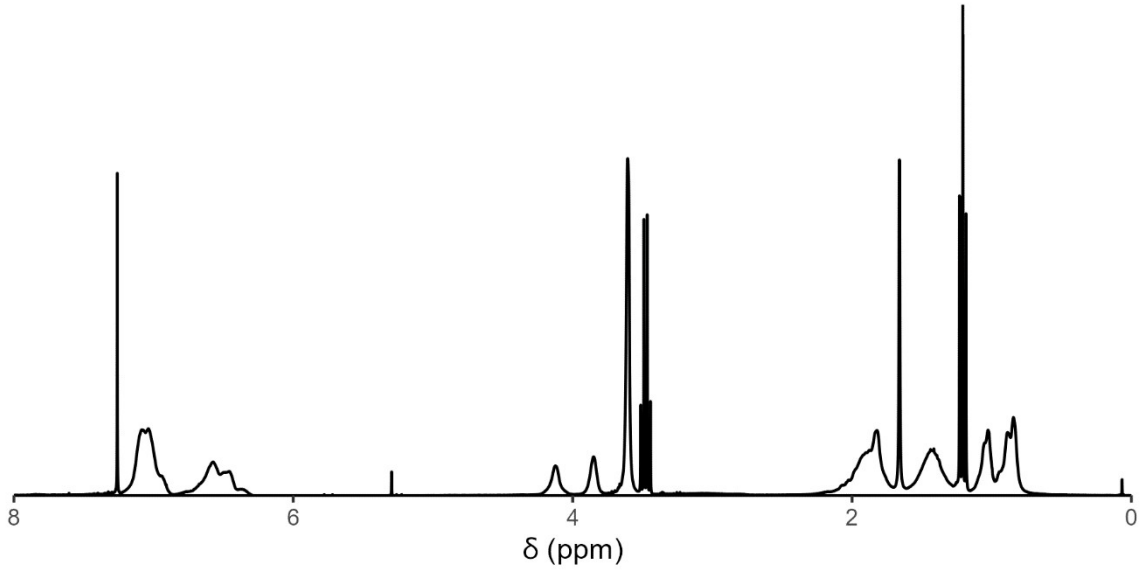


Figure S39: $^1$H NMR spectrum of $S_{0.39}$-$MH_{0.61}$-*35* in $CDCl_3$.

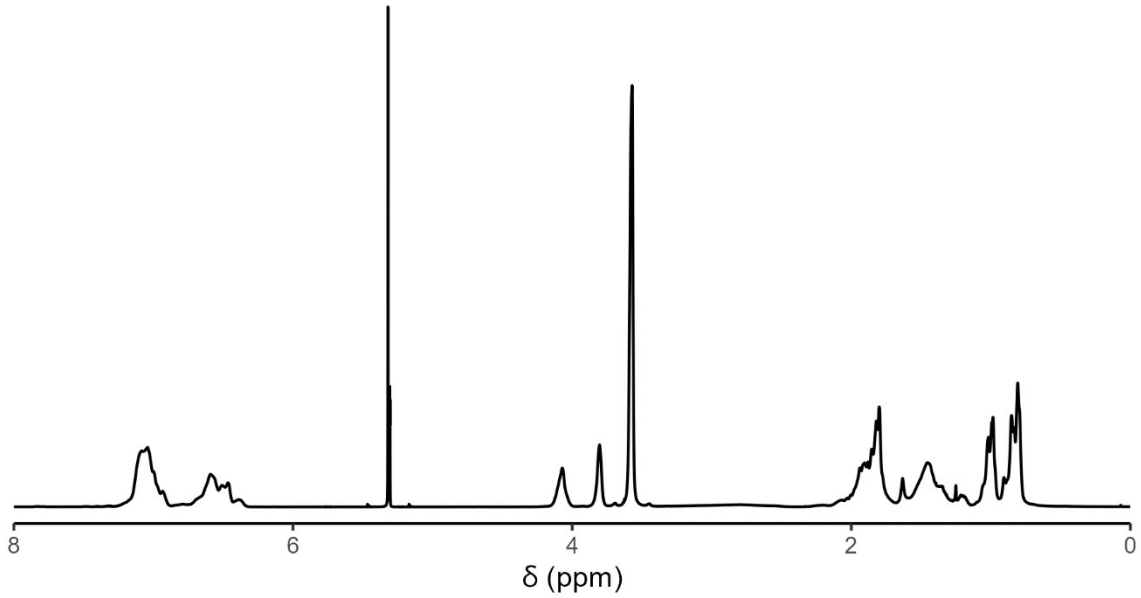


Figure S40: $^1$H NMR spectrum of $S_{0.37}$-$MH_{0.63}$-*65* in $CDCl_3$.

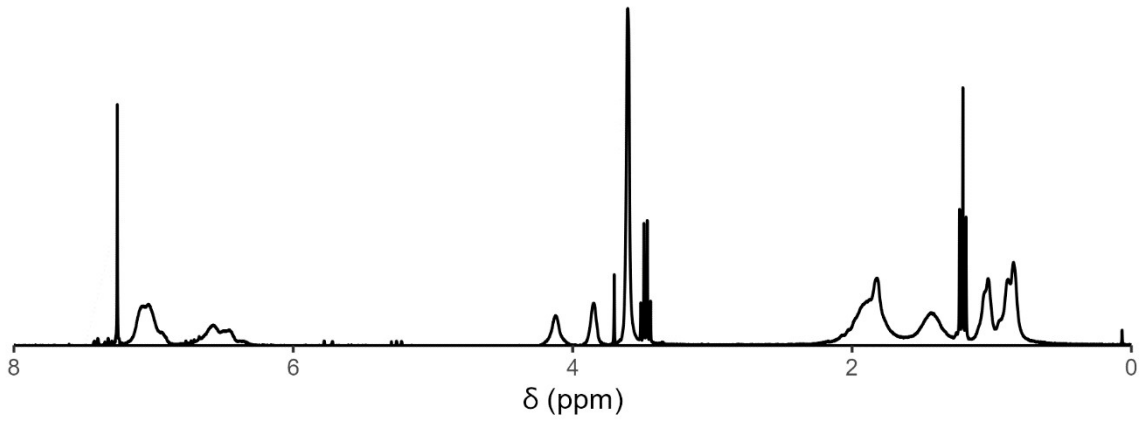


Figure S41: $^1$H NMR spectrum of $S_{0.31}$-$MH_{0.69}$-*48* in $CDCl_3$.

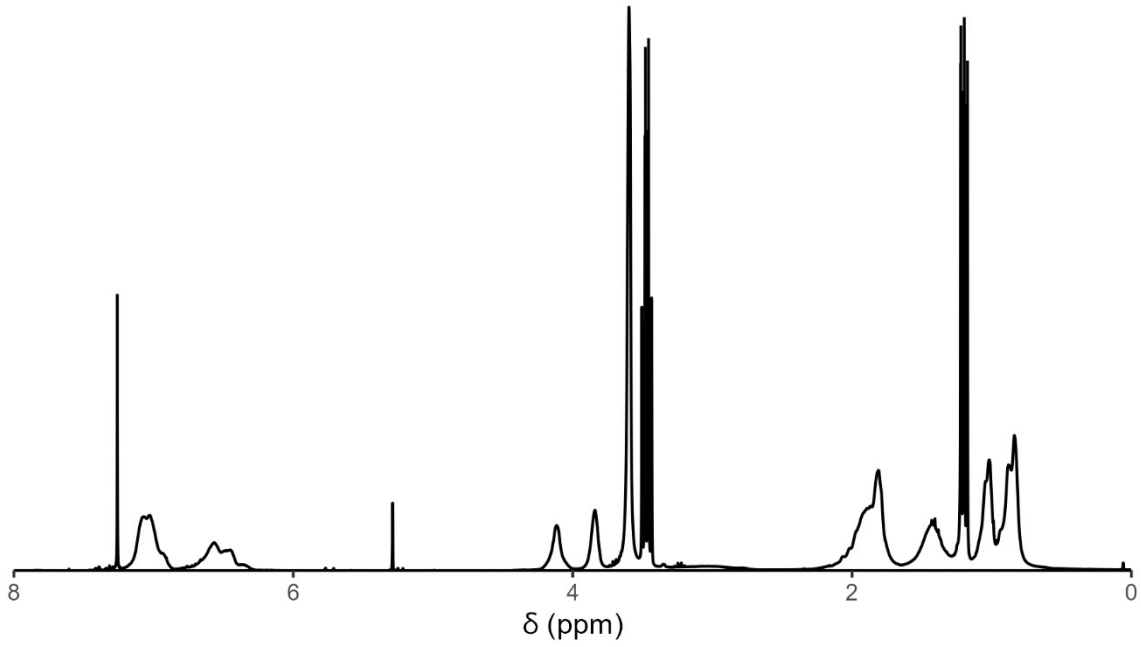


Figure S42: $^{1}$H NMR spectrum of $S_{0.28}$-$MH_{0.72}$-*67* in $CDCl_3$.

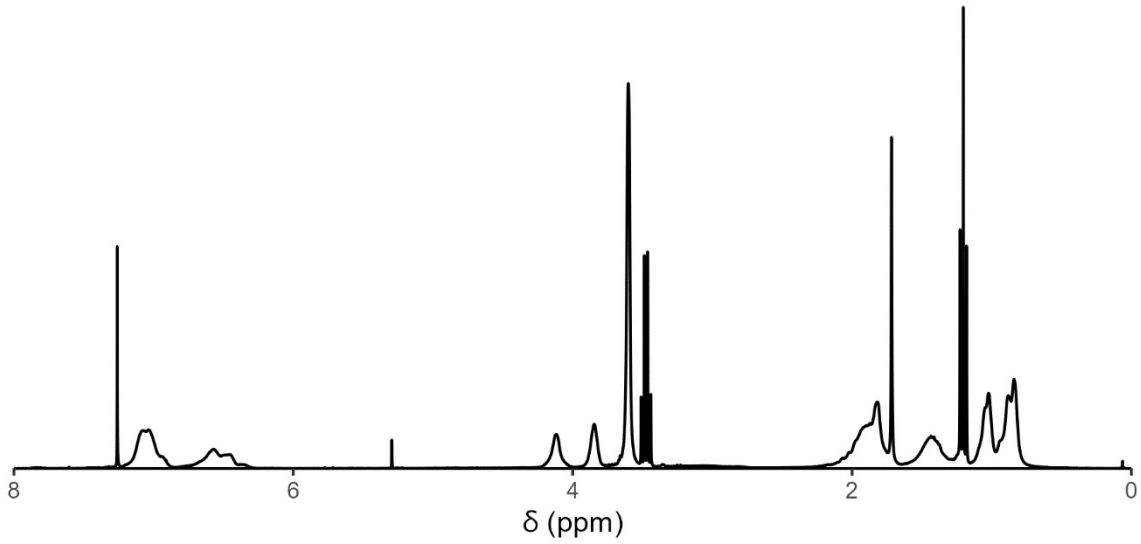


Figure S43: $^{1}$H NMR spectrum of $S_{0.28}$-$MH_{0.72}$-*29* in $CDCl_3$.

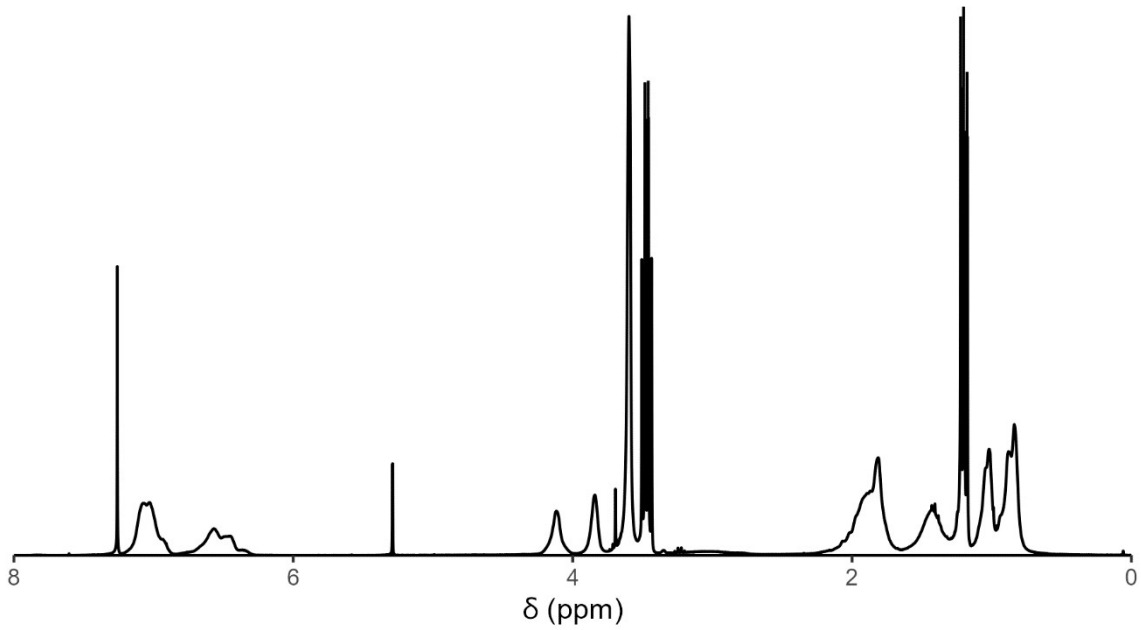


Figure S44: $^{1}$H NMR spectrum of $S_{0.27}$-$MH_{0.73}$-*70* in $CDCl_3$.

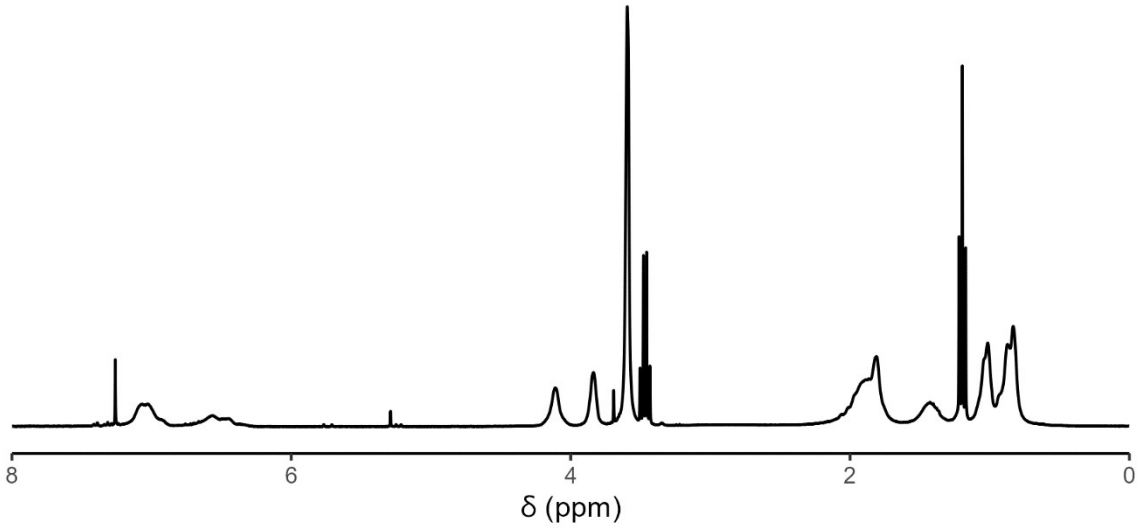


Figur

e S45: $^{1}$H NMR spectrum of $S_{0.16}$-$MH_{0.84}$-*45* in CDCl3.

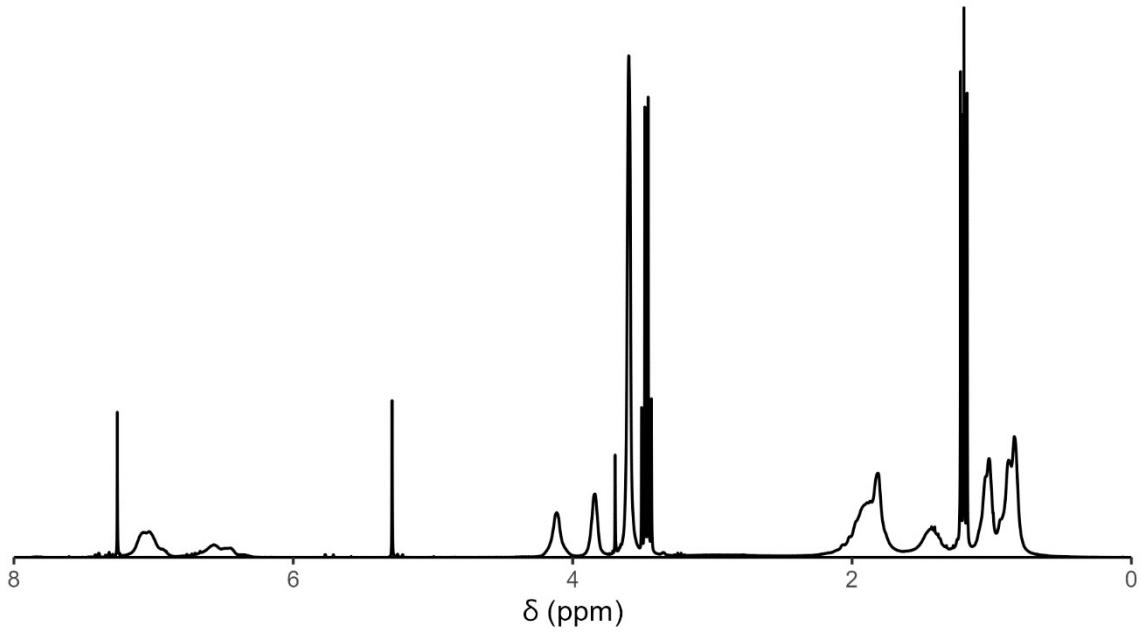


Figure S46: $^{1}$H NMR spectrum of $S_{0.16}$-$MH_{0.84}$-*43* in $CDCl_3$.

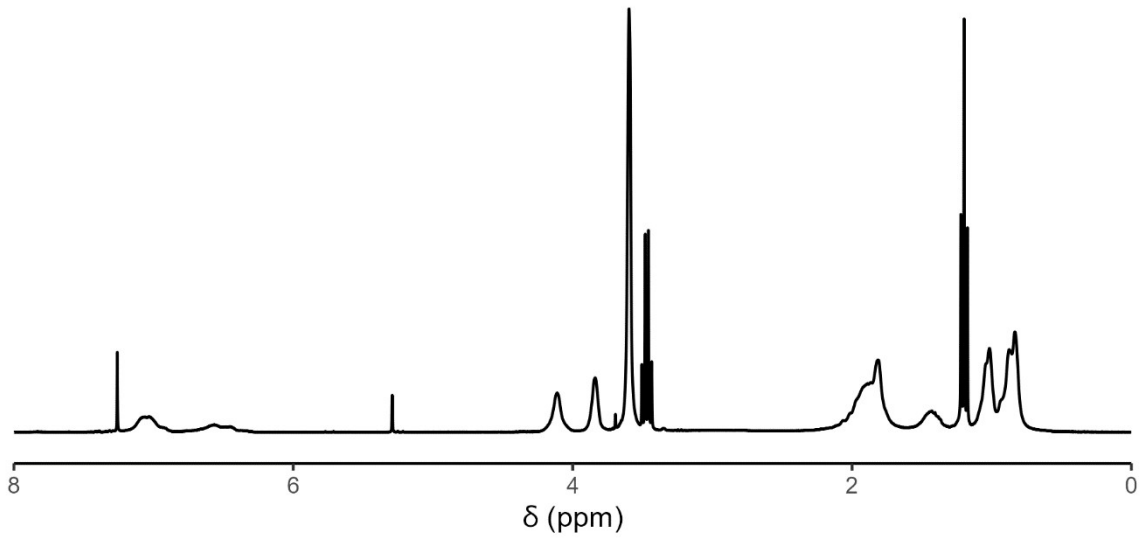


Figure S47: 1H NMR spectrum of $S_{0.12}$-$MH_{0.88}$-*40* in CDCl3.

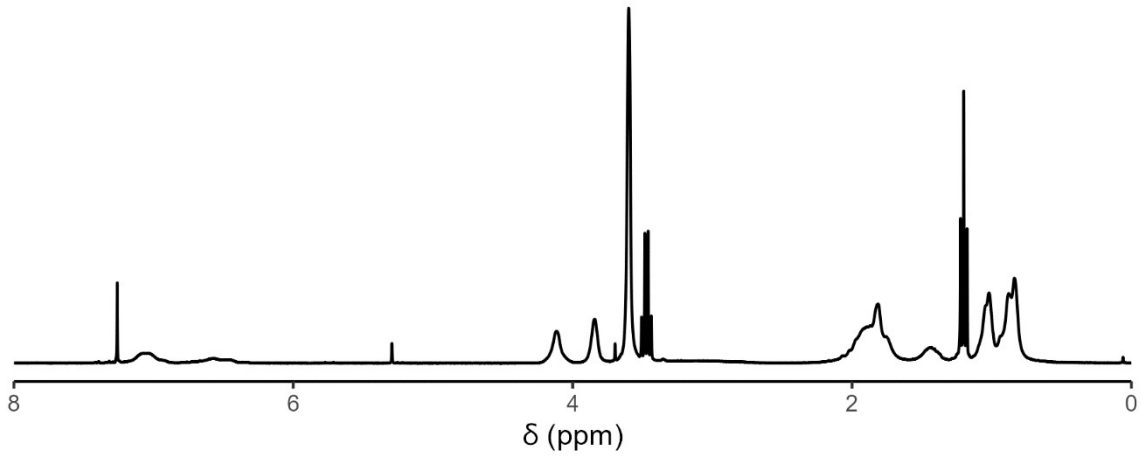


Figure S48: $^{1}$H NMR spectrum of $S_{0.09}$-$MH_{0.91}$-*39* in $CDCl_3$.

GPC chromatograms of PS-*b*-P(MMA-*stat*-HEMA) BCPs

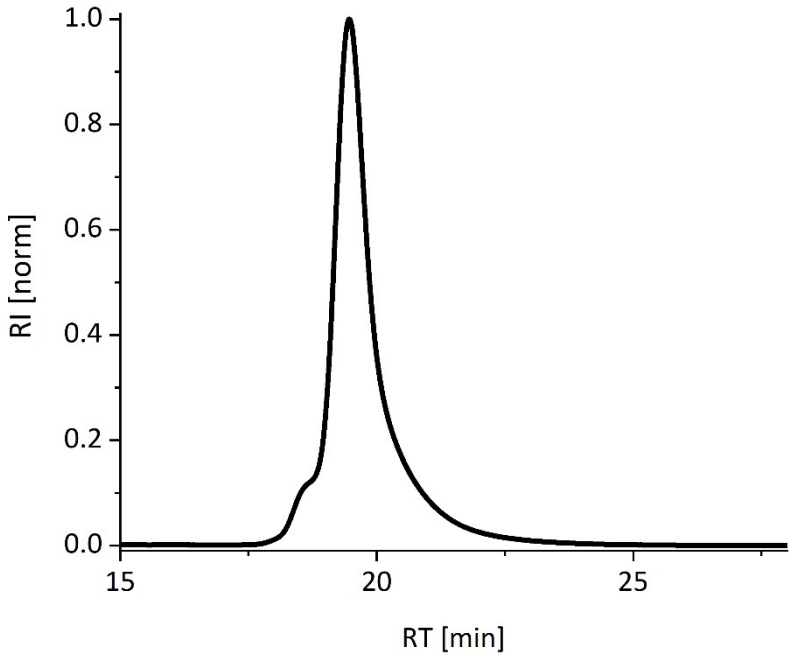


Figure S49: GPC chromatogram (RI detector) of $S_{0.75}$-$MH_{0.25}$-*66*.

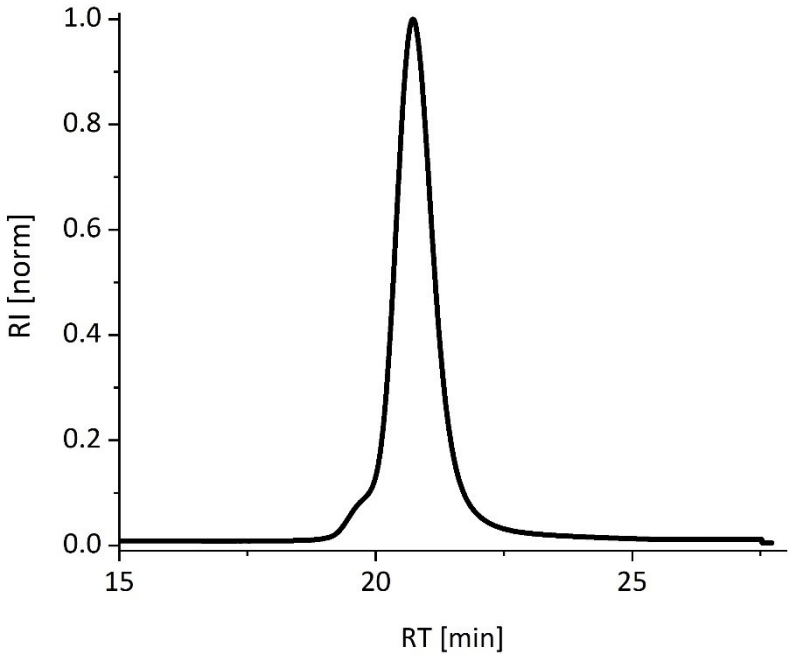


Figure S50: GPC chromatogram (RI detector) of $S_{0.68}$-$MH_{0.32}$-*33*.

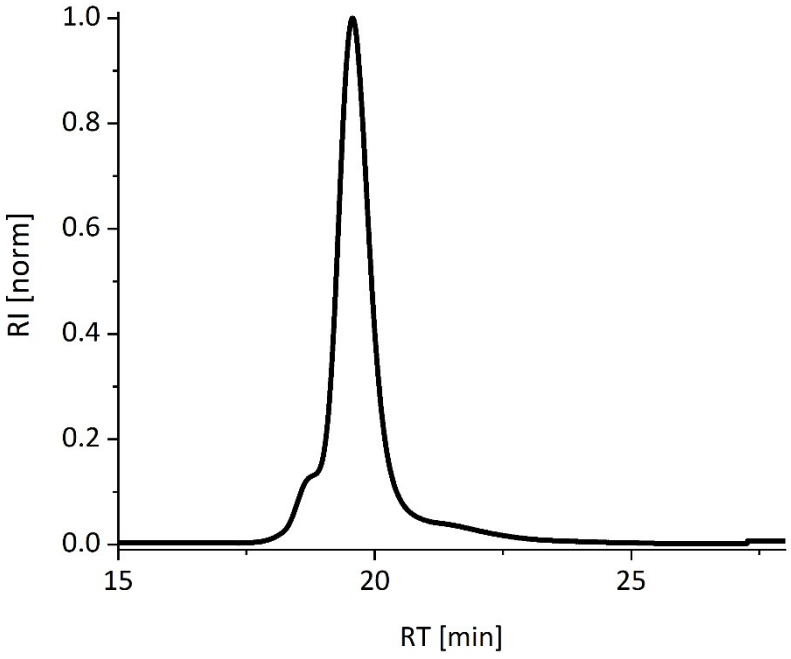


Figure S51: GPC chromatogram (RI detector) of $S_{0.66}$-$MH_{0.34}$-*70*.

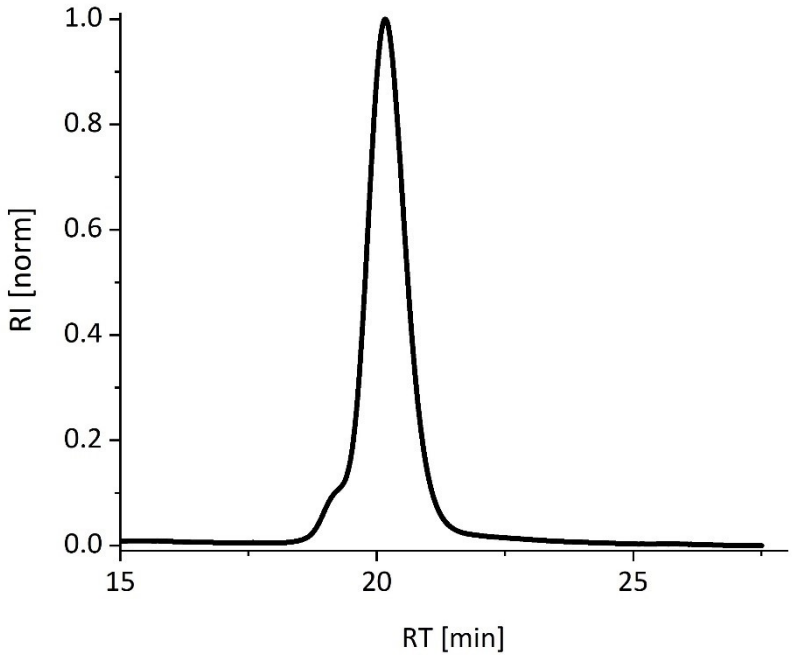


Figure S52: GPC chromatogram (RI detector) of $S_{0.56}$-$MH_{0.44}$-*52*.

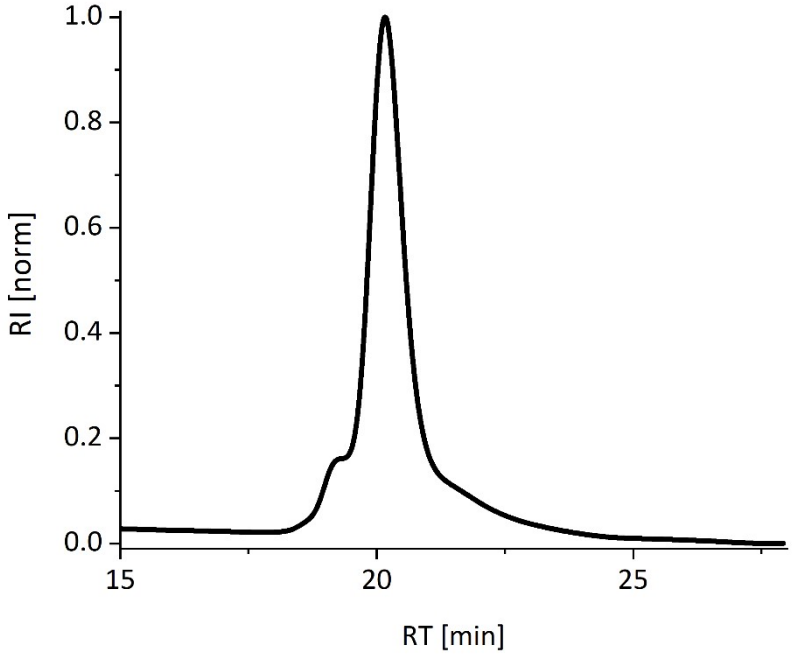


Figure S53: GPC chromatogram (RI detector) of $S_{0.54}$-$MH_{0.46}$-*45*.

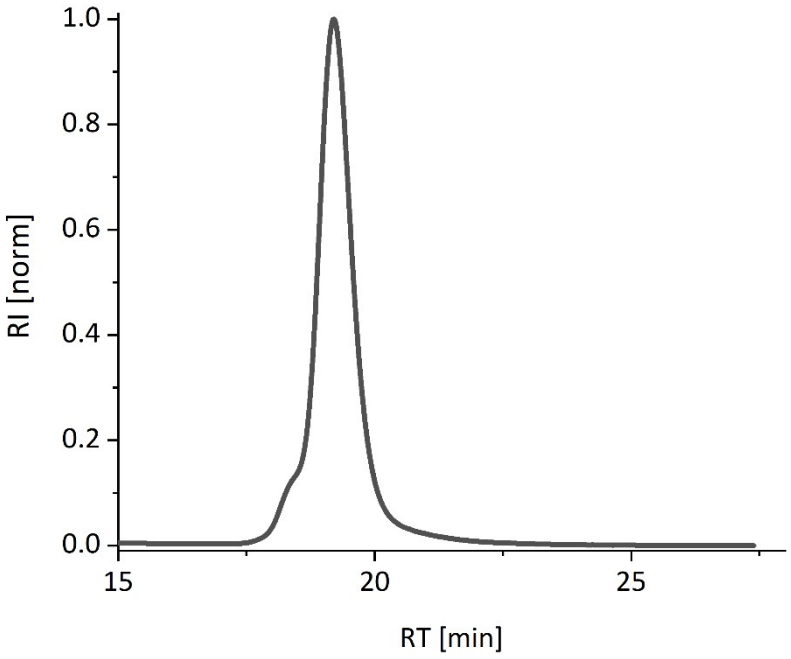


Figure S54: GPC chromatogram (RI detector) of $S_{0.53}$-$MH_{0.47}$-*94*.

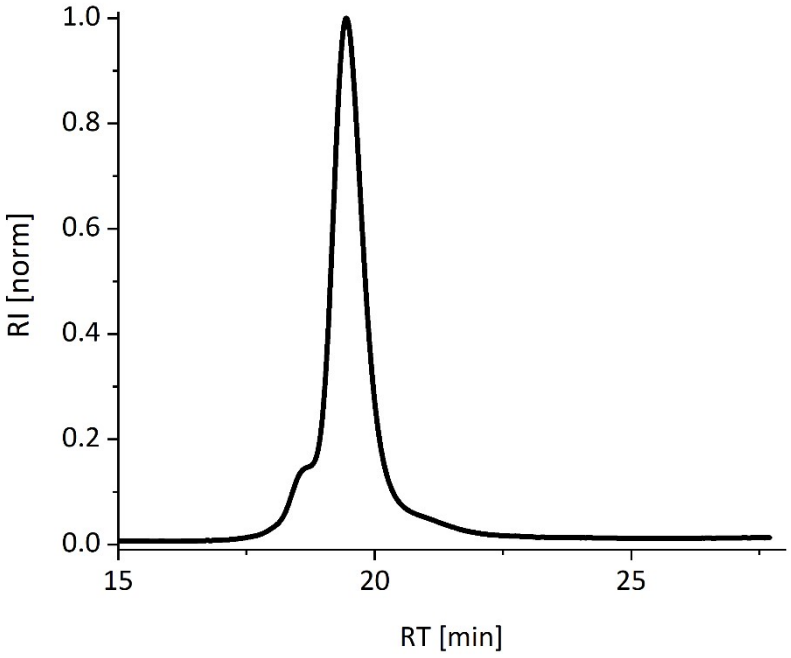


Figure S55: GPC chromatogram (RI detector) of $S_{0.52}$-$MH_{0.48}$-*67*.

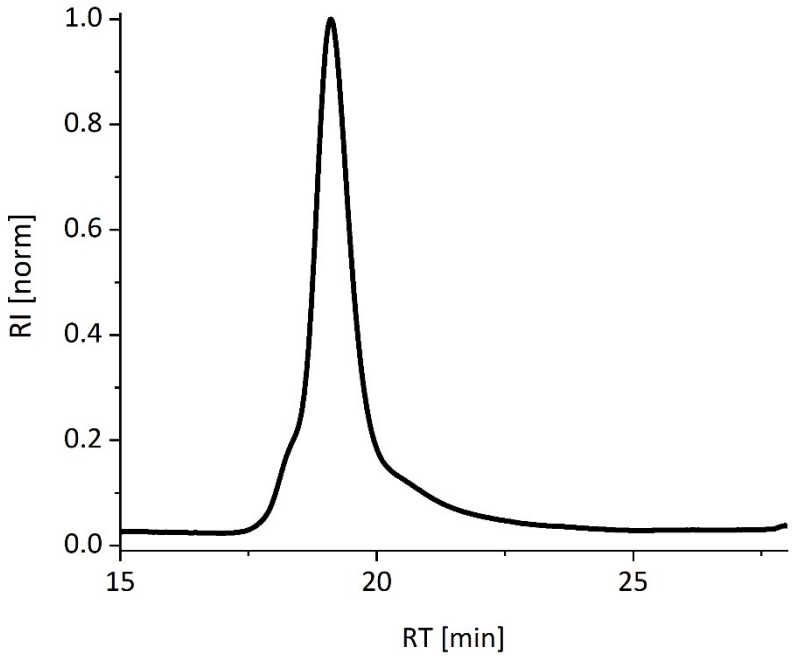


Figure S56: GPC chromatogram (RI detector) of $S_{0.50}$-$MH_{0.50}$-*91*.

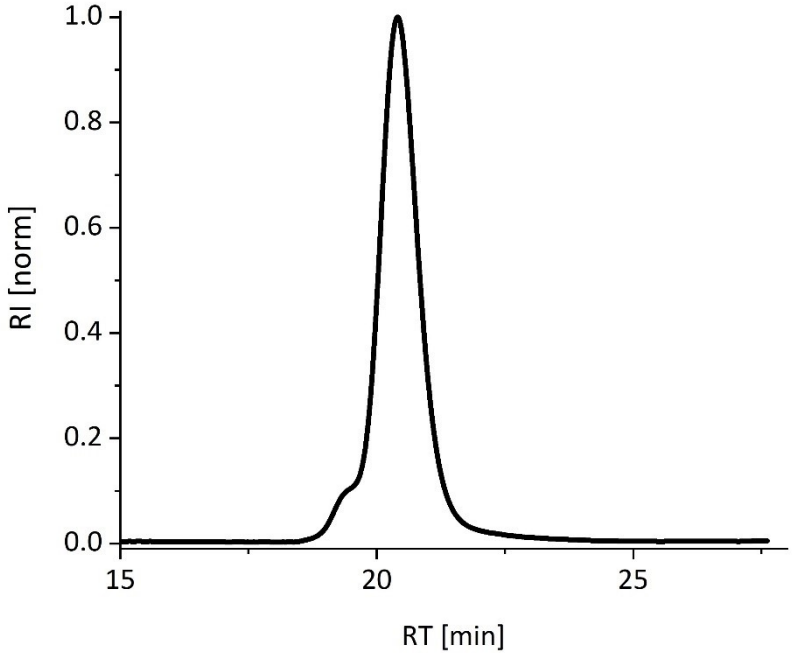


Figure S57: GPC chromatogram (RI detector) of $S_{0.50}$-$MH_{0.50}$-*45*.

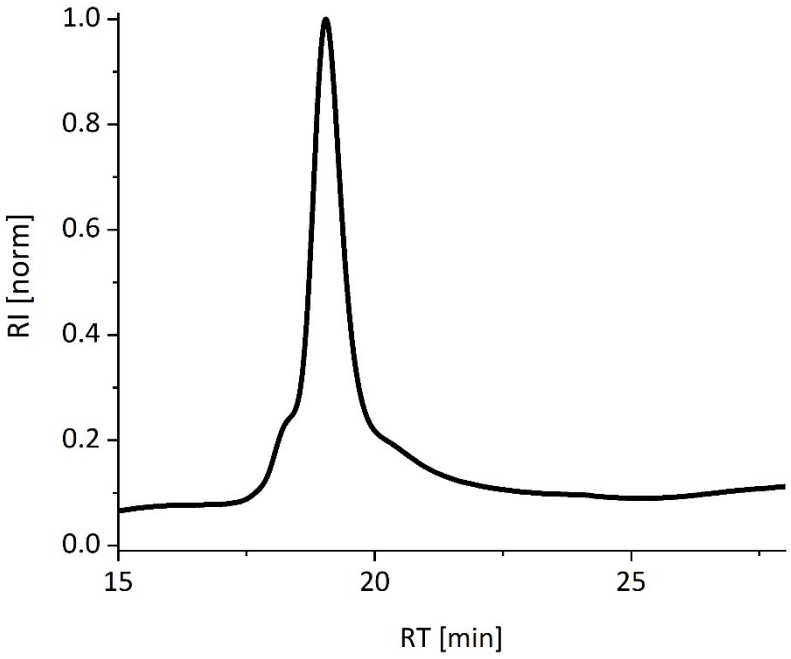


Figure S58: GPC chromatogram (RI detector) of $S_{0.49}$-$MH_{0.51}$-*92*.

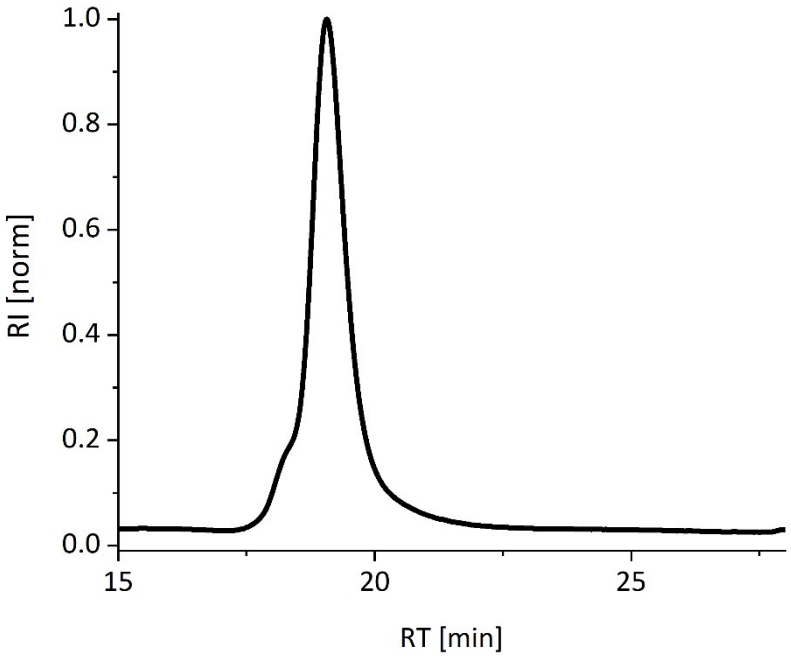


Figure S59: GPC chromatogram (RI detector) of $S_{0.46}$-$MH_{0.54}$-*81*.

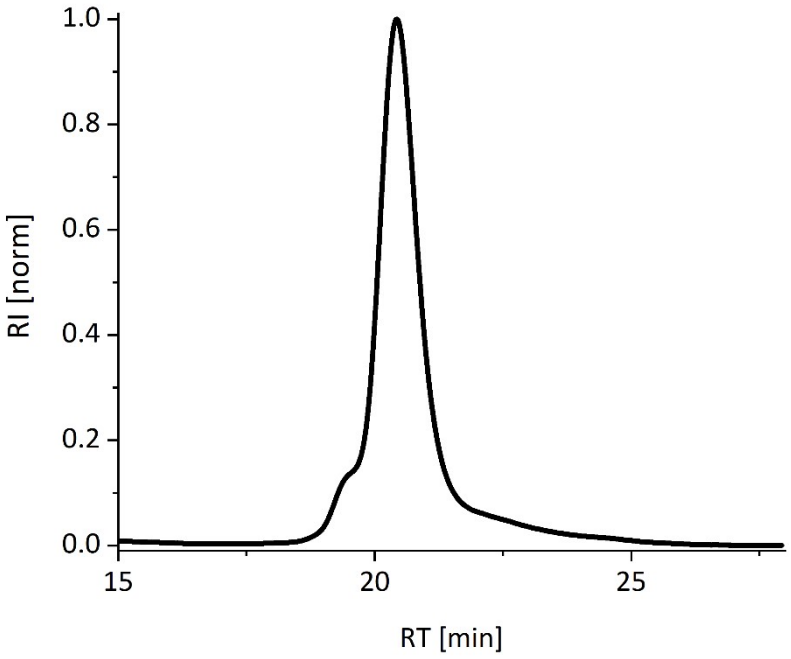


Figure S60: GPC chromatogram (RI detector) of $S_{0.45}$-$MH_{0.55}$-*42*.

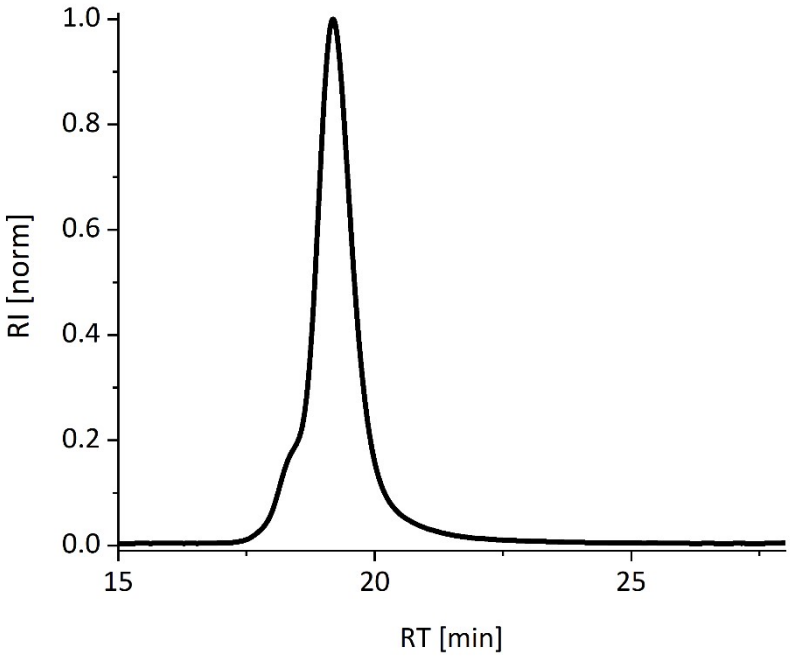


Figure S61: GPC chromatogram (RI detector) of $S_{0.42}$-$MH_{0.58}$-*89*.

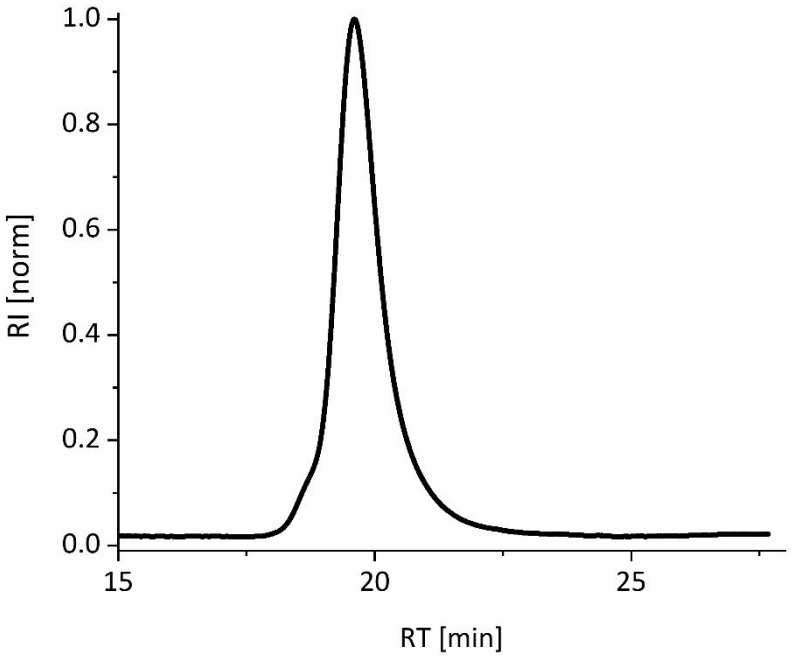


Figure S62: GPC chromatogram (RI detector) of $S_{0.42}$-$MH_{0.58}$-*57*.

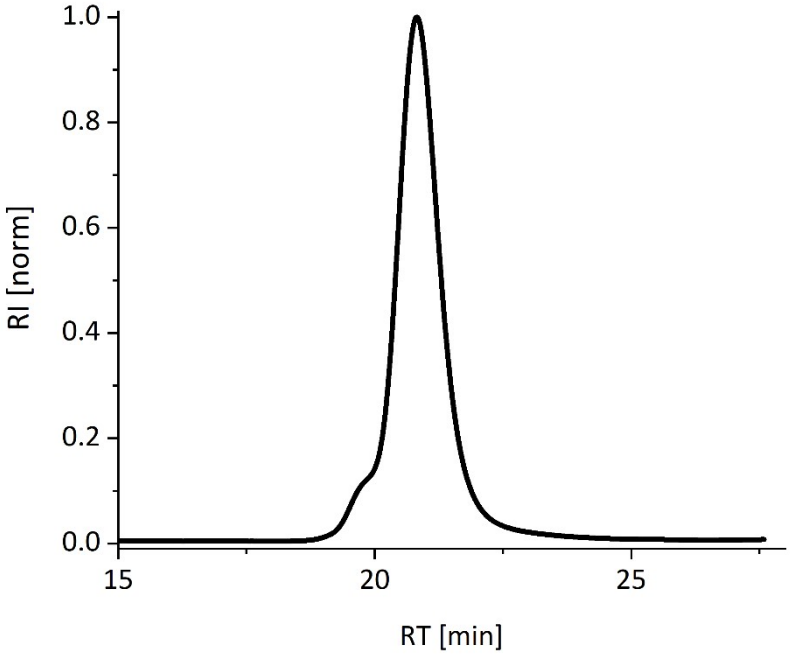


Figure S63: GPC chromatogram (RI detector) of $S_{0.39}$-$MH_{0.61}$-*35*.

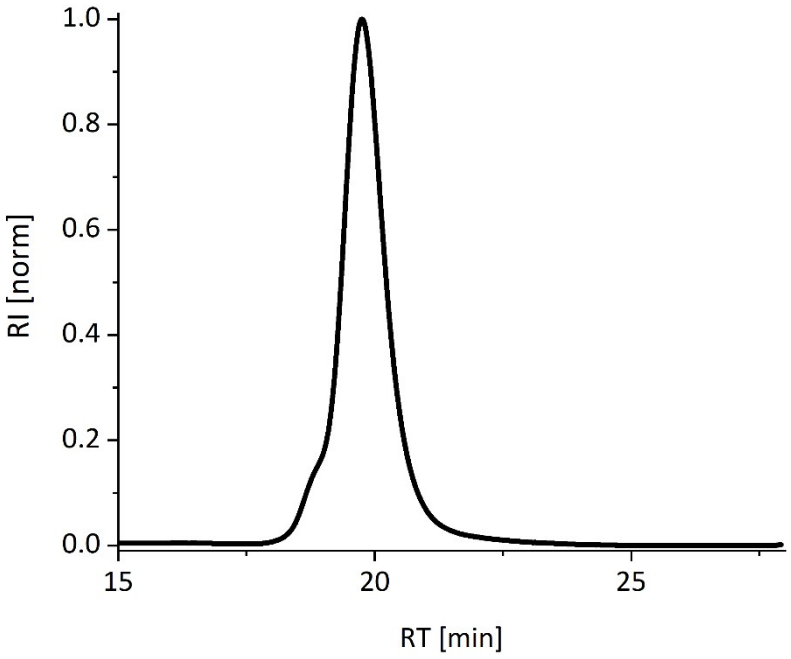


Figure S64: GPC chromatogram (RI detector) of $S_{0.37}$-$MH_{0.63}$-*65*.

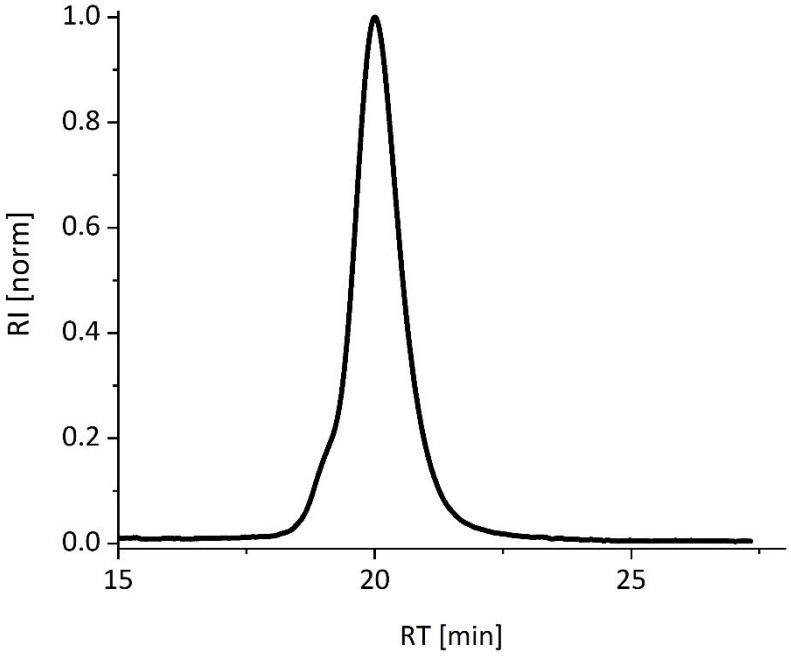


Figure S65: GPC chromatogram (RI detector) of $S_{0.31}$-$MH_{0.69}$-*48*.

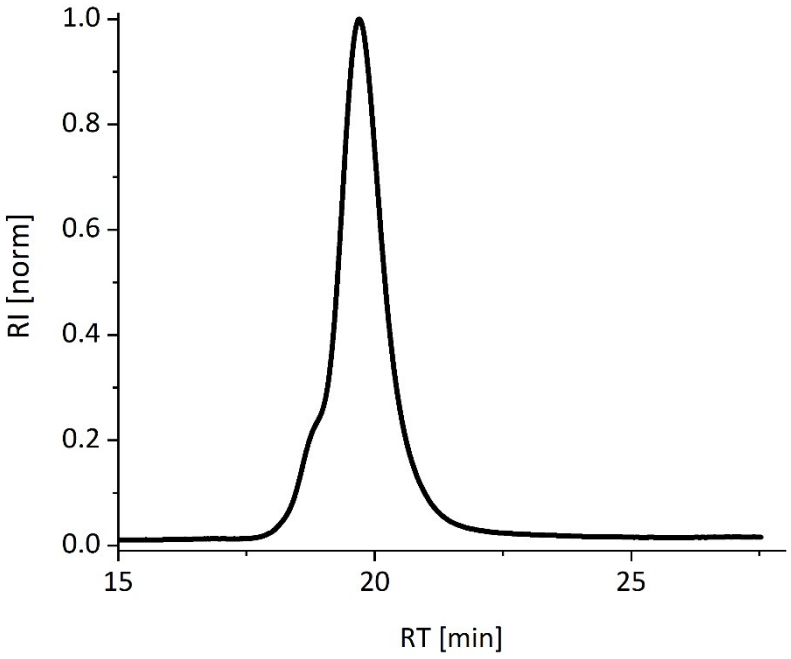


Figure S66: GPC chromatogram (RI detector) of $S_{0.28}$-$MH_{0.72}$-*67*.

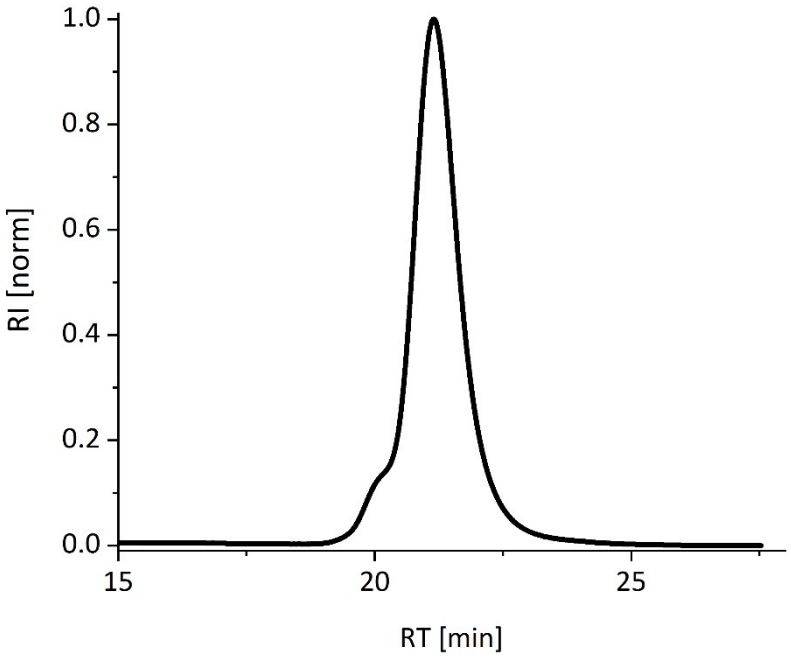


Figure S67: GPC chromatogram (RI detector) of $S_{0.28}$-$MH_{0.72}$-*29*.

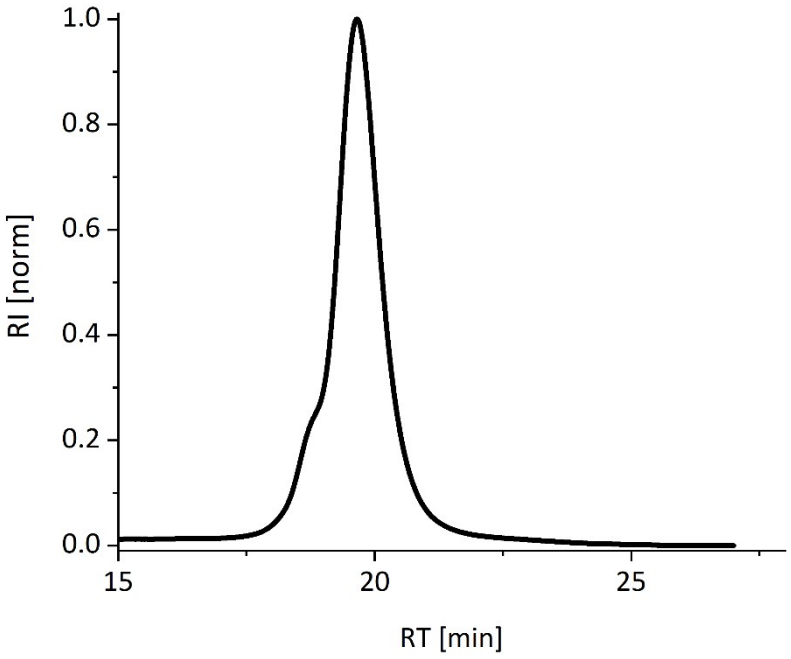


Figure S68: GPC chromatogram (RI detector) of $S_{0.27}$-$MH_{0.73}$-*70*.

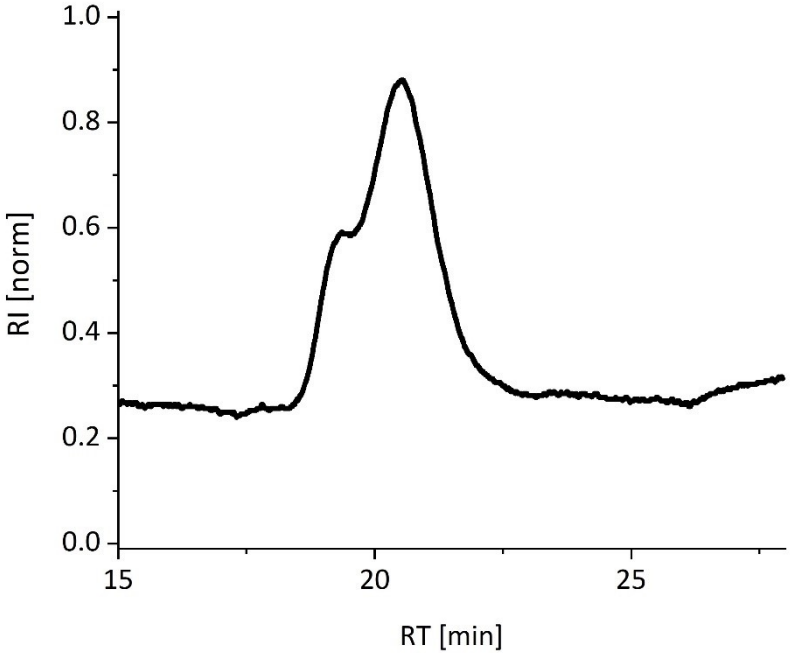


Figure S69: GPC chromatogram (RI detector) of $S_{0.16}$-$MH_{0.84}$-*45*.

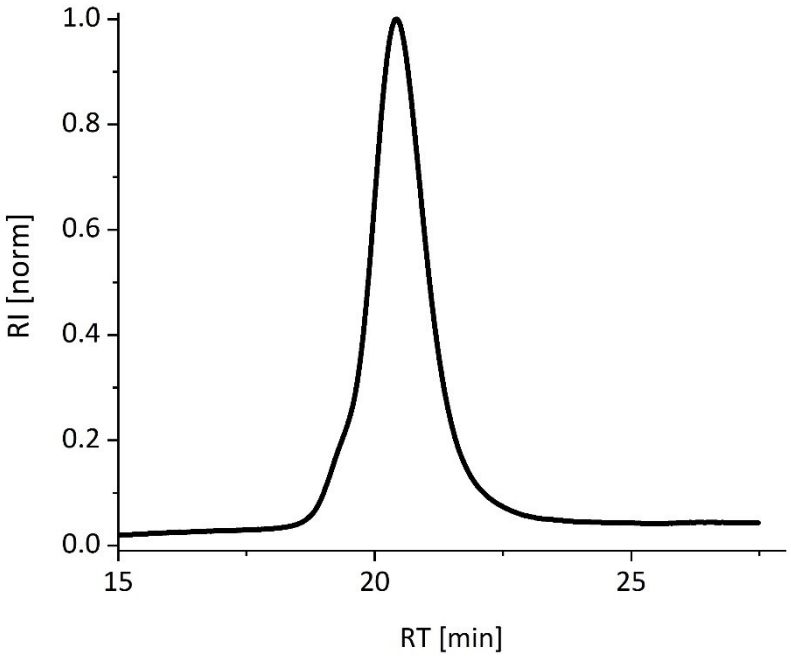


Figure S70: GPC chromatogram (RI detector) of $S_{0.16}$-$MH_{0.84}$-*43*.

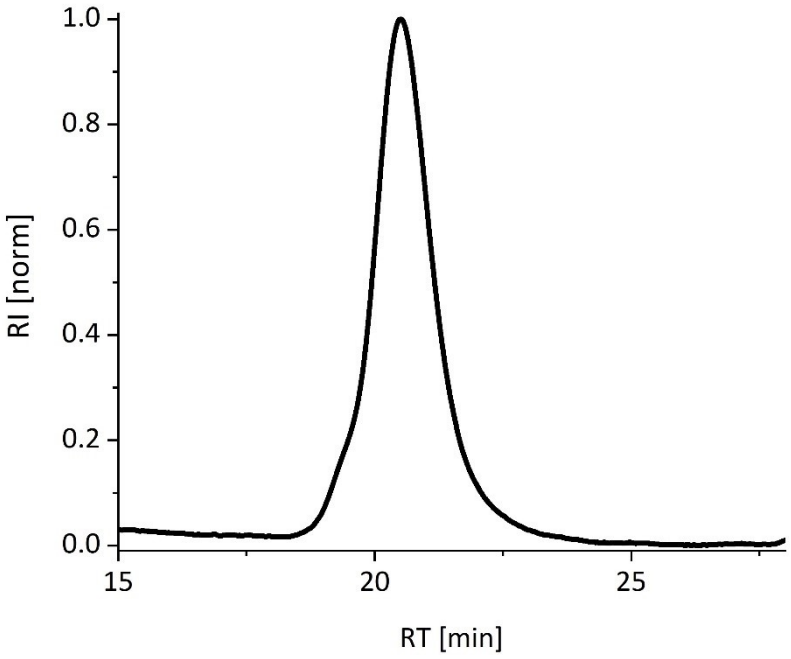


Figure S71: GPC chromatogram (RI detector) of $S_{0.12}$-$MH_{0.88}$-*40*.

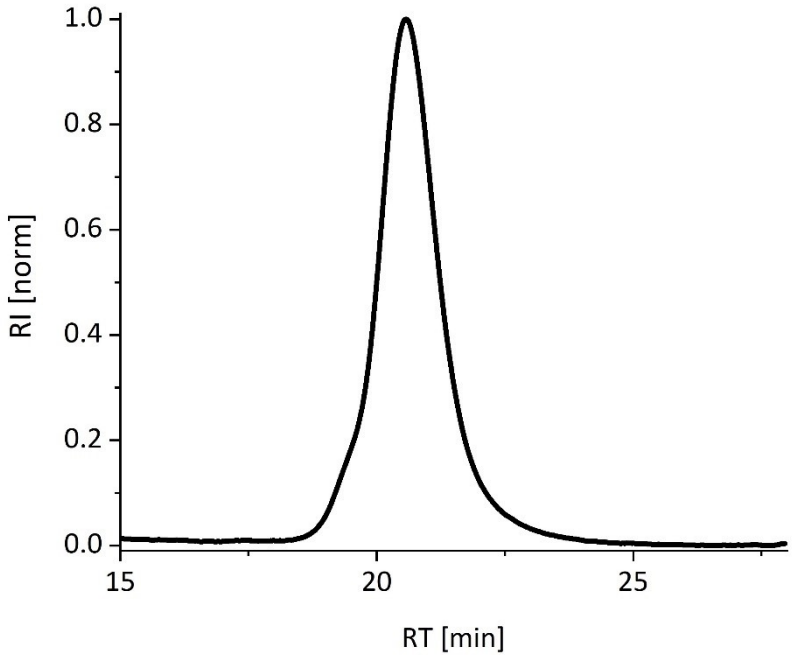


Figure S72: GPC chromatogram (RI detector) of $S_{0.09}$-$MH_{0.91}$-*39*.

### *1.3* Functionalized BCPs

Exemplary synthesis of functionalized BCPs

$S_{0.53}$-$MH_{0.47}$-*94* (250 mg, MW = 93566, 2.67 µmol, 207 µmol OH-groups) was added to a Schlenk flask. After flushing with nitrogen, dry DCM (19 mL) was added. After dissolving, $NEt_3$ (592 µL, 430 mg, 4.24 mmol, 20 eq.) was added, the solution was cooled to 0 °C and methacryloyl chloride (348 µL, 389 mg, 3.74 mmol, 18 eq.) was added slowly under stirring. After stirring at 0°C to RT for 16-72 h, most of the DCM was removed in vacuo. MeCN (65 mL) was added and the mixture was poured into aqueous $NaHCO_3$ (5%, 130 mL). After extracting with DCM (3 x 65 mL) the united organic fractions were dried over $Na_2SO_4$, the solvent was removed in vacuo and the washing step was repeated if $NEt_3HCl$ was still present. After precipitation in $Et_2O$, $S_{0.53}$-$MH^*_{0.47}$-*94* was obtained as a solid.

$^1$H NMR 600 MHz ($CD_2Cl_2$): $\delta$ [ppm] = 7.80 (m), 7.47 (m), 7.31 (m), 7.28 - 6.31 (m), 6.12 (bs), 5.63 (bs), 4.32 (bs), 4.17 (bs), 3.56 (s), 2.14 - 0.63 (m).

NMR spectra of functionalized BCPs

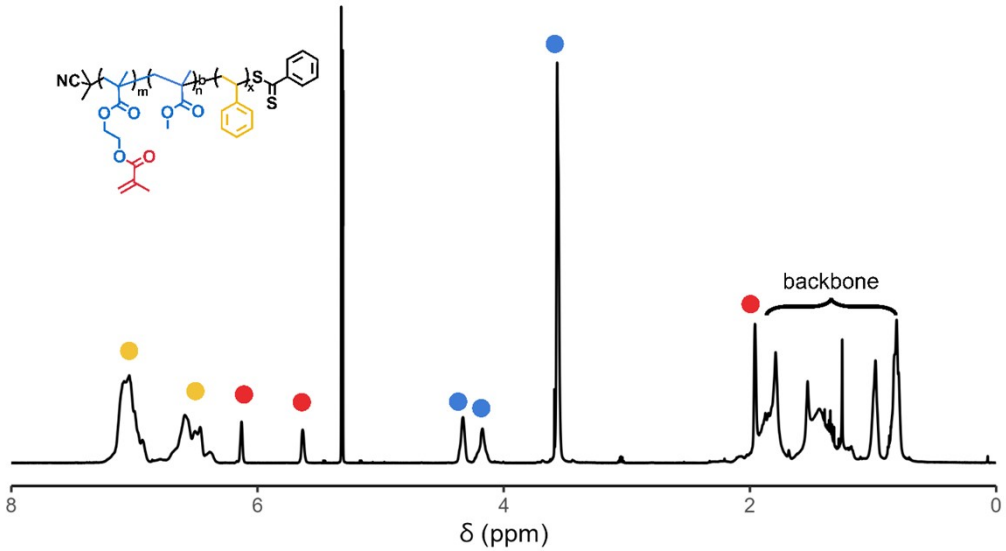


Figure S73: $^{1}$H NMR spectrum of $S_{0.53}$-MH*$_{0.47}$-*94* in $CD_2Cl_2$ with peak assignment.

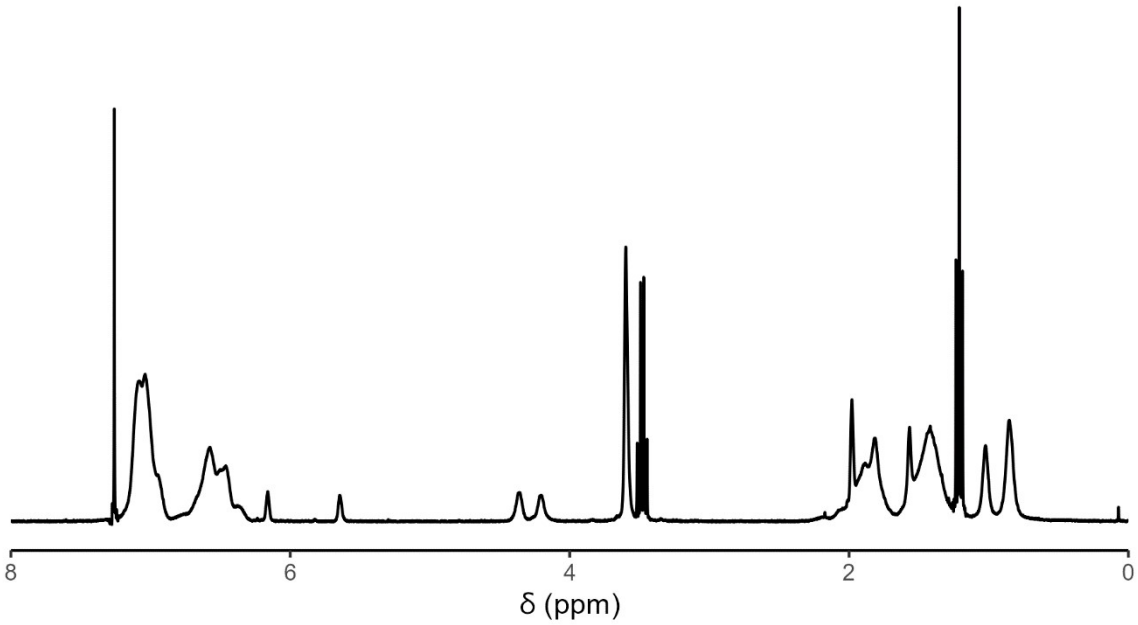


Figure S74: $^{1}$H NMR spectrum of $S_{0.75}$-MH*$_{0.25}$-*66* in $CDCl_3$.

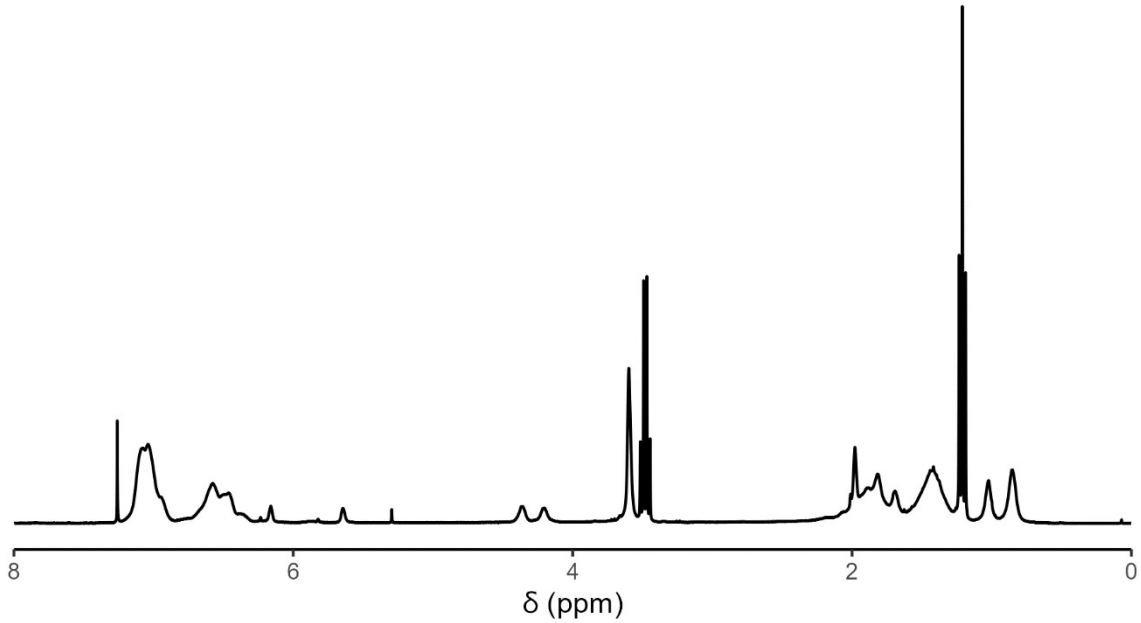


Figure S75: $^{1}$H NMR spectrum of $S_{0.68}$-MH*$_{0.32}$-*33* in $CDCl_3$.

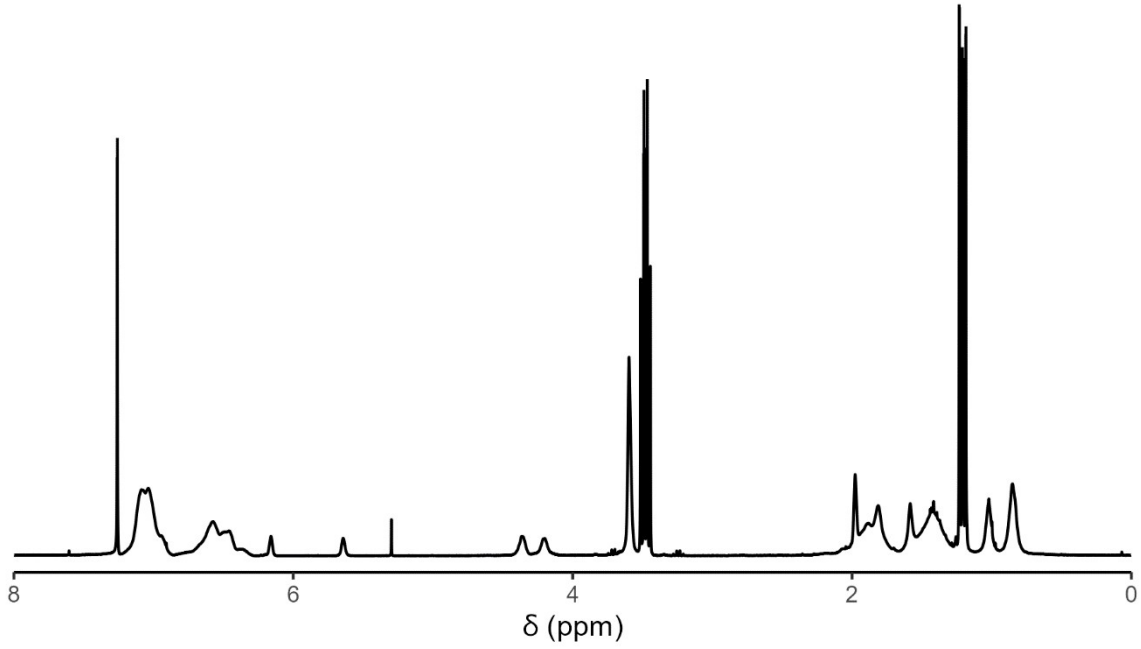


Figure S76: $^{1}$H NMR spectrum of $S_{0.66}$-MH*$_{0.34}$-*70* in $CDCl_3$.

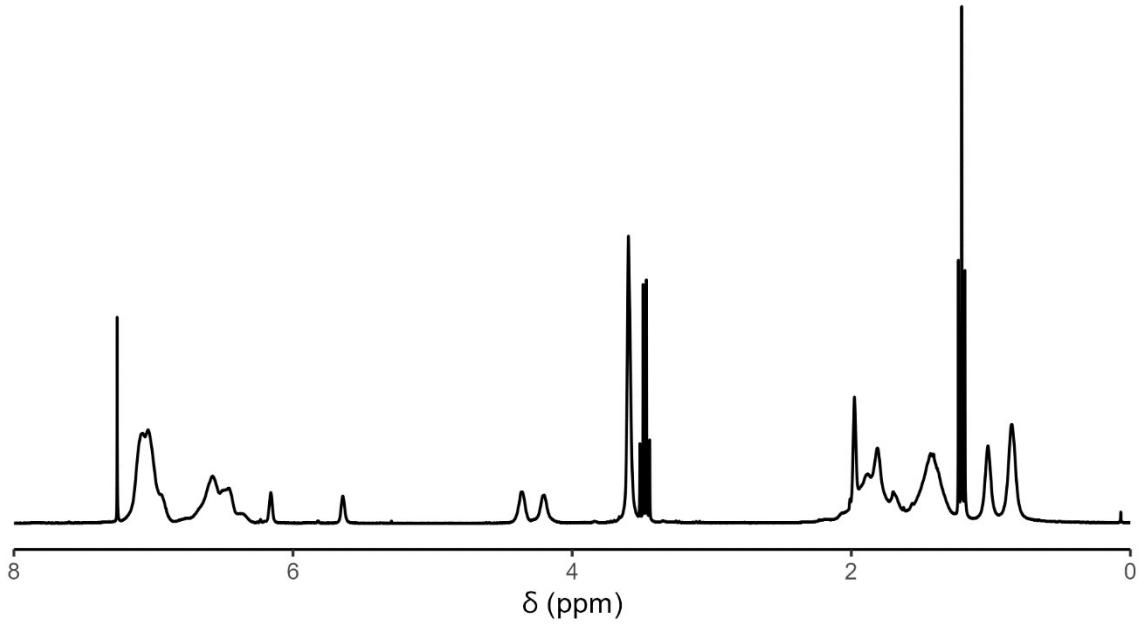


Figure S77: $^{1}$H NMR spectrum of $S_{0.56}$-MH*$_{0.44}$-*52* in $CDCl_3$.

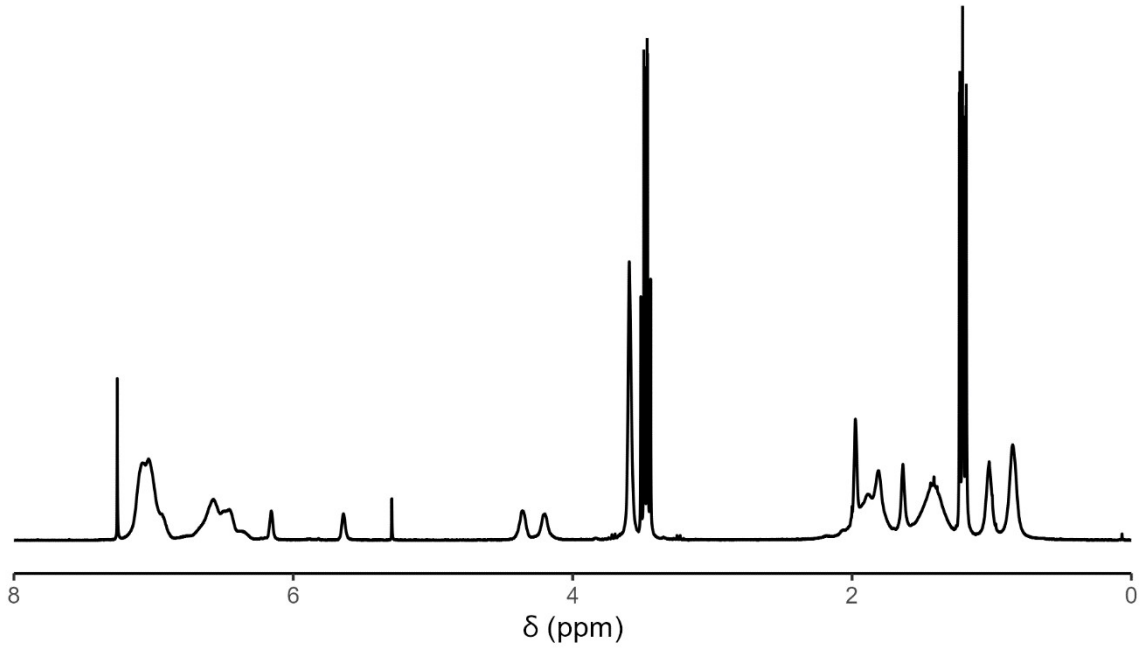


Figure S78: $^{1}$H NMR spectrum of $S_{0.52}$-MH*$_{0.48}$-*67* in $CDCl_3$.

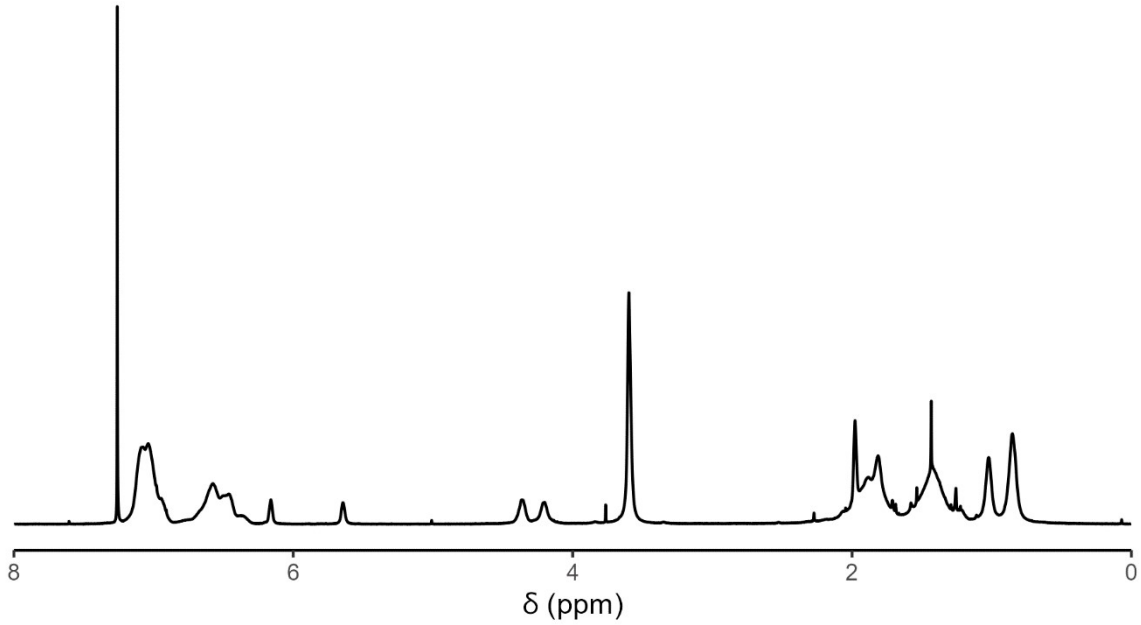


Figure S79: $^{1}$H NMR spectrum of $S_{\mathbf{0.50}}$-MH*$_{\mathbf{0.50}}$-*91* in $CDCl_3$.

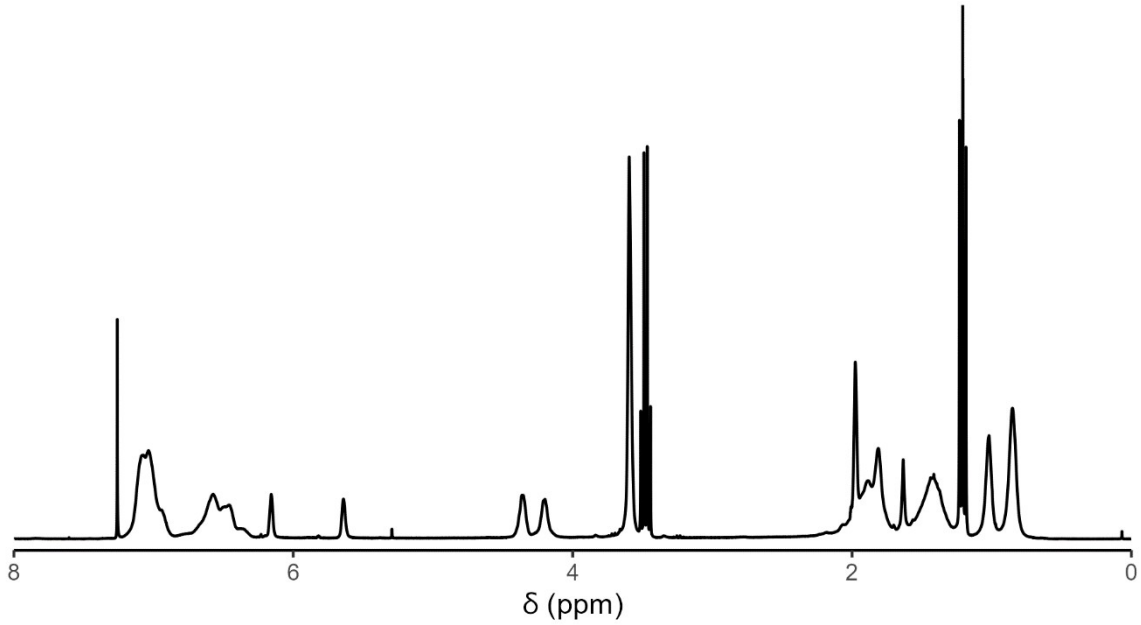


Figure S80: $^{1}$H NMR spectrum of $S_{\mathbf{0.50}}$-MH*$_{\mathbf{0.50}}$-*45* in $CDCl_3$.

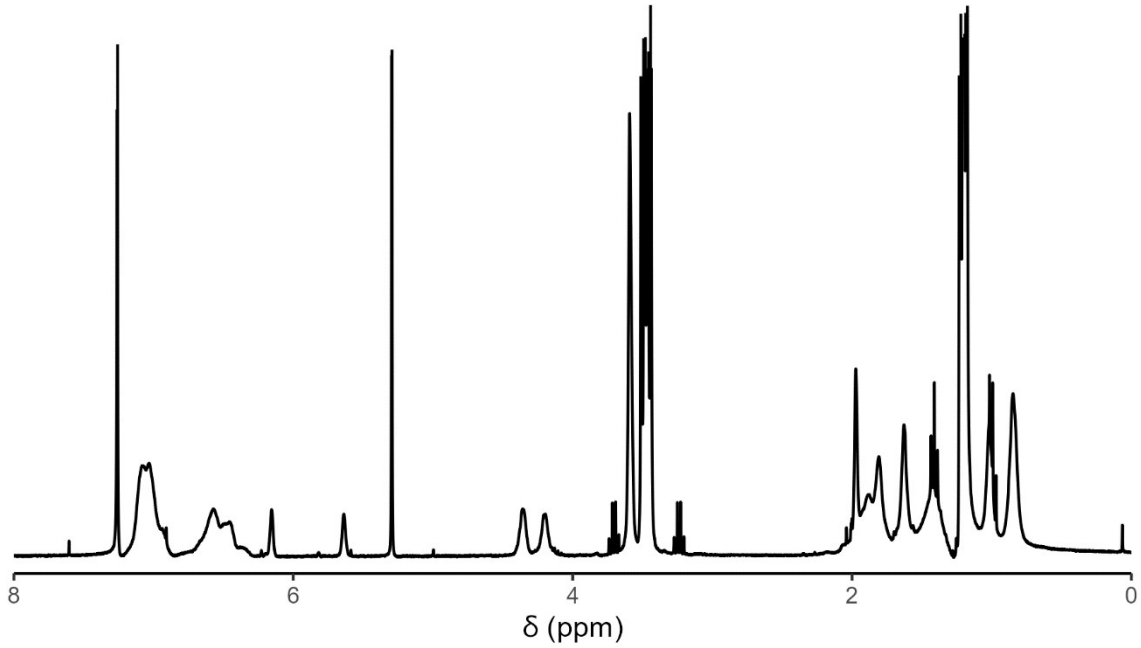


Figure S81: $^{1}$H NMR spectrum of $S_{0.46}$-MH*$_{0.54}$-*81* in $CDCl_3$.

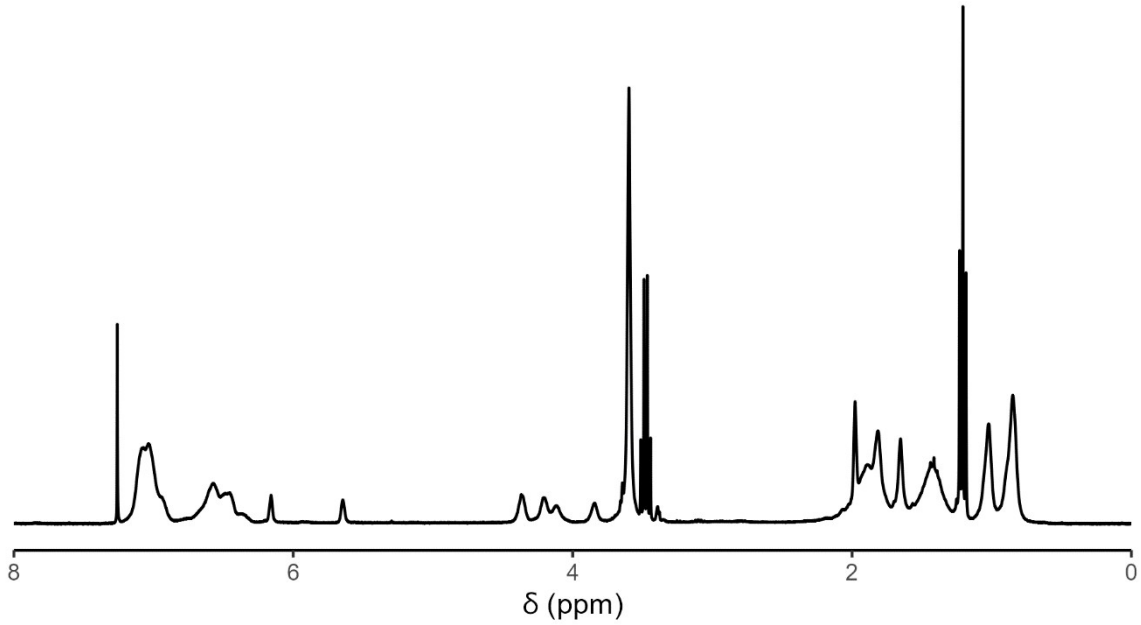


Figure S82: $^{1}$H NMR spectrum of $S_{0.45}$-MH*$_{0.55}$-*42* in $CDCl_3$.

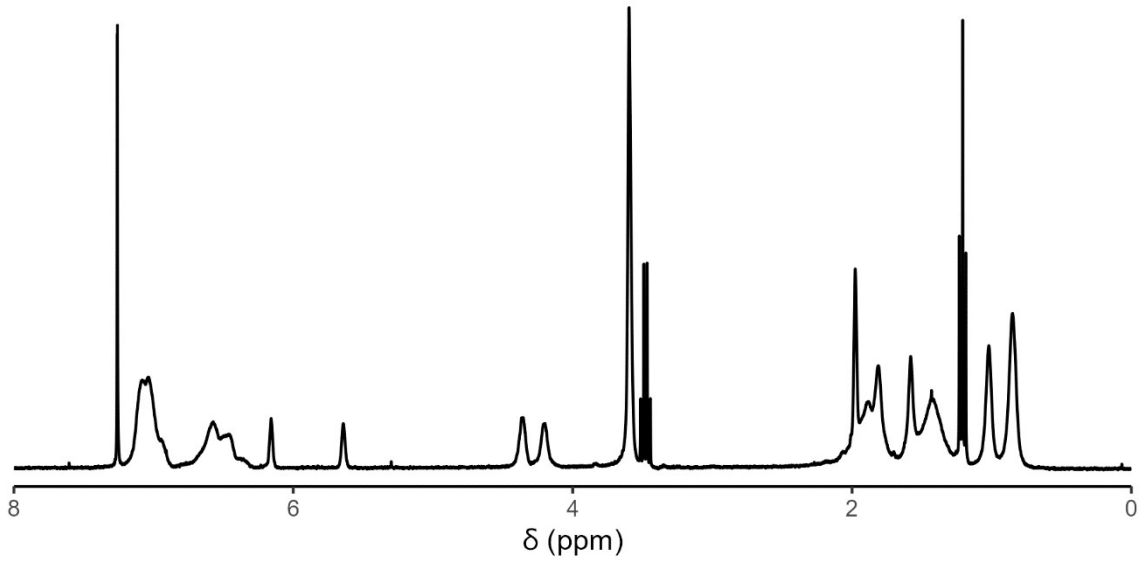


Figure S83: $^{1}$H NMR spectrum of $S_{0.42}$-MH*$_{0.58}$-*89* in $CDCl_3$.

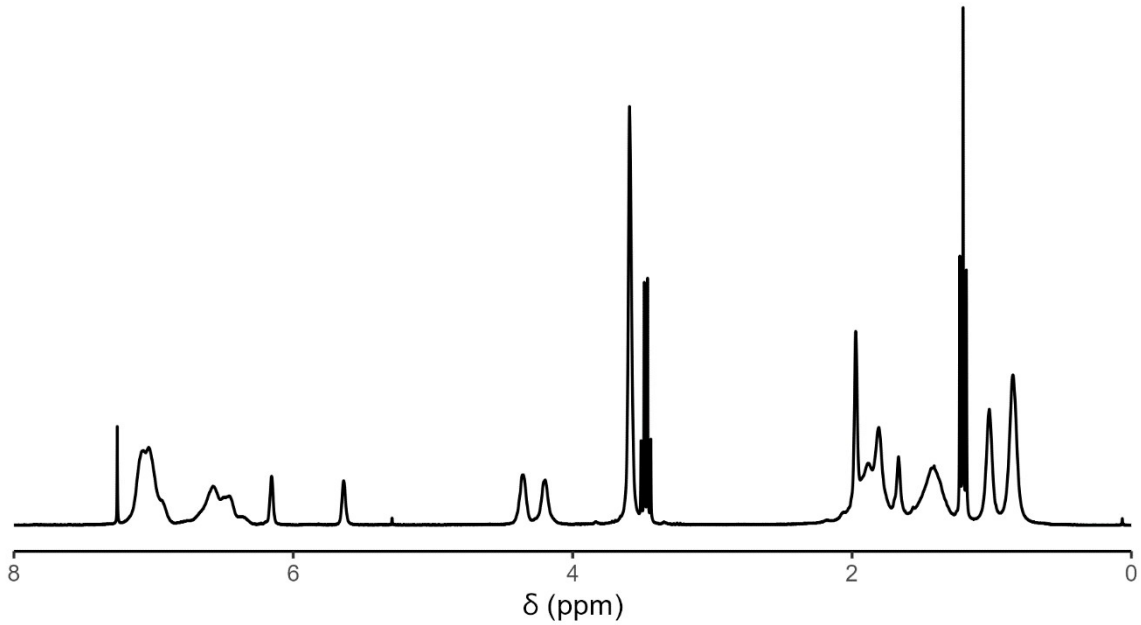


Figure S84: $^{1}$H NMR spectrum of $S_{0.42}$-MH*$_{0.58}$-*57* in $CDCl_3$.

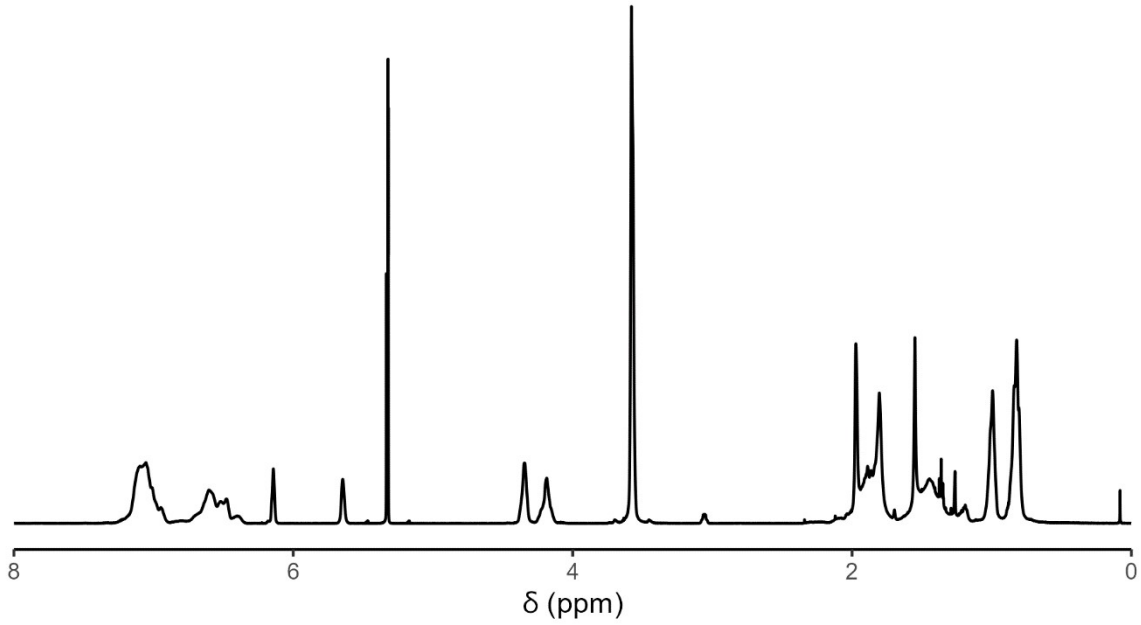


Figure S85: $^{1}$H NMR spectrum of $S_{\mathbf{0.37}}$-MH*$_{\mathbf{0.63}}$-*65* in $CD_2Cl_2$.

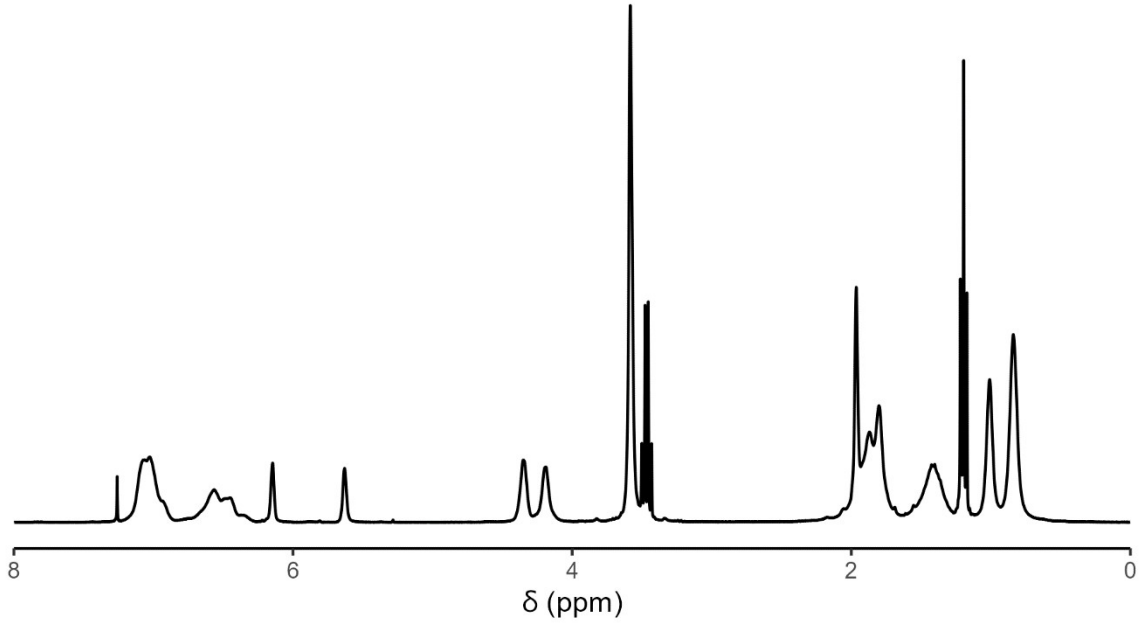


Figure S86: $^{1}$H NMR spectrum of $S_{\mathbf{0.31}}$-MH*$_{\mathbf{0.69}}$-*48* in $CDCl_3$.

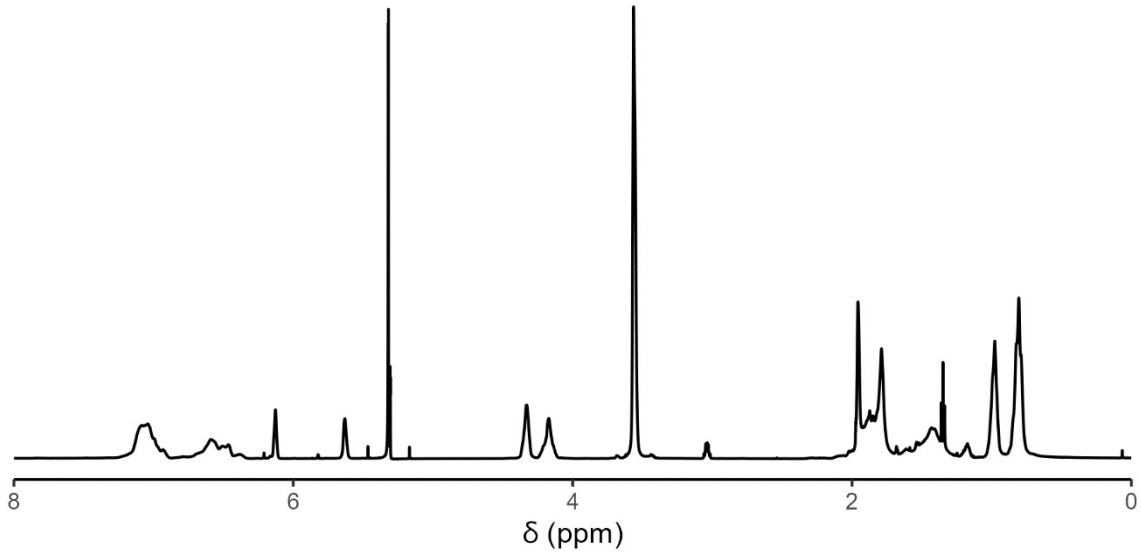


Figure S87: $^{1}$H NMR spectrum of $S_{\mathbf{0.28}}$-MH*$_{\mathbf{0.72}}$-*67* in $CD_2Cl_2$.

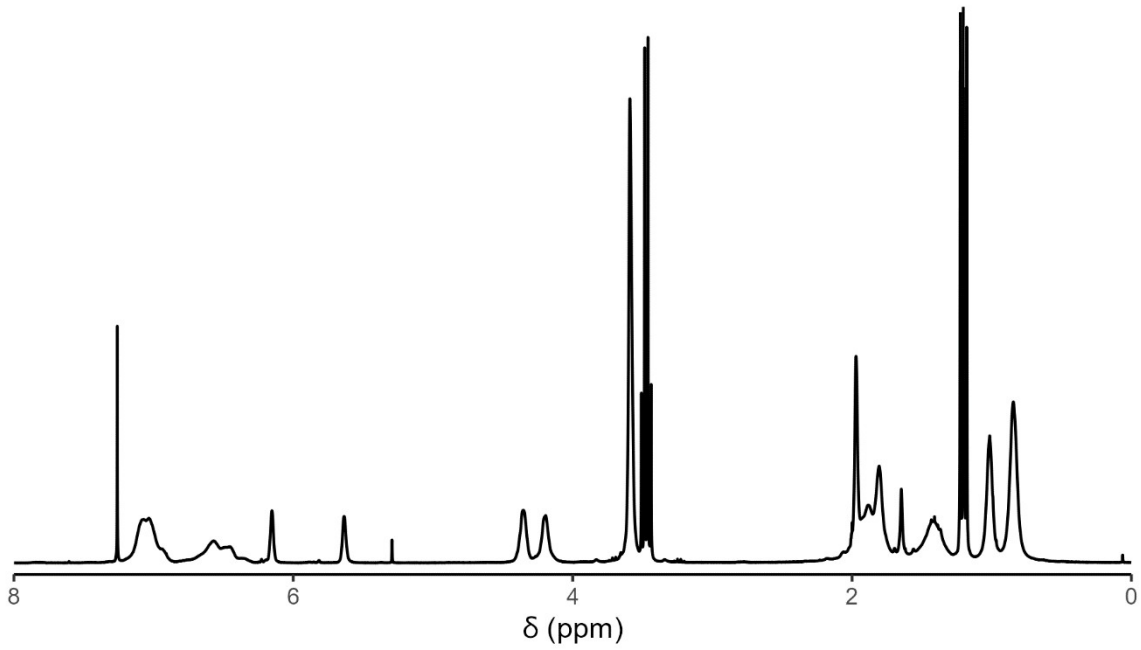


Figure S88: $^{1}$H NMR spectrum of $S_{\mathbf{0.28}}$-MH*$_{\mathbf{0.72}}$-*29* in $CDCl_3$.

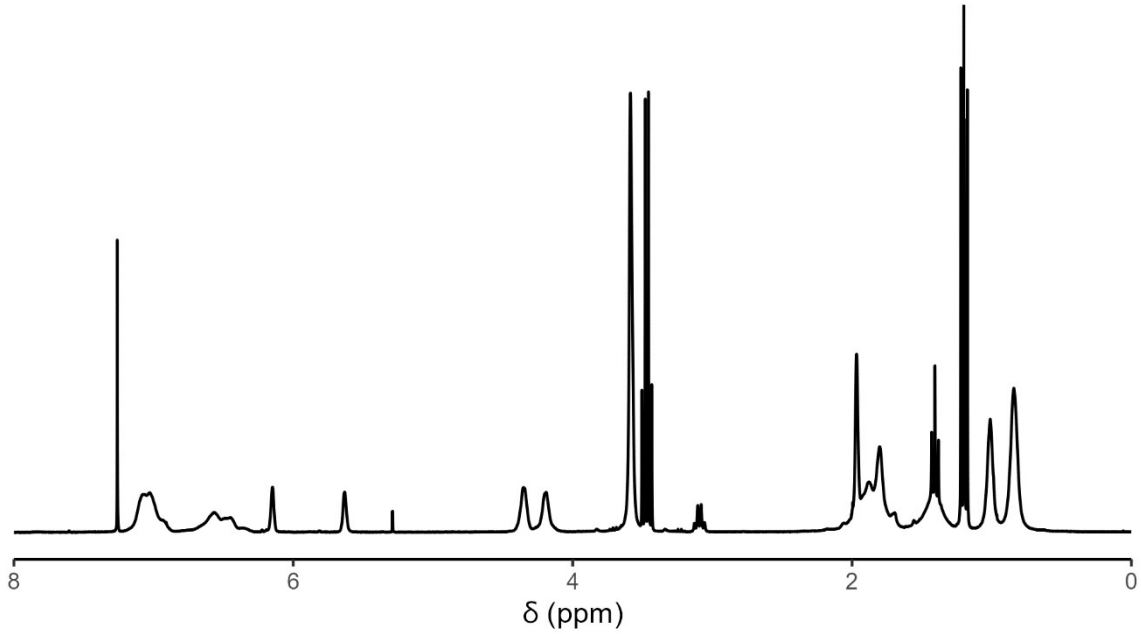


Figure S89: $^{1}$H NMR spectrum of $S_{\mathbf{0.27}}$-MH*$_{\mathbf{0.73}}$-*70* in $CDCl_3$.

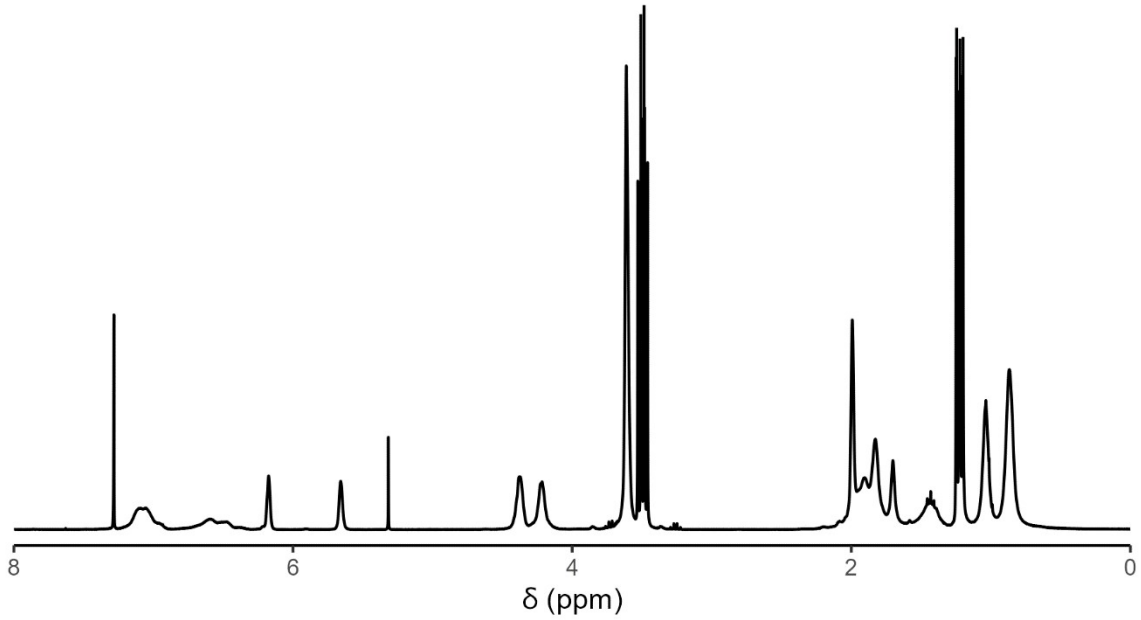


Figure S90: $^{1}$H NMR spectrum of $S_{\mathbf{0.16}}$-MH$_{\mathbf{0.84}}$-*43* in $CDCl_3$.

## 2. Morphology characterization

SEM images and SAXS spectra

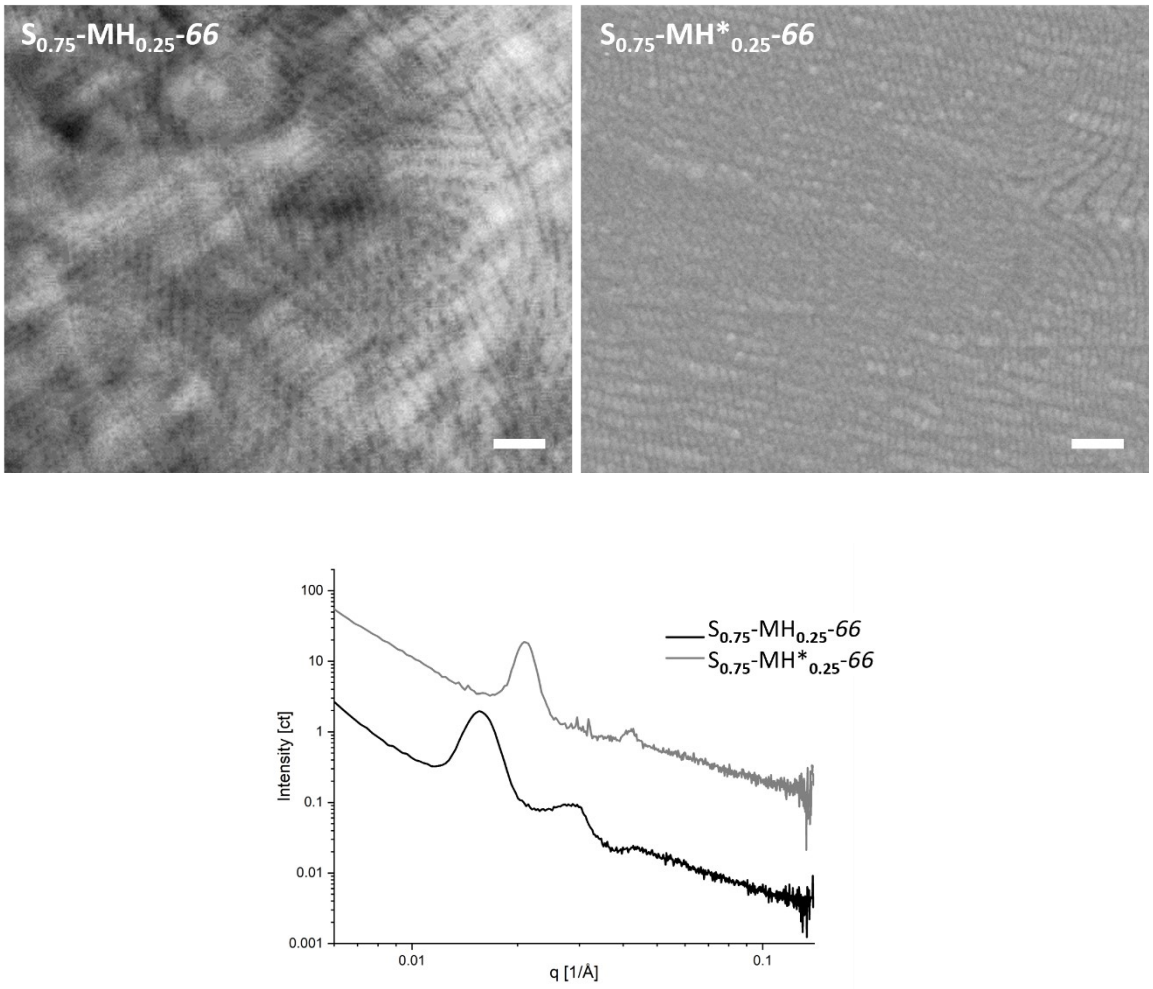


Figure S91: SEM images and SAXS spectra for $S_{0.75}$-$MH_{0.25}$-*66* and $S_{0.75}$-$MH^*_{0.25}$-*66*. Scale bars = 200 nm.

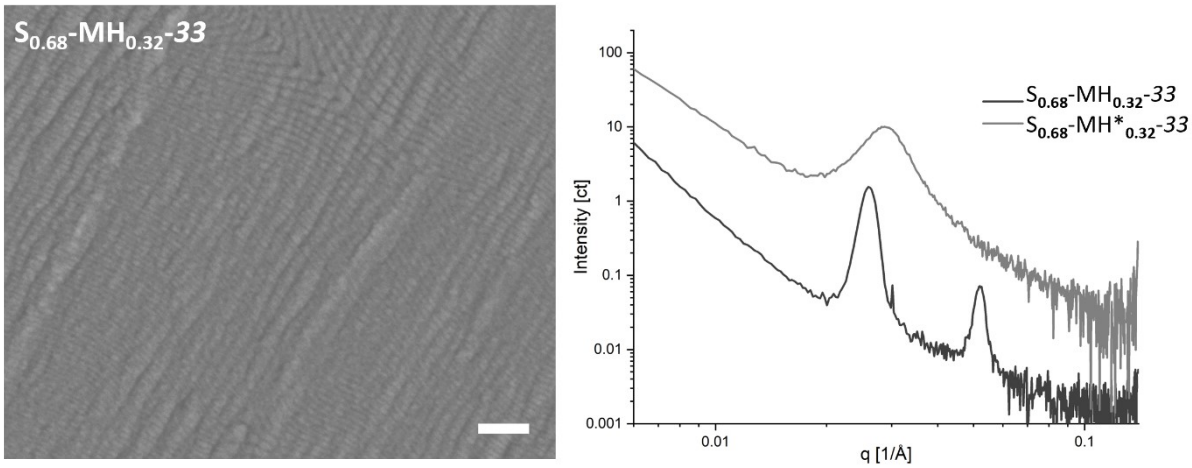


Figure S92: SEM image and SAXS spectra for $S_{0.68}$-$MH_{0.32}$-*33* and $S_{0.68}$-$MH^*_{0.32}$-*33*. Scale bar = 200 nm.

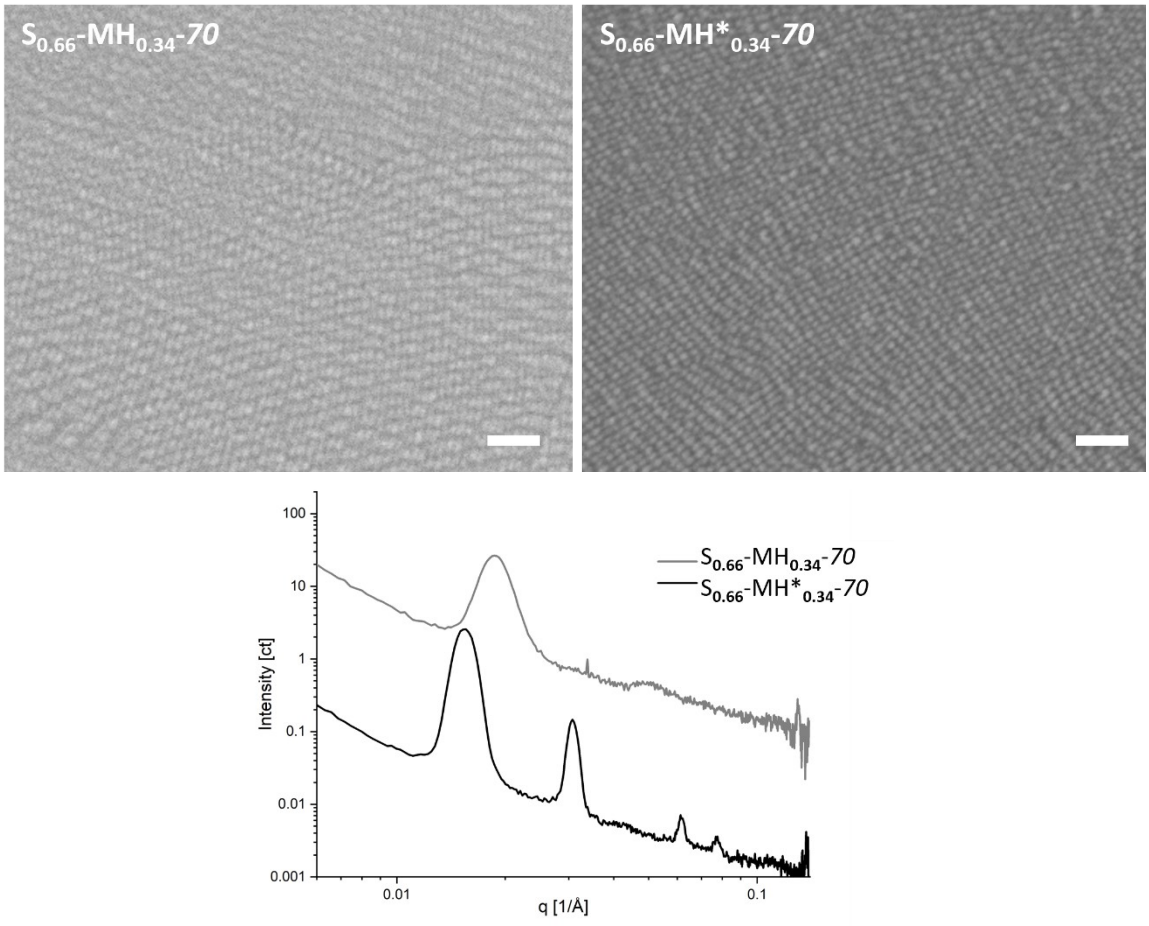


Figure S93: SEM images and SAXS spectra for $S_{0.66}$-$MH_{0.34}$-*70* and $S_{0.66}$-$MH^*_{0.34}$-*70*. Scale bars = 200 nm.

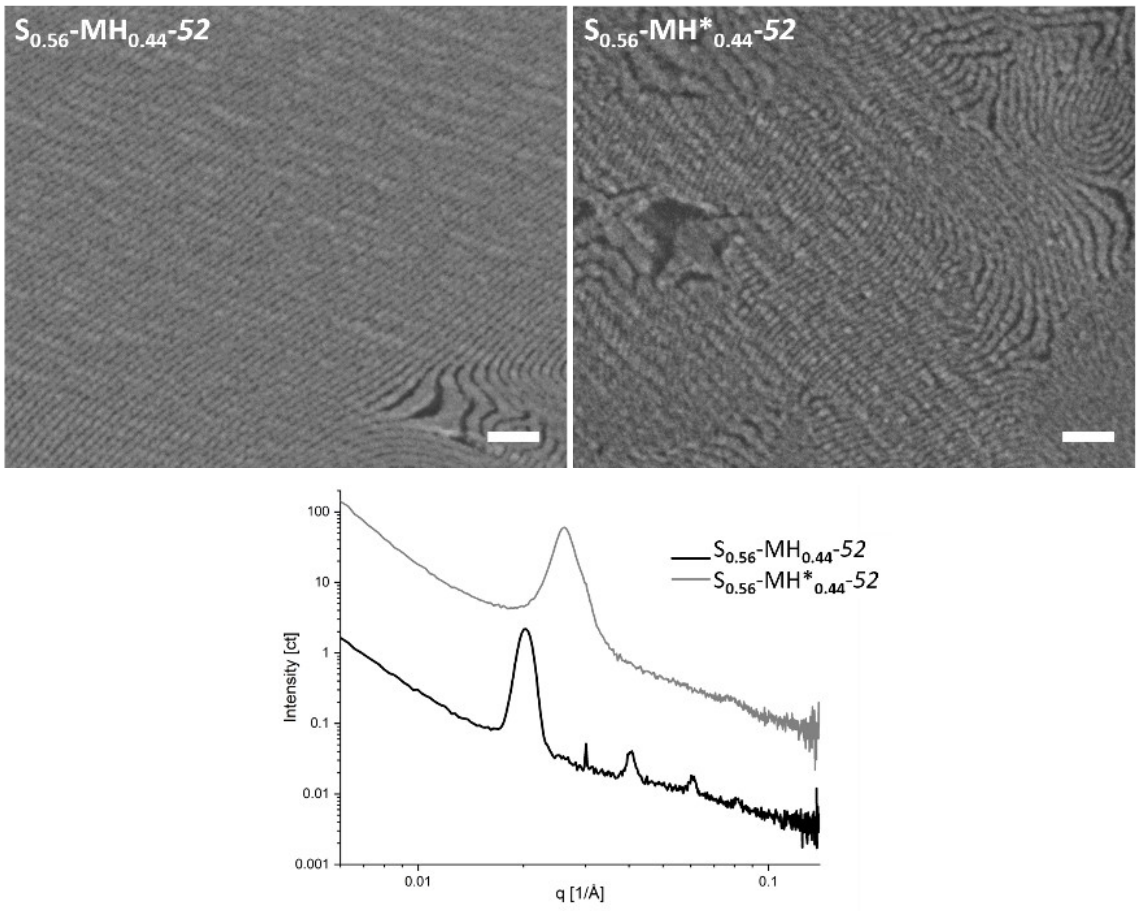


Figure S94: SEM images and SAXS spectra for $S_{0.56}$-$MH_{0.44}$-*52* and $S_{0.56}$-$MH^*_{0.44}$-*52*. Scale bars = 200 nm.

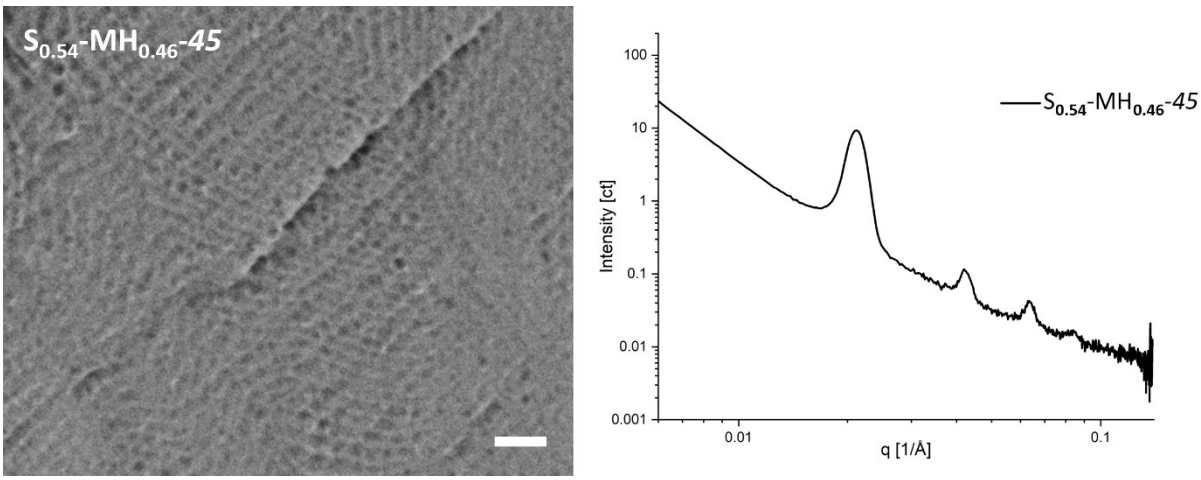


Figure S95: SEM image and SAXS spectrum for $S_{0.54}$-$MH_{0.46}$-*45*. Scale bar = 200 nm.

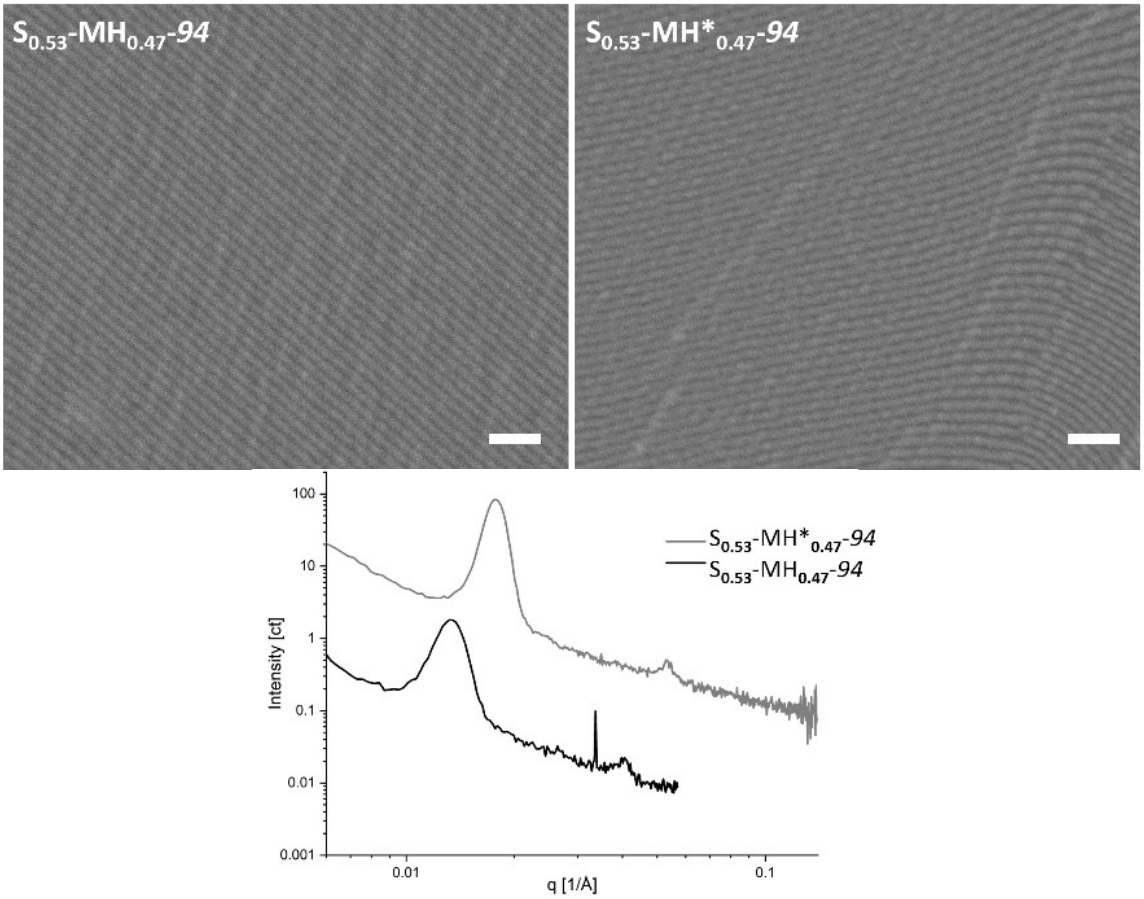


Figure S96: SEM images and SAXS spectra for $S_{0.53}$-$MH_{0.47}$-*94* and $S_{0.53}$-$MH^*_{0.47}$-*94*. Scale bars = 200 nm.

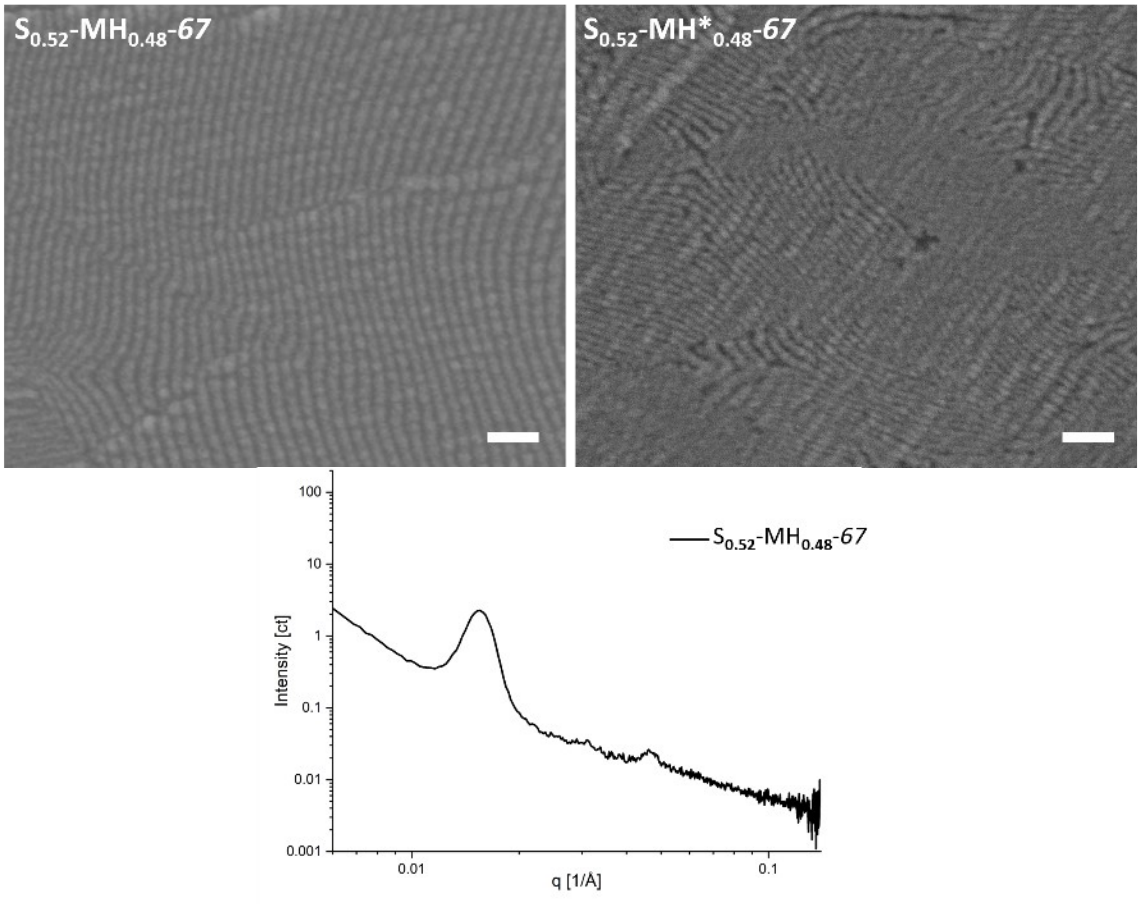

Figure S97: SEM images and SAXS spectrum for $S_{0.52}$-$MH_{0.48}$-*67* and $S_{0.52}$-$MH^*_{0.48}$-*67*. Scale bars = 200 nm.

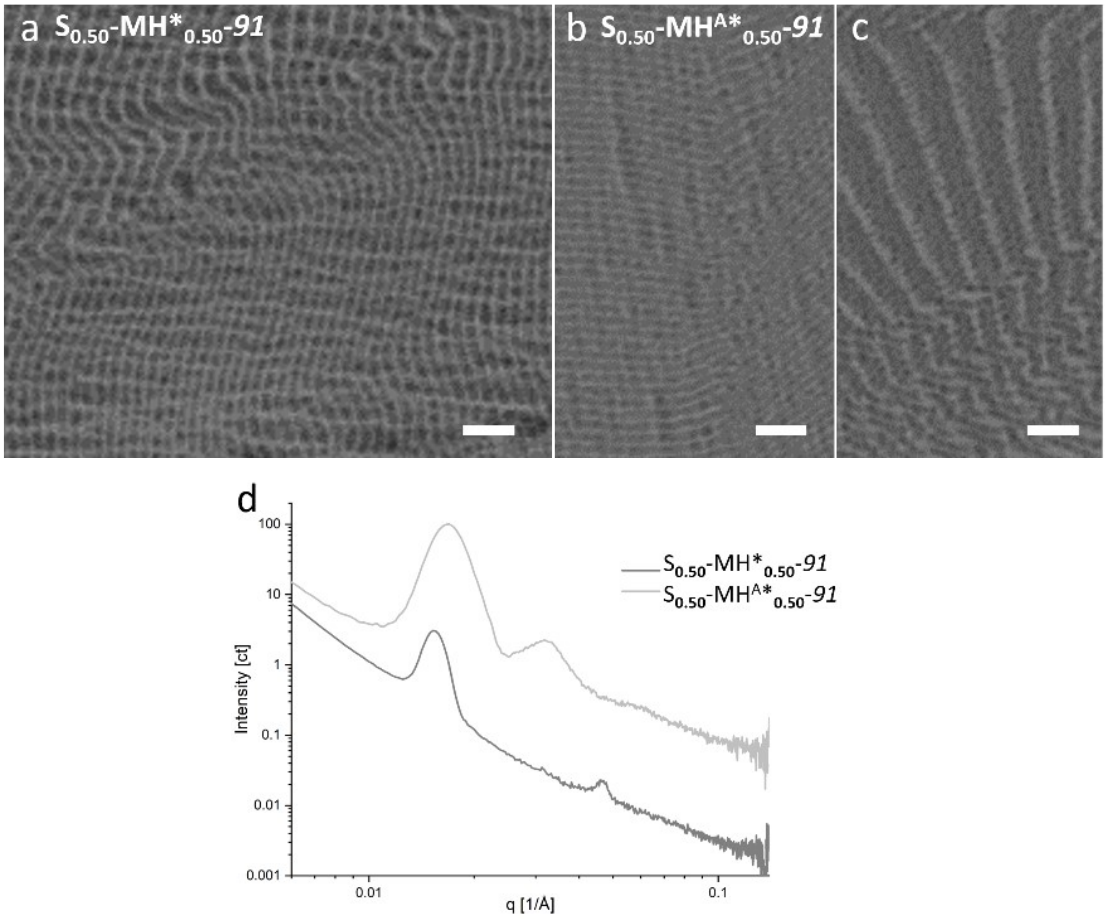


Figure S98: SEM images and SAXS spectra for $S_{0.50}$-$MH^*_{0.50}$-*91* and $S_{0.50}$-$MH^{A*}_{0.50}$-*91*. Scale bars = 200 nm.

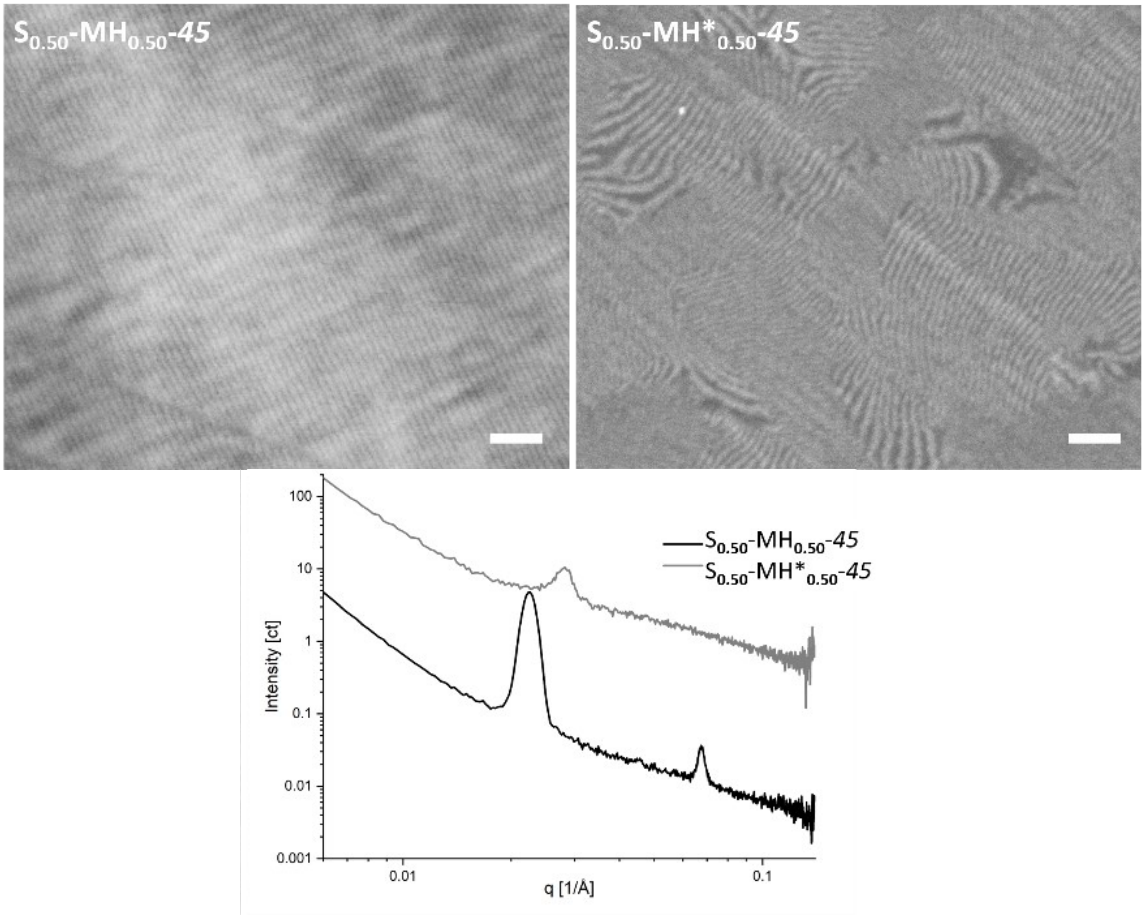


Figure S99: SEM images and SAXS spectra for $S_{0.50}$-$MH_{0.50}$-45 and $S_{0.50}$-$MH^*_{0.50}$-*45*. Scale bars = 200 nm.

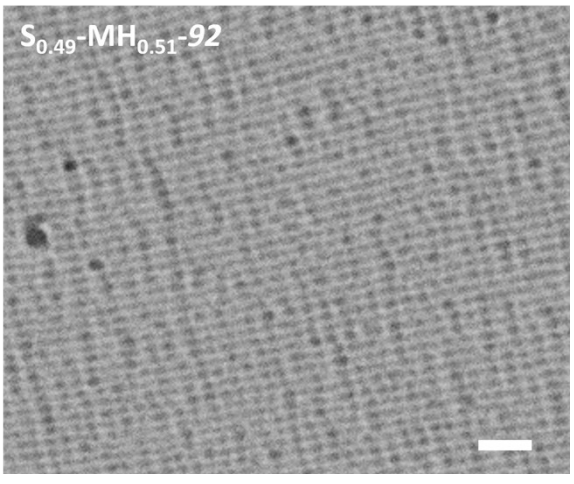


Figure S100: SEM image for $S_{0.49}$-$MH_{0.51}$-*92*. Scale bar = 200 nm.

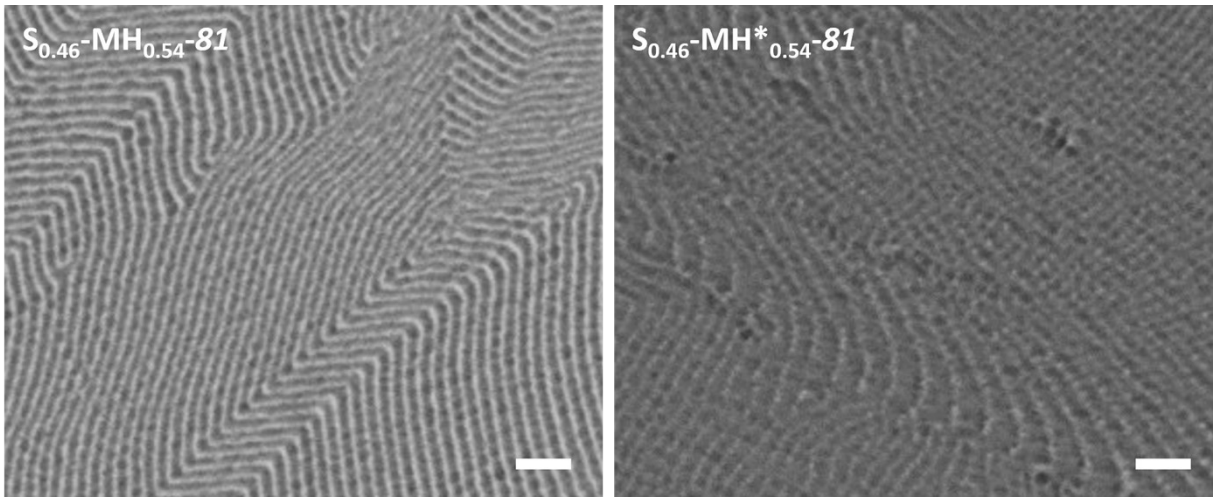


Figure S101: SEM images for $S_{0.46}$-$MH_{0.54}$-81 and $S_{0.46}$-$MH^{*}_{0.54}$-*81*. Scale bars = 200 nm.

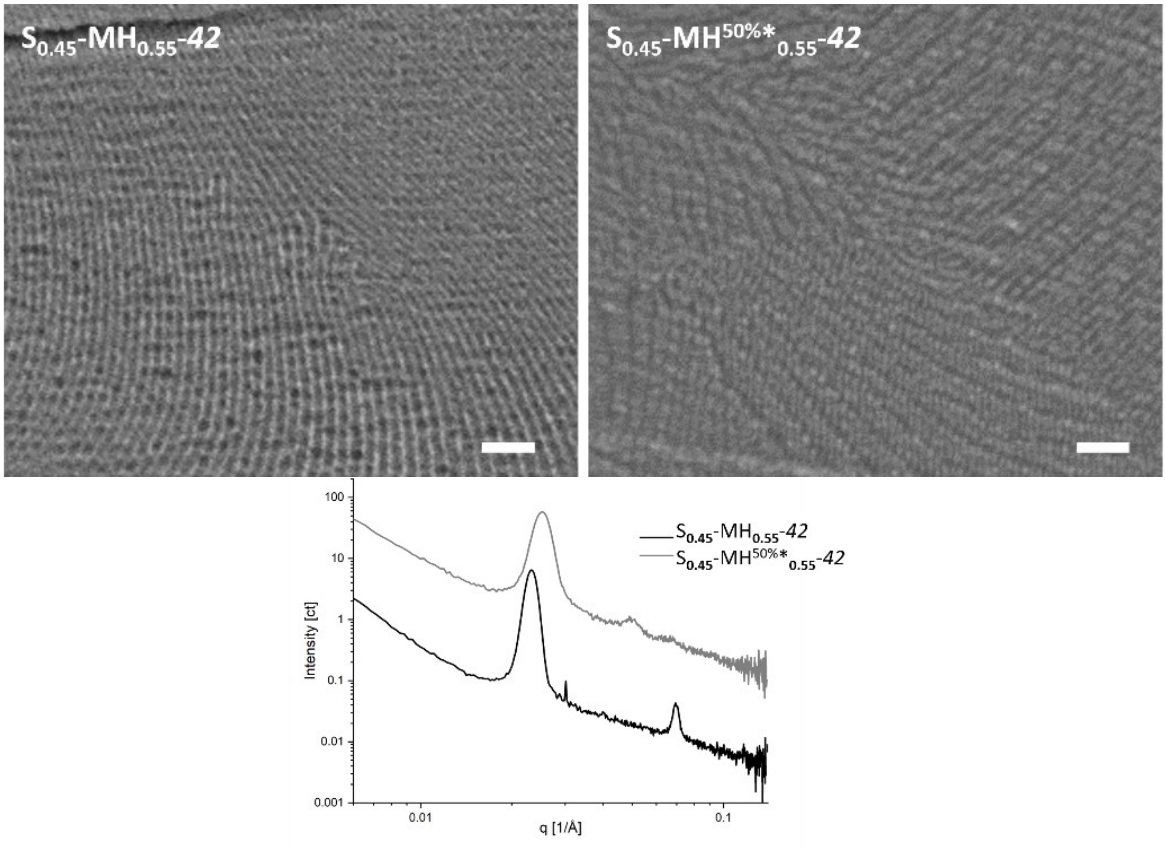


Figure S102: SEM images and SAXS spectra for $S_{0.45}$-$MH_{0.55}$-*42* and $S_{0.45}$-$MH^{50\%*}_{0.55}$-*42*. Scale bars = 200 nm.

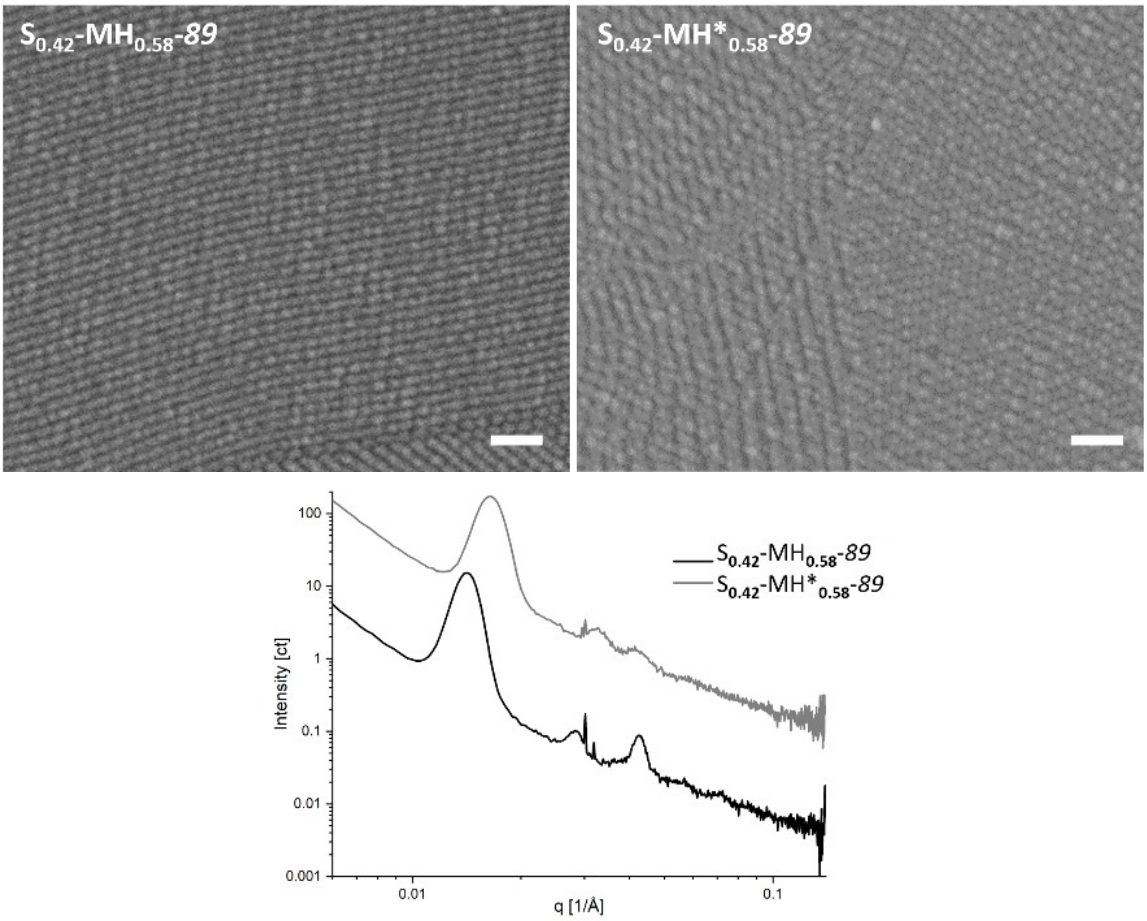


Figure S103: SEM images and SAXS spectra for $S_{0.42}$-$MH_{0.58}$-*89* and $S_{0.42}$-$MH^*_{0.58}$-*89*. Scale bars = 200 nm.

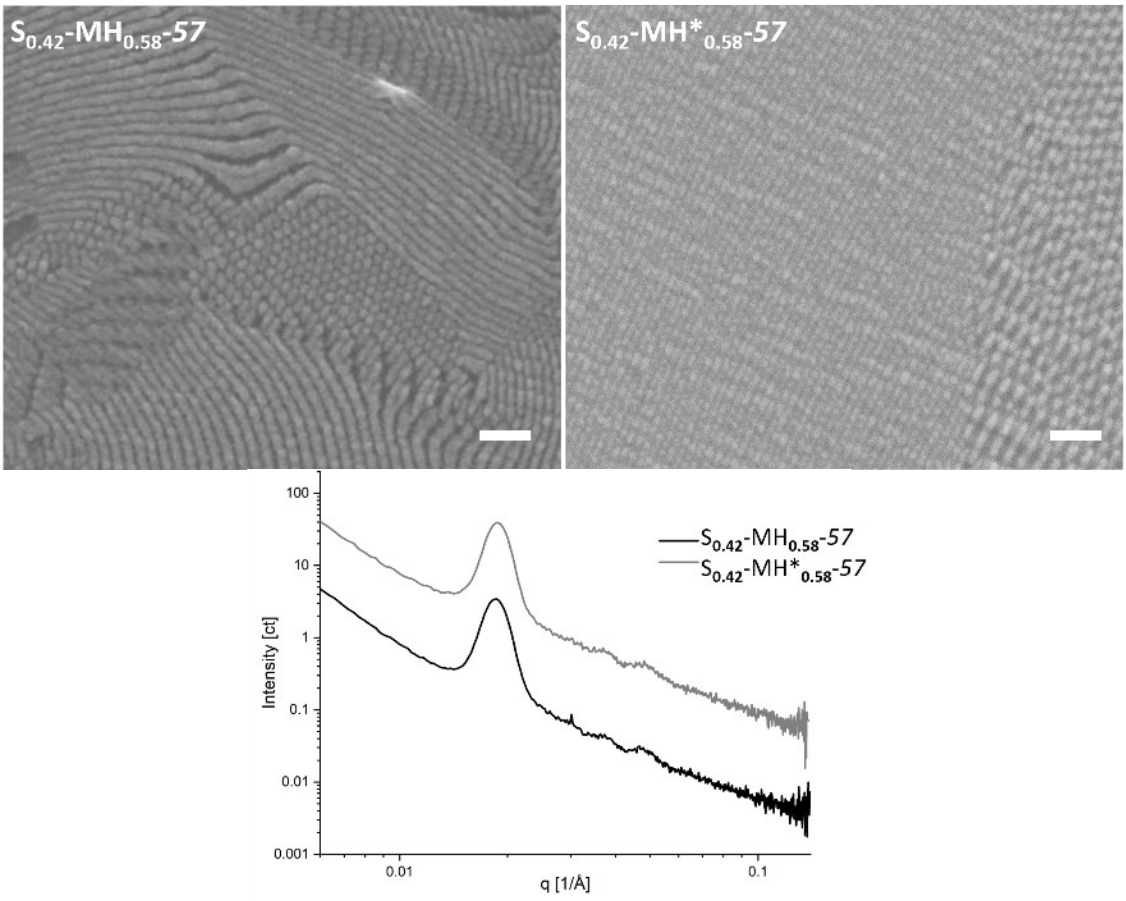


Figure S104: SEM images and SAXS spectra for $S_{0.42}$-$MH_{0.58}$-*57* and $S_{0.42}$-$MH^*_{0.58}$-*57*. Scale bars = 200 nm.

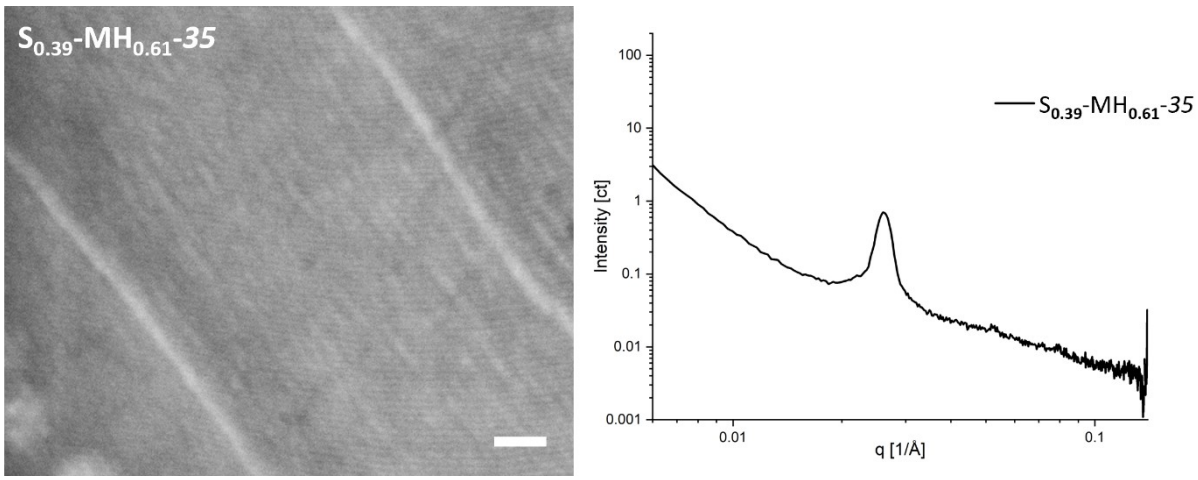


Figure S105: SEM image and SAXS spectrum for $S_{0.39}$-$MH_{0.61}$-*35*. Scale bar = 200 nm.

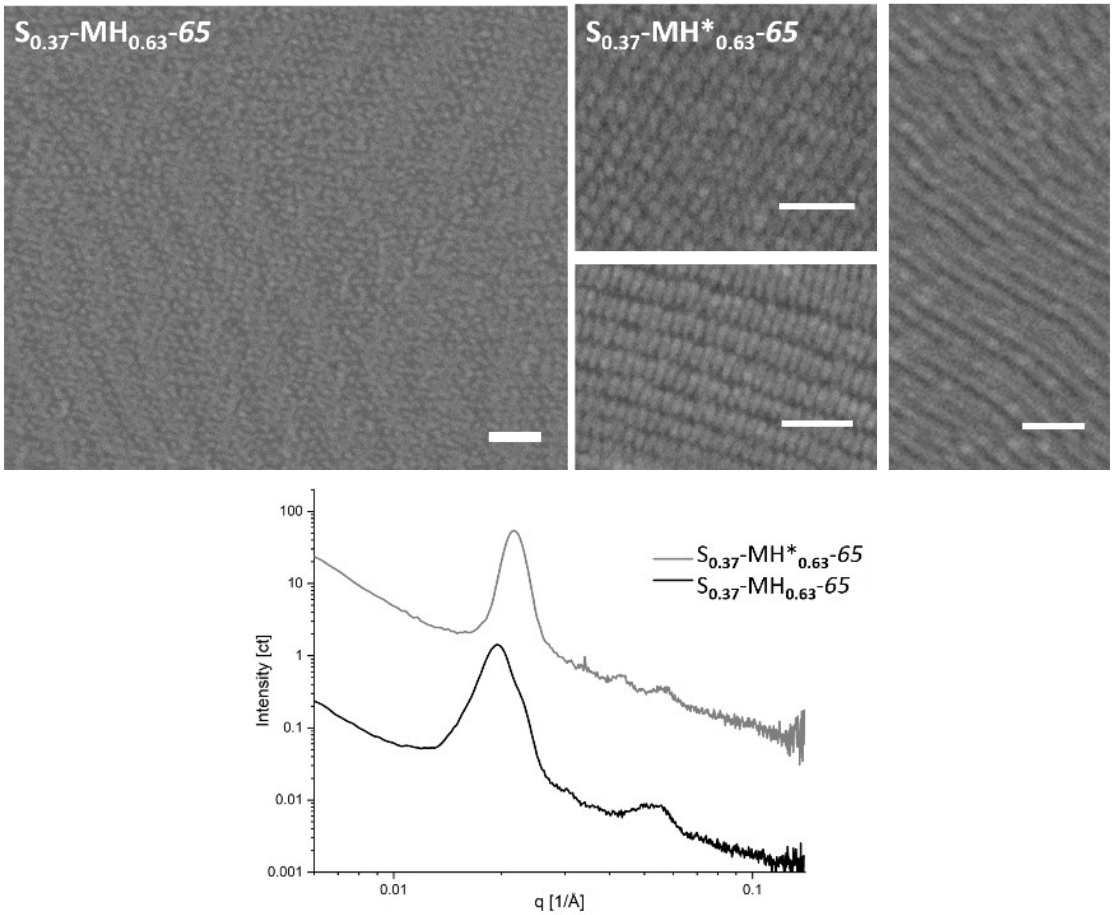


Figure S106: SEM images and SAXS spectra for $S_{0.37}$-$MH_{0.63}$-*65* and $S_{0.37}$-$MH^*_{0.63}$-*65*. Scale bars = 200 nm.

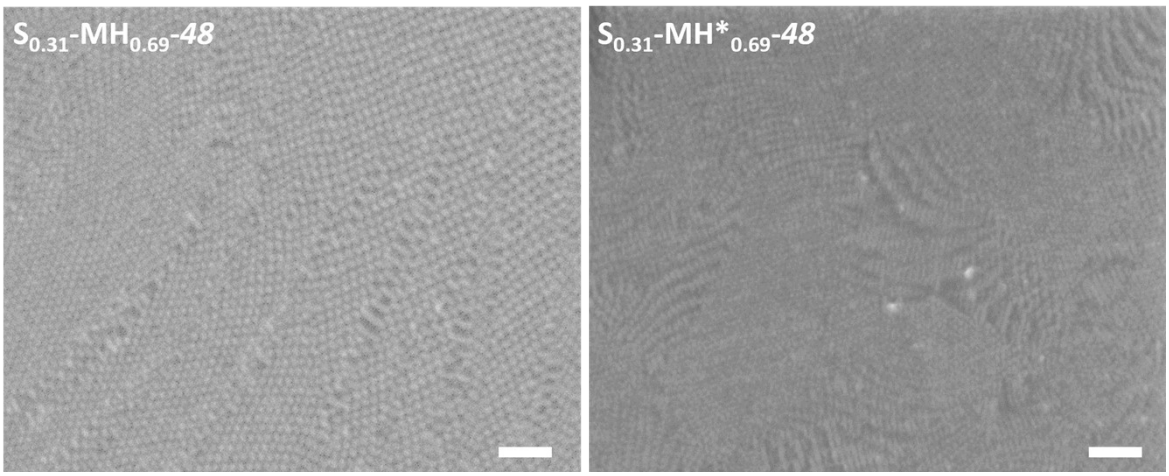


Figure S107: SEM images for $S_{0.31}$-$MH_{0.69}$-*48* and $S_{0.31}$-$MH^*_{0.69}$-*48*. Scale bars = 200 nm.

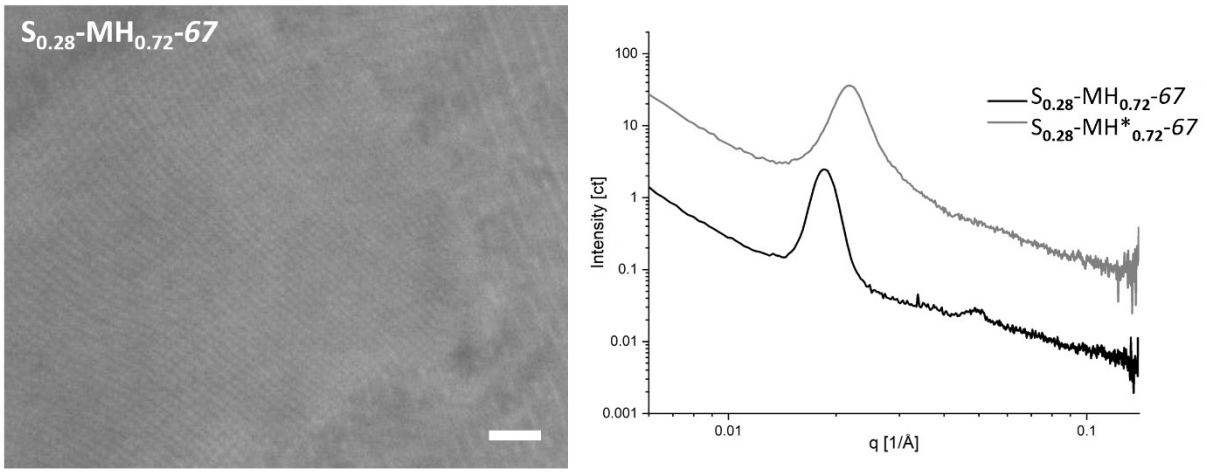


Figure S108: SEM image and SAXS spectra for $S_{0.28}$-$MH_{0.72}$-*67* and $S_{0.28}$-$MH^*_{0.72}$-*67*. Scale bar = 200 nm.

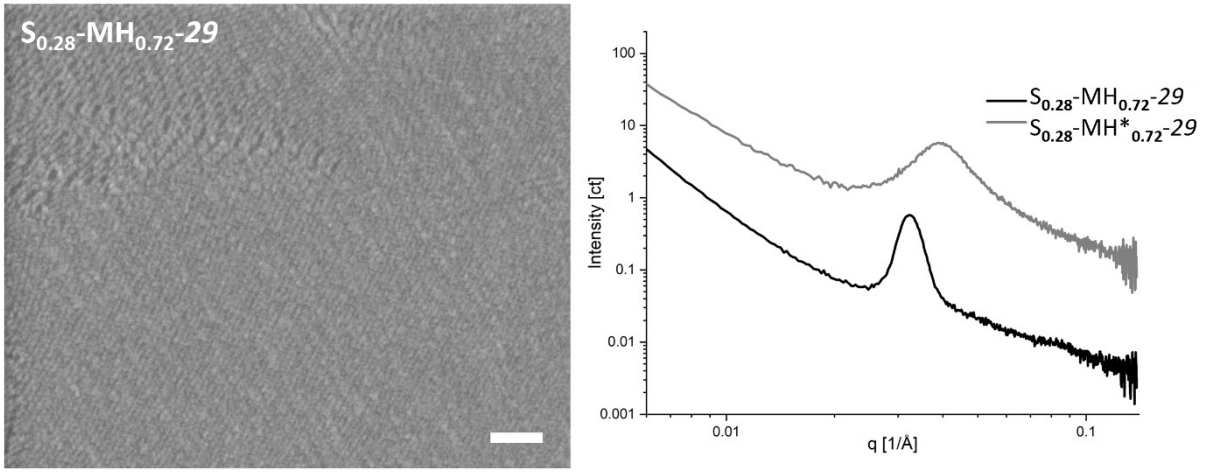


Figure S109: SEM image and SAXS spectra for $S_{0.28}$-$MH_{0.72}$-*29* and $S_{0.28}$-$MH^*_{0.72}$-*29*. Scale bar = 200 nm.

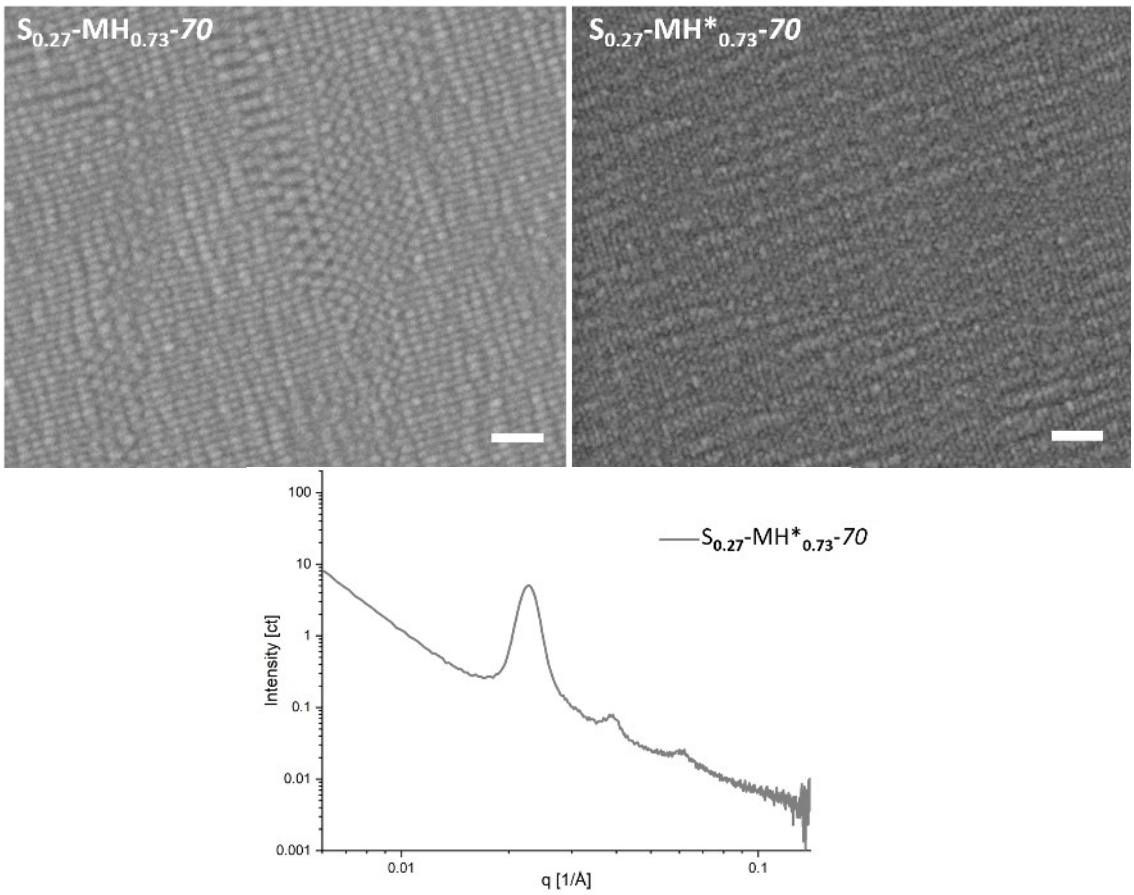


Figure S110: SEM images and SAXS spectrum for $S_{0.27}$-$MH_{0.73}$-*70* and $S_{0.27}$-$MH^*_{0.73}$-*70*. Scale bars = 200 nm.

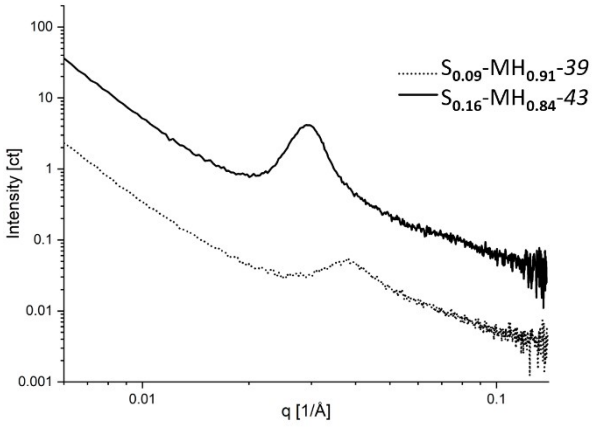


Figure S111: SAXS spectra for $S_{0.16}$-$MH_{0.84}$-*43* and $S_{0.09}$-$MH_{0.91}$-*39*.

AFM and IR-SNOM phase images

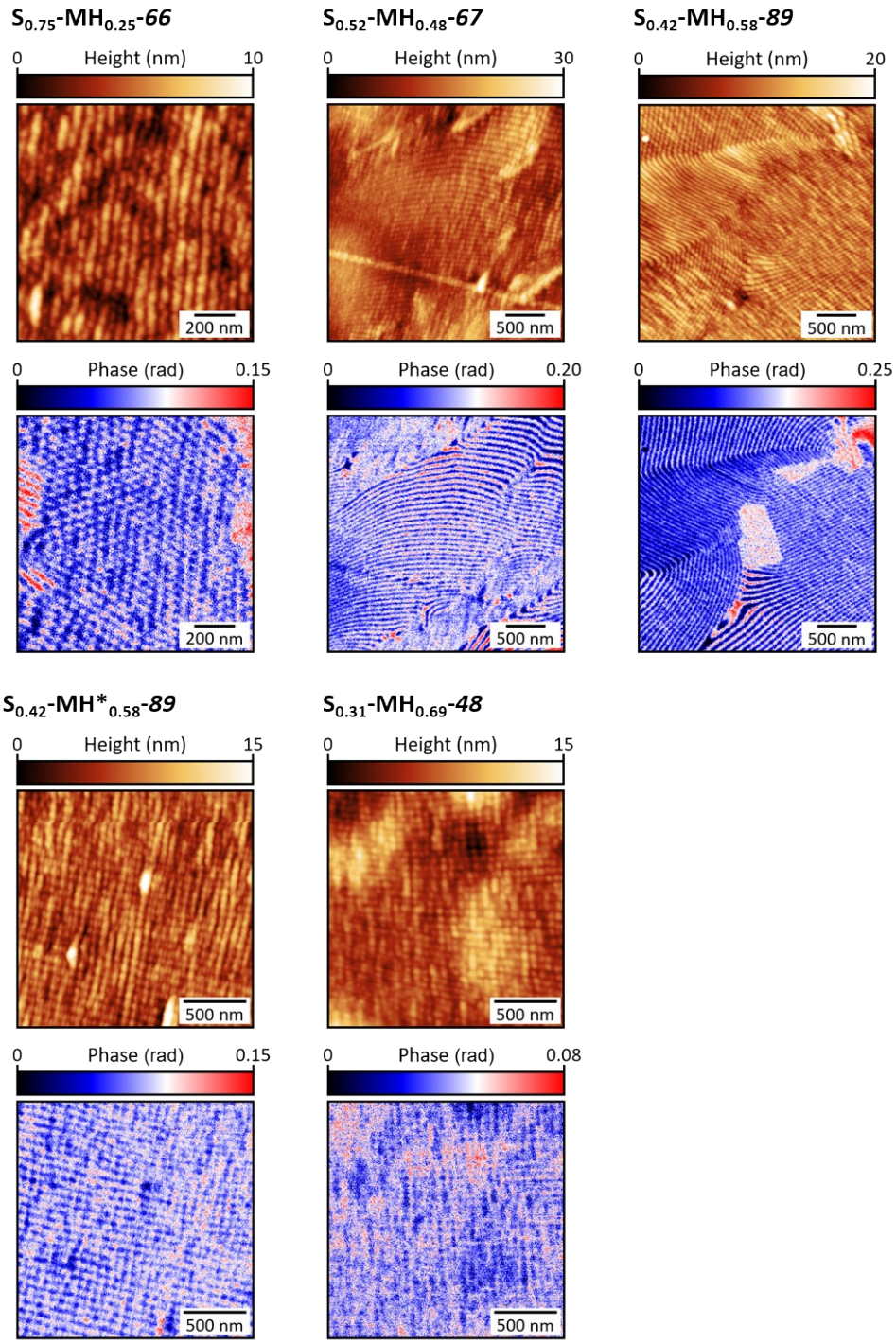


Figure S112: AFM height images (top) and corresponding IR-SNOM near-field optical phase images (bottom), mapped at an independently addressable absorption band of the PMMA block at 1152 $cm^{-1}$.

Cuts along different planes of cylindrical and gyroidal morphologies

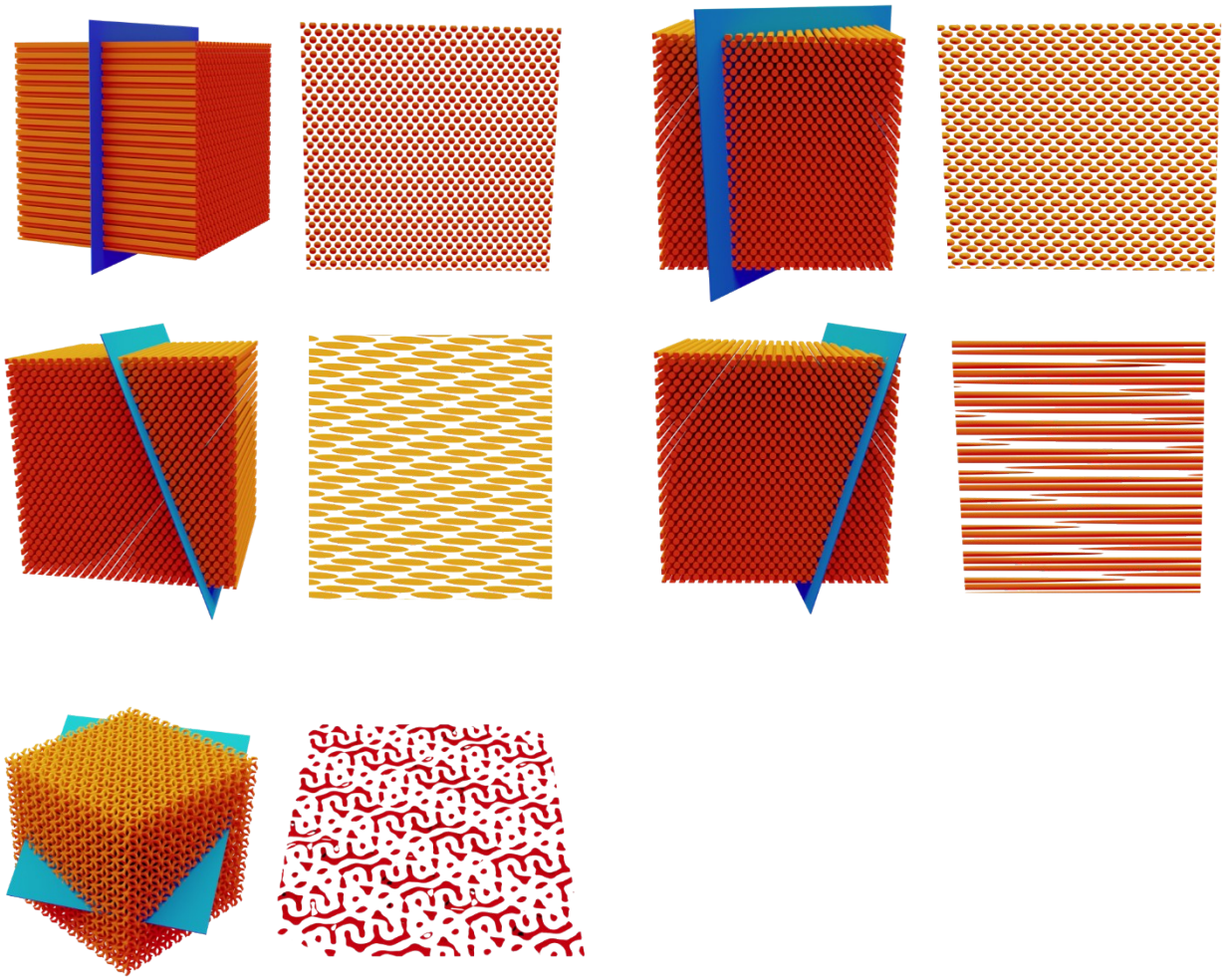

Figure S113: 3D modeled, rendered images cut along different planes of the ordered cylindrical (top and middle row) and gyroidal (bottom row) morphologies.

Domain spacings

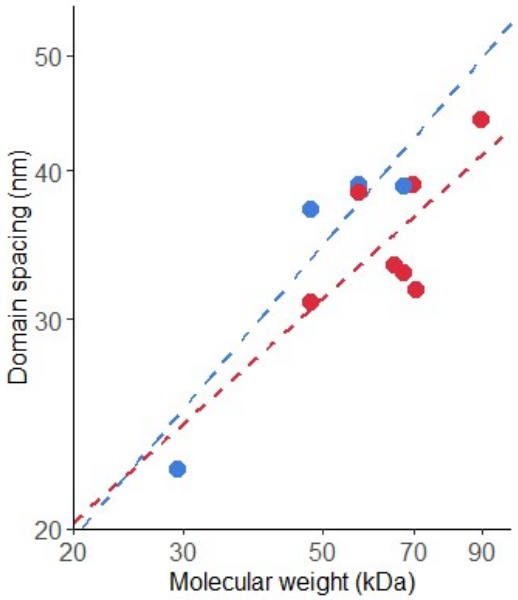


Figure S114: Double logarithmic plot of the domain spacing $d_{SAXS}$ against the molecular weight for the cylindrical samples. The dotted lines are the power law fits with the parameters stated below in Table S3. Blue = precursor BCP and red = functionalized BCP.

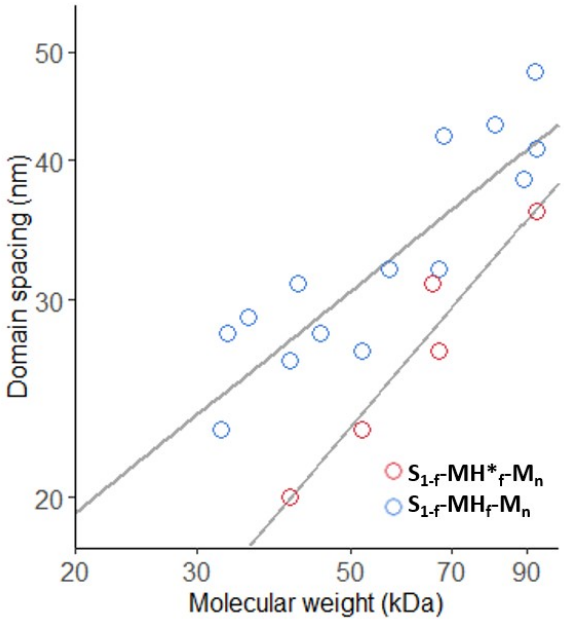


Figure S115: Double logarithmic plot of the domain spacing against the molecular weight for the lamellar morphology determined from $d_{SEM}$. The dark grey lines are the power law fits to $d=a*MW^b$.

Table S3: Fit data for the power law for the different polymer types

| Morphology | Fit to power law | $d \sim MW^b$ | $R^2$ |
|---|---|---|---|
| Lamella ($d_{SAXS}$) | $0.036^{+/-0.012} * MW^{0.63 +/- 0.03}$ | 0.63 | 0.98 |
| Lamella functionalized ($d_{SAXS}$) | $0.040^{+/- 0.035} * MW^{0.59 +/- 0.08}$ | 0.59 | 0.95 |
| Lamella ($d_{SEM}$) | $0.141^{+/- 0.011} * MW^{0.50 +/- 0.07}$ | 0.50 | 0.80 |
| Lamella functionalized ($d_{SEM}$) | $0.009^{+/-0.012} * MW^{0.73 +/- 0.12}$ | 0.73 | 0.93 |
| Cylinder | $0.043^{+/- 0.001} * MW^{0.62 +/- 0.20}$ | 0.62 | 0.85 |
| Cylinder functionalized | $0.187^{+/- 0.490} * MW^{0.47+/- 0.32}$ | 0.47 | 0.43* |